

REVIEWS OF TOPICAL PROBLEMS

PACS numbers: 42.25.Kb, 42.55.Vc

Angular divergence and spatial coherence of X-ray laser radiation

P D Gasparyan, F A Starikov, A N Starostin

Contents

Abstract. **X-ray lasers have been the subject of intense research since the mid-1980s owing to continuous advances in technology and computer engineering. By the mid-1990s, extreme ultraviolet (XUV) and soft X-ray lasing has already been achieved for approximately a hundred lines, with a lower boundary within the 'water window.' At present, the generation of highly directional and highly coherent laser radiation is of great interest for a variety of scientific, technological and medical applications. The formation of X-ray laser radiation is only one aspect of the general field of X-ray lasing, where a number of interrelated atomic physics, plasma physics, and quantum electronics problems are also to be solved. In the present paper, the historical development and current state of theoretical and experimental work on the angular divergence and spatial coherence of X-ray laser radiation is reviewed. Various approaches to the dynamics of laser-amplified radiation are considered and prospects for improving laser beam quality and increasing radiation intensity discussed. A comparison is made between the experimental results and theoretical predictions.**

1. Introduction

From the first steps of the development of quantum electronics and the advent of optical lasers, the quest to move to the shorter-wavelength region, in particular, to create an X-ray laser was natural and attractive. Efficient X-ray lasers promise to provide substantial progress in numerous fields of science, techniques, and medicine. One of the examples of application of X-ray lasers, which cannot leave the scientific and simply human imagination indifferent, is the possibility of studying in detail the structure of a biological cell *in vivo* with a high spatial resolution.

The X-ray wavelength range corresponds to electronic transitions between inner shells of atoms or outer shells of multiply-charged ions in a plasma. The pumping intensity required for obtaining the inverse population is proportional to $\nu^3 \Delta\nu$ and is quite high for the X-ray range. According to the first estimates [1], it should be equal to $10^{17} - 10^{18}$ W/cm^2, which corresponds to a thermal radiation source with a huge (for the Earth's conditions) temperature of 1 – 3 keV. The only radiation source of this type is a nuclear or thermonuclear explosion. For this reason, the development of X-ray lasers in the 1960s could proceed only within the framework of military programs and was the privilege of a few research groups of the Nuclear Powers. The reality of the development of X-ray lasers pumped by nuclear explosion radiation was accepted by experimental studies of X-ray lasers in the USA reported in 1981 [2]. Papers [3, 4] report the successful engineering of an X-ray laser pumped by a nuclear explosion with a power of 20 – 100 kilotons.

As of now, the full-scale experimental work at this project is not to proceed in view of the nuclear test moratorium. At the same time, in the late 1970s — early 1980s substantial progress was achieved in the development of multi-beam optical laser systems producing nanosecond pulses with powers from 0.01 to 10 TW for studies in the field of controlled thermonuclear fusion. Powerful optical lasers used as drivers for laser thermonuclear fusion were applied for pumping laboratory plasma X-ray lasers in the XUV and soft X-ray wavelength ranges. This stimulated extensive studies of X-ray lasers, although with moderate parameters (wave-

P D Gasparyan, F A Starikov Russian Federal Nuclear Centre, All-Russian Research Institute of Experimental Physics (VNIIEF), 607190 Sarov (Arzamas-16), Nizhegorodskaya region, Russia
Tel. (7-831-30) 4-55-22, 4-58-93, 4-56-46; Fax (7-831-30) 5-45-65
E-mail: pdg@albatross.md08.vniief.ru; starikov@otd13.vniief.ru
A N Starostin State Research Centre of the Russian Federation – Troitsk Institute for Innovation and Fusion Research (TRINITI), 142092 Troitsk, Moscow region, Russia
Tel. (7-095) 334-06-97; Fax (7-095) 334-57-76
E-mail: staran@fly.triniti.troitsk.ru

Received 22 October 1997
Uspekhi Fizicheskikh Nauk **168** (8) 843 – 876 (1998)
Translated by M N Sapozhnikov; edited by A Radzig

lengths and powers), but under laboratory conditions. The first successful laboratory experiments on X-ray lasing in a multiply-charged ion plasma were performed in 1984 [5–7].

In experiments [5] at the Lawrence Livermore National Laboratory (LLNL), USA, an extended X-ray laser plasma was produced by transverse focusing of radiation from an Nd:glass laser to a line on an ultrathin foil covered with a selenium film 750 A in thickness [6]. A schematic of this experiment is shown in Fig. 1. The target was irradiated with 0.45-ns laser pulses at 0.53 μm of 1 kJ energy and an intensity of $(5\times10^{13}-10^{14})$ W/cm^2. In [5, 6], a collisional excitation X-ray laser operating on the transitions between discrete excited states in Ne-like ions was demonstrated, which has been originally suggested in [8]. In this laser scheme, the absorption of intense laser radiation causes heating and evaporation of the target with the formation of a high-temperature multiply-charged expanding coronal plasma. In the low-density region, the ionized plasma corona contains Ne-like ions at a high concentration. In the plasma produced by the foil explosion, soft X-ray lasing was detected on two $1s^22s^22p^53p$ $J=2$ — $1s^22s^22p^53s$ $J=1$ transitions of Ne-like selenium at 20.6 and 20.9 nm. Lasing was observed during pumping for ~ 200 ps. The measured gain coefficient and output power were 4–5 cm^{-1} and 2–5 MW, respectively. The population inversion on the 3p–3s transitions was achieved in the three-level pumping scheme (Fig. 2). Pumping of the upper laser levels of the $1s^22s^22p^53p$ configuration occurs upon monopole excitation from the ground state of Ne-like ions (the $1s^22s^22p^6$ configuration) in collisions with free electrons. The radiative decay of these levels to the ground state is strongly suppressed. The lower laser levels of the $1s^22s^22p^53s$ configuration are predominantly depopulated via radiative decay to the ground state, whose rate in the multiply-charged plasma substantially exceeds the rate of electronic excitation of these levels from the ground state. The population inversion produced in this way in the plasma with slowly varying temperature and density has a quasi-steady-state nature, because the rates of collisional and radiative processes are significantly higher than the energy-exchange rates in the plasma. This scheme can be implemented in a pure form only in an infinitely thin, optically transparent (in transverse direction) layer of an open plasma. Under real conditions, the thickness of the X-ray laser medium is finite, and the rate of radiative decay of the lower laser level decreases because of its pumping by radiation from the ground state, i.e. due to reabsorption of the resonance radiation. This effect, which is substantial in most multiply-charged ion X-ray laser schemes, restricts the gain-medium lateral dimension to the mean free path of resonance photons. In the X-ray laser scheme under consideration, an increase in the probability of emission of the resonance photons from the gain medium due to the Doppler frequency shift reduces the spurious effect of reabsorption of the resonance radiation. Indeed, for the large transverse gradient of the plasma velocity typical of the reaffection wave of the plasma corona, the Doppler shift for the resonance quanta of the X-ray laser medium emitted in the transverse direction is comparable and even greater than the Doppler width of the resonance lines. Under such conditions, the X-ray laser medium becomes more transparent for the resonance radiation, which allows one to produce inversion over a sufficiently wide gain region. At the same time, the transverse velocity gradient does not affect the line shift and does not prevent X-ray lasing in the longitudinal direction (the gain direction)†.

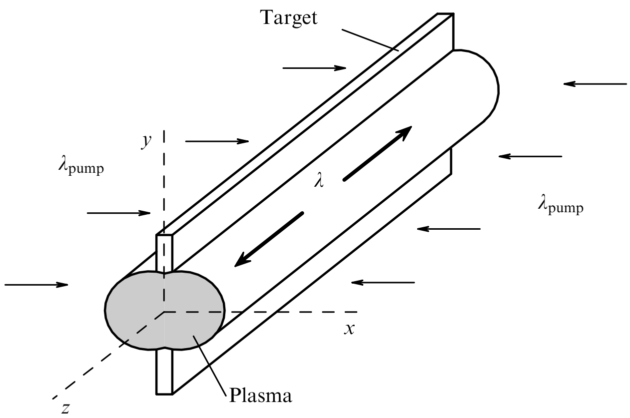

Figure 1. Schematic of experiments on X-ray lasing upon irradiation of a thin foil [5, 6].

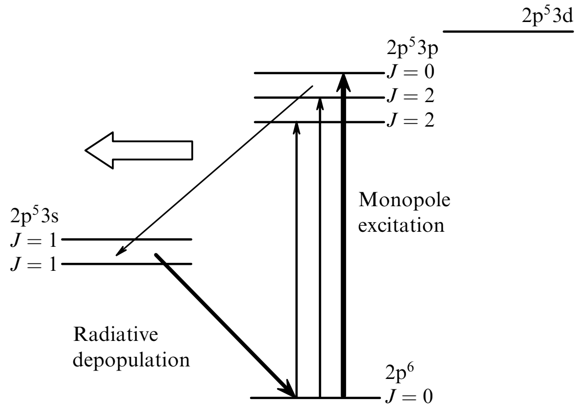

Figure 2. Energy diagram of the X-ray laser operating on the 3p–3s transition of the Ne-like ion.

The three-level Ne-like ion X-ray laser scheme considered above is simplified. Note that pumping of the upper laser level is also facilitated by recombination of the F-like ions and subsequent cascade transitions from the Ne-like highly excited states. Under real conditions, a variety of kinetic effects (a great number of levels and reactions in the multiply-charged plasma, the nonequilibrium distribution functions of free electrons, diffusion processes, etc.) also plays a certain role.

In experiments [7] performed at Princeton University, USA, the pumping radiation (a wavelength of 10 μm, a pulse duration of ~ 50 ns, and an energy of ~ 1 kJ) was focused onto a small spot on a solid target. During expansion of the magnetically confined plasma the plasma

† Reabsorption of the resonance radiation, being spurious in the collisional pumping scheme, is advantageous in X-ray lasers with resonance optical pumping [15]. In these laser schemes, the lasing medium is surrounded by an optically thick converter of the resonance radiation with photon energy equal to the excitation energy of the upper laser level. The resonance photons are accumulated in the converter and the lasing medium due to reabsorption, providing optical pumping of the upper laser levels. In the resonance pumping schemes, it is important to ensure the absence of the plasma velocity gradients which enhance the loss of photons.

column was formed in the direction opposite to the pumping direction. In [7], the laser action was observed on the $n = 3-2$ transition of H-like carbon at $\lambda = 18.2$ nm upon recombination pumping when the plasma was subjected to complete ionization followed by rapid cooling, recombination, and cascade electronic transitions from highly excited levels of the hydrogen-like ion [9]. The rapid plasma cooling can be achieved during its hydrodynamic expansion or during processes of radiation emission and heat conduction, as in [7]. The duration of the X-ray laser pulse in [7] was 10 – 30 ns.

The first experiments on laboratory optical-laser-pumped X-ray lasers [5 – 7] were followed by rapid progress in this field of research described in reviews [10 – 14], monograph [15], and the proceedings of regular International Conferences on X-Ray Lasers [16 – 19]. A number of physical mechanisms of pumping and operating X-ray laser schemes are discussed in detail in monograph [15]. By the mid-1990s, X-ray lasing had been obtained at ~ 100 lines in the wavelength range down to 3.56 nm [14]. This lower wavelength boundary is located within the 'water window' (2.3 – 4.4 nm) suitable for biological and medical applications of X-ray lasers. The observed small-signal gains are equal to several cm^{-1} for an X-ray laser plasma length from several millimetres to ~ 10 cm. For pumping energies of 1 kJ and higher, a gain saturation was demonstrated which requires a gain length, i.e. the product of the small-signal gain by the X-ray plasma length, of the order of 15 – 20. The maximum power, energy, and brightness of the X-ray laser radiation are ~ 10 MW, ~ 5 mJ, and $\sim 10^{23}$ photon/(s mm^2 mrad^2) in the 0.01% band, respectively [10].

In the last years, great efforts have been expended on reducing the required pump energy and producing lasing without the use of large laser facilities of which only a few exist in the world [14, 18, 19]. Recent progress has resulted in the development of the first small-scale X-ray lasers pumped by ultrashort laser pulses with energies of the order of several joules only and even lower. Thus, in Ref. [20] X-ray lasing was observed at 32.6 nm on the 3p – 3s $J = 0-1$ transition in Ne-like titanium by heating a preliminary prepared plasma with a picosecond pulse. The pumping intensity was $\sim 10^{15}$ W/cm^2. In contrast to the quasi-steady-state scheme of producing population inversion in Ne-like ions, the inversion is created here during rapid plasma heating (in a time of the order of intraion relaxation) due to transient collisional processes proceeding with different rates [21]. Such a sharply nonstationary regime allowed the authors of Ref. [20] to obtain a gain coefficient of 19 cm^{-1} and a gain length of about 10. The X-ray laser pulse duration was about 20 ps.

A new interesting possibility for the development of the X-ray laser appeared with the advent of femtosecond optical lasers operating at repetition rates from 10 Hz to 1 kHz. The passage to femtosecond pumping results in a substantial increase in power. The irradiation of a gas or preliminary prepared plasma by a femtosecond pulse causes tunnelling ionization in superstrong fields. The mechanism of producing the inverse population substantially depends on the type of polarization of the pump radiation (see a brief review [22]). In the case of linear polarization, the ionized electrons are cold, and the population of the depleted laser levels occurs via recombination. In the case of circular polarization, hot electrons are produced, and the laser levels are collisionally populated. The maximum gain length ~ 11 was achieved for the 41.8-nm line of the $4d^9 5d\,^1S_0 - 4d^9 5p\,^1P_1$ transition in the Pd-like xenon upon excitation of a cell with xenon by ~ 40-fs, ~ 70-mJ laser pulses [23].

A remarkable achievement was the engineering of a tabletop X-ray laser operating at 46.9 nm on the 3p – 3s $J = 0-1$ transition in Ne-like argon in a capillary discharge where the quasi-stationary X-ray lasing was obtained without laser pumping [24]. The energy of the laser was 30 μJ, and gain saturation was achieved [25]. Although tabletop X-ray lasers have modest parameters compared to those of X-ray lasers pumped by powerful optical lasers, their advent is quite important. The lower cost of their fabrication facilitates more extensive distribution and makes them available as an object and a research tool for many laboratories.

While the main goal of the first studies on X-ray lasers was the demonstration of lasing, in the course of the development of this field, along with the search for new lasing conditions and media and further shortening of the laser wavelength [26], increasing attention is being paid to experimental and theoretical studies aimed at controlling and optimizing the quality of the X-ray laser radiation. Notwithstanding the fact that the present-day brightness and monochromaticity of X-ray lasers substantially exceeds those of the conventional alternative X-ray sources (X-ray tubes, synchrotrons, relativistic electron beams, a dense laser plasma, and an electric-discharge plasma). For this reason, X-ray lasers are already used for interferometric and X-ray diffraction diagnostics of plasmas [19]. Nevertheless, the complete set of properties of X-ray lasers required for studies of elementary processes in atomic physics, X-ray microscopy and holography, X-ray lithography, etc. [15, 27] has not been obtained so far. For the X-ray laser to become a true laser satisfying its promising applications, the X-ray laser radiation should be not only powerful but also of low-divergence and highly coherent. As was experimentally shown [28], the X-ray laser radiation is characterized by the degree of monochromaticity $\Delta\lambda/\lambda < 10^{-4}$, which yields, for the soft X-ray region, a longitudinal coherence length equal to tens and hundreds of micrometers, which is sufficient for many X-ray laser applications.

More important for X-ray lasers is the problem of angular divergence and transverse spatial coherence [29]. In the case of optical lasers, open resonators are often used to obtain single-mode lasing, and it would be reasonable to apply this approach in the X-ray range. However, for X-ray lasers it is difficult to realize the multipass gain mode in the open resonator. Firstly, although modern technology permits the fabrication of multilayer mirrors for the soft X-ray range with reflection coefficients equal to tens of percent at normal incidence [30], their parameters still are poor according to laser standards, and, in addition, there exists the problem of radiation stability of the mirrors. Secondly, the multipass gain mode is hindered by the short time of the population inversion occurrence in a plasma. The X-ray laser can operate, as a rule, in the single- or double-pass amplified-spontaneous-emission (ASE) mode. In the ASE mode, spontaneous emission of ions with the inverse population is amplified when the magnitude of inversion, the transition probability, and the linewidth are unsuitable for the appearance of superfluorescence [31]. The maximum ASE signal is observed in the direction of the maximum length of the medium. To obtain a noticeable level of induced emission, a high-gain plasma medium extended in one direction should be produced (see Fig. 1). For the laser line to be distinctly detectable against the background of nonlaser lines, the noise should be usually amplified at least by a factor of e^5. A number of fundamental principles of the development of ASE have been experimentally verified for mirrorless IR gas lasers with a homogeneous lasing medium [32, 33]. The properties of the X-ray ASE are determined by a number of physical effects observed in the X-ray laser plasma and substantially depend on the optical inhomogeneities present in the plasma gain medium. The specific ASE mode and optical inhomogeneities affect the quality of the X-ray laser radiation and hinder producing a single-mode regime.

This review is devoted to the specific features of forming the angular divergence and spatial coherence of ASE in X-ray lasers and the possibilities of improving the quality of the X-ray laser beam. The results of theoretical considerations are compared with experimental data obtained in this field.

It is important to note that the problem of X-ray lasers, being related to atomic physics, plasma physics, and quantum electronics, has many aspects. A complete theoretical description of the X-ray laser involves, along with the ASE dynamics, first of all such aspects as (1) the two-dimensional (and three-dimensional) radiative plasma hydrodynamics, and (2) the radiative-collisional kinetics of populations of ion levels. The combined solution to the equations of hydrodynamics, the population kinetics, and radiation transfer can be only obtained by the methods of numerical simulation. The numerical computations are quite expensive even in the case of a one-dimensional geometry for the X-ray laser targets because of the multidimensionality of the problems (spectral, angular, spatial, and time dependences) and the different scales of physical processes in X-ray lasers. For this reason, theoretical calculations of X-ray lasers are performed by steps, based on physical conditions and concepts. Hydrodynamic processes are much more inertial than kinetic and radiative processes. Because of its low energetics, ASE does not usually affect the hydrodynamic behaviour of the X-ray laser plasma. Therefore, hydrodynamic calculations can be performed without consideration of the ASE dynamics. Moreover, these computations can be restricted to simplified models of the plasma kinetics which take into account only the slowest processes of energy exchange and ionization. The space-time distribution of the ion composition, temperatures, and densities of ions and free electrons obtained from hydrodynamic calculations is used in refined calculations of the population kinetics (not completely compatible with the gasdynamics) with a great number of ion states. These, as a rule, quasi-steady-state calculations, which use the high rate of population of the excited ionic levels, yield the distributions of the gain coefficients and spontaneous sources in the X-ray laser medium which govern the ASE dynamics. At this stage of calculations, a careful consideration of reabsorption of line emission in the X-ray laser medium is important, because in most physical schemes the lower state of the operating transitions is depopulated mainly due to radiative decay. Calculations of the linear gain coefficient should take into account the nonunidimensional geometry of the gain medium and the Doppler line shift in an accelerated plasma.

A system of kinetic equations for populations of the ionic levels and nonlaser radiation transfer can be solved independently of the ASE dynamics equations if the gain saturation is absent. In some cases, the effect of gain saturation can noticeably change the temporal dynamics of inverse population of the operating ionic levels, and the ASE dynamics should be calculated conformingly by taking into account the influence of ASE on the level populations (the cases of lasing at close lines on strongly-coupled transitions). The specific features of computations of X-ray lasers, based on many approximations and simplifications, require an estimate of their accuracy. The usual approach to such problems on numerical simulation of plasma kinetics consists in the simplification of the dimensionality of the initial statement of the problem and calibration of approximations against the benchmark calculations. The estimate of the accuracy of simplified models for the population kinetics is generally performed in the local statement of the problem or in the one-dimensional approximation.

Note that new information, new approaches to the solution of problems, and explanations of observed anomalies rapidly change the state and the general picture of the problem. Studies of X-ray lasers are undergoing rapid expansion due to the continuous development of technological and calculation possibilities. At present, a sufficiently consistent and comprehensive discussion of different aspects of X-ray laser research is not available in the literature. It is necessary to make up for this drawback in order to consider the interrelation between all these aspects. Monograph [15] was written immediately after first successful laboratory experiments and represents the first book in this field. However, it virtually does not discuss the problems of divergence and coherence of ASE in X-ray lasers which will be considered in this review.

The review outline is as follows. Section 2 is devoted to theoretical approaches describing the amplification of short-wavelength noise radiation in an optically inhomogeneous plasma. Section 3 considers the principal features of the angular divergence and coherence of ASE in X-ray lasers with typical parameters of the gain medium. Finally, Section 4 discusses the methods for producing gain media aimed at the improvement of the X-ray laser beam quality and the enhancement of radiation brightness.

2. Theoretical methods for studying the radiation dynamics of X-ray lasers

The complexity of the problem of ASE dynamics requires various approaches to its solution. The use of alternative methods based on close physical approximations enhances the reliability of the data obtained. In addition, various approaches can take into account different physical effects and complement each other. ASE dynamics in an inhomogeneous X-ray laser medium is studied by methods of geometrical or wave optics. In the first case, the transport equation for the ASE intensity is used, while in the second case, the parabolic equation for the complex amplitude of the ASE field and the equation for the transverse correlation function. Because of the smallness of the wavelength in the XUV and soft X-ray ranges ($\lambda = 0.2-100$ nm) compared to the size of possible optical inhomogeneities, the X-ray laser medium is assumed continuous.

2.1 The transport equation

The line radiation transfer plays a dominant role in kinetic processes in a multiply-charged X-ray laser plasma. First of all, this is explained by the fact that the intensity of radiative processes in a multiply-charged plasma, which is proportional to Z^4, sharply increases as compared to collisional processes whose intensity is proportional to Z^{-2}. It is this circumstance that allows one to produce the substantial nonequilibrium state and population inversion of levels in a hot open multiply-charged ion plasma using one of the classical (three- or four-level) pumping schemes. In many X-ray laser schemes, the population inversion of ionic levels is maintained in the quasi-steady state of the gain medium, which is close to the coronal plasma state, with radiative decay of the lower laser levels. The 'quasi-particle' theory of line radiation transfer in a weakly dispersive plasma and gases in the approximation of complete redistribution over frequencies under photon scattering and with allowance made for the effects of partial redistribution over frequencies [34, 35] was developed for the cases of a low-density weakly nonideal plasma and isolated lines (transitions between the levels). The theory is used in balance radiative-collisional models of the X-ray laser plasma kinetics for description of the transfer both of laser and nonlaser line radiation. In a number of cases, the balance approximation of the level population kinetics in the radiative-collisional model is invalid (transitions between strongly degenerate levels that undergo Stark splitting in plasma microfields). Then, the level population kinetics and radiation transfer should be described taking into account nonlinear interference effects [36]. At present, a rigorous theory of radiation transfer is absent for these cases, except for optically-thin media [37]. Recently, the theory of resonant radiation transfer in dense dispersive strongly-absorbing media was developed [38], in which the equation for the generalized radiation 'intensity' was derived using the formalism of the kinetic Green functions.

For the laser radiation, the quasi-particle transport equation for radiation intensity introduces a maximum error near the lasing threshold when the effects of the ASE frequency and amplitude fluctuations are strong. For this reason, along with the quasi-particle approach, ASE dynamics in X-ray lasers is studied by semiclassical and classical methods developed in the theory of optical lasers (see, for example, Ref. [39]). Below, we describe these methods and their applications for studying the divergence and coherence of X-ray laser radiation. We consider the simplest case of lasing at isolated lines in the case of homogeneously-broadened levels involved in the operating transitions.

2.1.1 The content of the transport equation. The transport equation for the radiation intensity I_ω (measured in $\mathrm{W/(cm^2\,sr\,Hz)}$) in the spectral range ω — $\omega + \mathrm{d}\omega$ has the form [34, 40, 41]

$$\left[\frac{1}{v}\frac{\partial}{\partial t} + \mathbf{n}(\mathbf{R})\frac{\partial}{\partial \mathbf{R}} - \alpha(I_\omega, \mathbf{R}, t) + \beta(\mathbf{R}, t)\right] I_\omega(\mathbf{n}, \mathbf{R}, t) = Q_\omega(\mathbf{n}, \mathbf{R}, t)\,, \qquad (1)$$

where v is the speed of light in a medium. The intensity I_ω has the conventional photometric meaning, i.e. represents the energy characteristic of a light beam at the point $\mathbf{R}$ in the direction of the unit vector $\mathbf{n} = \mathbf{k}/k$. This corresponds to the geometrical optics approximation, which is valid only in the case of statistically quasi-uniform radiation fields when the mean radiation parameters weakly change on the scale of the statistical inhomogeneity [41]. In accordance with this condition, the diffraction effects that restrict the ASE divergence from below are neglected. In the case of X-ray lasers, the neglect of diffraction effects is substantiated by the smallness of λ. The wave effects can be considered within the framework of the classical transport equation only upon passage to nonclassical photometry. In this case, the equation for the generalized 'intensity' is derived from the wave statistical theory [38, 41]. In this theory, the intensity represents the Fourier transform of the correlation function of a random radiation field over the difference (correlation) variable.

Equation (1) should be solved in the spatial region filled with the X-ray laser plasma and the surrounding passive plasma. Consider the terms entering (1).

The spatial derivative in (1) is taken along the direction of the beam whose path in the medium is determined from the principal equation of geometrical optics [42, 43]

$$\frac{\mathrm{d}}{\mathrm{d}s}\left(\eta\frac{\mathrm{d}\mathbf{R}}{\mathrm{d}s}\right) = \nabla\eta\,, \qquad (2)$$

where $\mathbf{R}$ is the radius vector of the beam position, $\mathrm{d}s$ is the increment of the path length, and η is the refractive index of the medium. The contribution from the resonance ions to the refractive index is usually small for the wavelengths, temperatures, and densities of interest, and the effect of anomalous dispersion can be neglected. In most real situations, the dielectric constant ε of a plasma (its real part) is determined by the contribution from free electrons. At the frequency ω, it takes the form [42]

$$\varepsilon = \eta^2 = 1 - \frac{N_\mathrm{e}}{N_\mathrm{c}}\,, \qquad (3)$$

where N_e is the density of free electrons, and $N_\mathrm{c} = m_\mathrm{e}\omega^2/(4\pi\mathrm{e}^2)$ is the critical density. For the soft X-ray and XUV ranges ($\lambda = 0.2-100$ nm), the critical density $N_\mathrm{c} \approx 3\times(10^{28}-10^{23})\ \mathrm{cm}^3$, which considerably exceeds the characteristic values of N_e in the X-ray laser plasma [15]. Thus, ε is close to unity. In most X-ray laser schemes, the active plasma exhibits regular large-scale inhomogeneity of ε caused by its macroscopic motion. The refractive index gradient causes refraction of radiation according to (2). The ASE dynamics is most sensitive to the transverse (relative to the optical axis, i.e. the direction of plasma extension) gradient of η. As follows from (2) and (3), for $\eta \neq \mathrm{const}$, the beam is deflected to lower values of N_e. For this reason, a plasma column produced upon irradiation of a solid target and freely expanding into vacuum, represents a defocusing medium. The quantitative parameters of the spatial distribution of N_e are found from hydrodynamic calculations of X-ray laser targets.

The gain coefficient in (1) for the laser radiation near the isolated transition at the frequency ω has the form (see, for example, Ref. [39])

$$\alpha = \frac{c^2}{4\omega^2}A_{ul}W\psi_{ul}(\omega)\,, \qquad (4)$$

where A_{ul} is the probability of spontaneous radiative transition between the upper u and lower l laser levels, $W = N_u - g_u N_l/g_l$ is the population inversion (g_u, g_l, N_u, and N_l are statistical weights and populations of the upper and lower levels, respectively), and $\psi_{ul}(\omega)$ is the gain line profile normalized to unity in area. For the linear amplification mode, the gain line profile takes into account the homogeneous broadening of laser transitions and inhomogeneous (Doppler) line broadening. The distribution of the gain coefficient α in (1) is generally nonuniform in space and time. The gain profile performs spatial, spectral, and angular filtration of ASE. The radiation propagating at comparatively large angles to the optical axis of a laser leaves more rapidly the active region through its side surface and makes small contribution to the total energy.

The absorption coefficient β in (1) characterizes the effective absorption of laser radiation in a plasma due to reverse bremsstrahlung, Compton scattering by free electrons, photoionization, and discrete-discrete transitions in ions. Usually, β is much lower than α, and the effect of absorption on ASE is significant only in the case of strong gain saturation.

The calculation of ASE requires consideration of the nature of light sources Q, which are distributed over the gain medium and are stochastical. In the transport equation method, they are modelled by an isotropic source of line radiation emitted upon spontaneous decay of the upper level of the operating transition. The specific power of spontaneous emission per unit solid angle in the right-hand part of Eqn (1) is determined by the population of the upper level:

$$Q = \frac{\hbar\omega A_{ul} N_u \psi_{ul}(\omega)}{4\pi} \,. \tag{5}$$

In the general case, equations (1), (4), and (5) are solved in combination with a system of local balance equations of the radiative-collisional kinetic model for M ionic levels (see, for example, Ref. [44]):

$$\frac{\mathrm{d}N_i}{\mathrm{d}t} = D_i + \sum_i K_{ji} N_j + d_i \int_{4\pi} \mathrm{d}\Omega_{\mathbf{n}} \int \mathrm{d}\omega \alpha \, \frac{I_\omega(\mathbf{n}, \mathbf{R}, t)}{\hbar\omega} \,,$$
$$i = 1, \ldots, u, \ldots, l, \ldots, M \,. \tag{6}$$

Here, K_{ji} is the relaxation matrix, D_j is the electron flux to the state j from the continuum and the states that were not taken into account in the relaxation matrix, $d_i = -1$ for $i = u$, $d_i = 1$ for $i = l$, and $d_i = 0$ in the remaining cases. To solve the system of transport equations and equations of the radiative-collisional kinetic model for ionic levels (1)–(6), one should calculate consistently the emission intensity in the medium at all frequencies, taking into account the geometry and movement of the active and inactive regions of X-ray lasers both for laser and nonlaser transitions. The numerical solution to this system of equations involves time-consuming calculations (because of the great dimensionality of the problem) and requires the development of a suitable difference method of solution, because the different physical nature of usual nonequilibrium plasma emission and ASE requires various methods for solving the transport equation in the corresponding regions of absorption coefficient variation for laser radiation (positive or negative). For this reason, the system of equations (1)–(6) is solved by approximate methods, of which we note the following. Firstly, the method of probabilities of escape for the approximate consideration of reabsorption of line radiation in equations of the radiative-collisional kinetic model, which makes kinetic equations almost local. Secondly, this is the 'angles of vision' approximation (see below Section 2.1.3) used for the calculation of the ASE dynamics, which takes into account the ASE directivity and simplifies the calculations of lasing in the saturation mode.

The intensity I_ω entering (1) and (6) as the Fourier transform of the correlation function of the radiation field, i.e. as a mean statistical quantity, does not take into account radiation pulsations due to the finite coherence time τ_c. The value of I_ω is in fact averaged over a time exceeding τ_c. This means that the radiation being amplified is assumed to be broadband and τ_c is assumed to be significantly shorter than the radiative decay time in Eqn (6). But if the spectral line is quite narrow (for example, if the external narrow-band signal is amplified or the ASE line narrows upon amplification) and this condition is not satisfied, the population kinetics should in some degree follow the field pulsations. In this case, the approach under consideration should be changed.

Despite the exclusion of wave effects from the consideration, the use of the method of geometrical optics for the description of the ASE dynamics in X-ray lasers is quite time-consuming. The total picture of the ASE formation is determined from a combined solution of equations (1) and (2) for frequencies near the laser transitions and from equations of the radiative-collisional model (6) for a set of beams emerging from different points of space in various input directions. In the linear approximation in ASE, when the effect of laser radiation on populations in Eqn (6) can be neglected, the system (6) can be solved independently of the transport equations (1) and (2) for laser radiation. Then, the set of equations (1) and (2) is integrated, taking into account the distributions of α, β, and Q obtained from (6), by the method of characteristics over each beam and yields the total distribution of the laser radiation intensity.

Most studies of qualitative features of the ASE dynamics use the quasi-steady-state two-dimensional approximation to (1) and model profiles of η, α, and Q [45, 46]. To model specific experiments (see, for example, Refs [47–50]), the gasdynamic parameters of the X-ray laser medium are calculated using transverse-one-dimensional or two-dimensional nonequilibrium hydrodynamics codes based on the simplified radiative-collisional kinetic models (LASNEX [51], ZARYA [52], SAGE [53], MIMOZA [54], FILM [55], etc.). The kinetic parameters of the laser plasma are computed using codes for detailed multilevel radiative-collisional models of the plasma kinetics in the local approximation ([56], XRASER [57], CC-9 [58], TARAN [59], etc.) or codes for the consistent solution of equations of nonequilibrium radiative hydrodynamics (CC-9 [58], GIDRA [60], EHYBD3 [61], etc.). Codes that calculate the gain along the beam paths in 3D space are in fact used for postprocessor computations.

2.1.2 The two-level quasi-steady-state model. The ASE intensity can become quite high during light amplification and will affect the level populations in (6). The case of gain saturation is interesting from a practical point of view, because in this case the potential of the X-ray laser medium is more fully realized. Equations (1), (2), and (6) should be solved simultaneously. In the simplest case, when in the saturation mode a single-lasing transition dominates (as a rule, the transition with the maximum margin of the population inversion) and ASE weakly affects the energy balance of the medium and relaxation of nonlasing levels, the system of equations (6) can be simplified by replacing the multilevel radiative-collisional kinetic model with the effective open two-level model [44]:

$$\frac{\mathrm{d}N_u}{\mathrm{d}t} = D_u^{\mathrm{eff}} - K_u N_u + K_{ul} N_l - \int_{4\pi} \mathrm{d}\Omega_{\mathbf{n}} \int \mathrm{d}\omega \alpha \frac{I_\omega(\mathbf{n}, \mathbf{R}, t)}{\hbar\omega} \,,$$
$$\frac{\mathrm{d}N_l}{\mathrm{d}t} = D_l^{\mathrm{eff}} - K_l N_l + K_{lu} N_u + \int_{4\pi} \mathrm{d}\Omega_{\mathbf{n}} \int \mathrm{d}\omega \alpha \frac{I_\omega(\mathbf{n}, \mathbf{R}, t)}{\hbar\omega} \,. \tag{7}$$

Here, the quantities D_u^{eff} and D_l^{eff} and the total decay rates K_u and K_l of the operating levels are found from the solution of complete system (6) in the absence of radiation. If the rate of changes in I_ω, D_l^{eff}, and D_u^{eff} are noticeably lower than the decay rates of laser levels, the quasi-steady-state approximation to the balance equations for populations can be applied. By assuming the derivatives in Eqn (7) to be zero, the populations N_u and N_l can be calculated and substituted into Eqns (4) and (5), which results in reducing of the set of equations (1) and (6) to one transport equation

$$\left[\frac{1}{c}\frac{\partial}{\partial t}+n(\mathbf{R})\frac{\partial}{\partial\mathbf{R}}-\frac{\alpha_0(\mathbf{R},t)}{1+\Phi(\mathbf{R},t)}+\beta(\mathbf{R},t)\right]I_\omega(\mathbf{n},\mathbf{R},t) = \frac{Q_0(\mathbf{R},t)+Q_1(\mathbf{R},t)\Phi(\mathbf{R},t)}{1+\Phi(\mathbf{R},t)}\,, \tag{8}$$

where

$$\alpha_0=\frac{c^2}{4\omega^2}A_{ul}W_0(\mathbf{R},t)\psi_{ul}(\omega) \tag{9}$$

is the gain coefficient of a weak signal;

$$W_0=\frac{D_u^{\mathrm{eff}}(K_l-K_{lu}\,g_u/g_l)+D_l^{\mathrm{eff}}(K_{ul}-K_u\,g_u/g_l)}{K_uK_l-K_{lu}K_{ul}}$$

is the inverse population in the absence of radiation effect;

$$Q_0=\frac{\hbar\omega A_{ul}}{4\pi}\,\frac{D_u^{\mathrm{eff}}K_l+D_l^{\mathrm{eff}}K_{ul}}{K_uK_l-K_{lu}K_{ul}}\,\psi_{ul}(\omega)\,,$$
$$Q_1=\frac{\hbar\omega A_{ul}}{4\pi}\,\frac{g_u(D_u^{\mathrm{eff}}+D_l^{\mathrm{eff}})}{g_u(K_u-K_{lu})+g_l(K_l-K_{ul})}\,\psi_{ul}(\omega) \tag{10}$$

are the powers of spontaneous radiation in the absence of radiation effect and in the case of complete saturation, respectively. The saturation function in (8) has the form

$$\Phi(\mathbf{R},t)=\int_{4\pi}\mathrm{d}\Omega_{\mathbf{n}}\int\mathrm{d}\omega\,\frac{\psi_{ul}(\omega)}{\psi_{ul}(\omega_0)}\,\frac{I_\omega(\mathbf{n},\mathbf{R},t)}{J_{\mathrm{sat}}}\,,$$

where $\psi(\omega_0)$ is the value of the spectral function at the line centre, and

$$J_{\mathrm{sat}}=\frac{4\hbar\omega^3}{c^2A_{ul}\psi_{ul}(\omega_0)}\,\frac{g_l(K_uK_l-K_{lu}K_{ul})}{g_u(K_u-K_{lu})+g_l(K_l-K_{ul})} \tag{11}$$

is the saturation flux density.

The nonstationary equation (8) takes into account sources of spontaneous radiation and determines the total intensity spectrum of the lasing medium. In the stationary case (with respect to radiation), the numerical solution of Eqn (8) for a homogeneous amplifying medium of finite length with cylindrical symmetry was obtained in Ref. [62]. The calculations showed that a significant part of the energy of X-ray ASE, as in the IR region [33], is contained within a comparatively narrow solid angle along the X-ray laser axis z in two mutually opposite directions. In the general case, the nonlinear equation (8) is solved numerically using iteration methods and specialized exact difference approximation schemes.

2.1.3 The 'angles of vision' approximation. The problem of calculation of the ASE intensity distribution in the gain saturation mode can be significantly simplified in the 'angles of vision' approximation suggested by A N Starostin and L P Feoktistov and developed by A N Anisimov for the nonstationary case. This approximation uses the presence of the distinctly manifested spatial selection of ASE in an extended amplifying medium and spectral selection of ASE in the vicinity of a quite narrow gain line.

Let us integrate equation (8) over frequency in the approximation of the narrow spectral line by introducing the integrated-in-frequency intensity I and assuming that the approximate equality

$$I(\mathbf{n},\mathbf{R},t)\cong\int\mathrm{d}\omega\,\frac{\psi_{ul}(\omega)}{\psi_{ul}(\omega_0)}\,I_\omega(\mathbf{n},\mathbf{R},t)\approx\int_\omega I(\mathbf{n},\mathbf{R},t)\,\mathrm{d}\omega$$

is satisfied. Then, the saturation function Φ in Eqn (8) is estimated as

$$\Phi(\mathbf{R},t)=\int_{4\pi}\mathrm{d}\Omega_{\mathbf{n}}\,\frac{I(\mathbf{n},\mathbf{R},t)}{J_{\mathrm{sat}}}\,. \tag{12}$$

Further, we will use for the transport equation (8) the approximation of two radiation fluxes with mean intensities I^+ and I^- counter-propagating along the optical axis. In this approximation, function (12) is approximated by the expression

$$\Phi(z,t)=\frac{I^-(z,t)\Delta\Omega^-(z,t)}{J_{\mathrm{sat}}}+\frac{I^+(z,t)\Delta\Omega^+(z,t)}{J_{\mathrm{sat}}}\,. \tag{13}$$

In Eqn (13), it is assumed that the laser radiation intensity weakly varies over the cross section of the X-ray laser medium and is mainly contained within the solid angle where the gain length is maximum. For the elongated geometry of the laser medium, the gain length is maximum in the directions of the X-ray laser axis and sharply changes when the beams leave the laser medium. The region of solid angles, in which the gain length is close to maximum, determines some angles $\Delta\Omega^+(z,t)$ and $\Delta\Omega^-(z,t)$ within which radiation intensities I^+ and I^- change weakly. Estimate (13) was obtained assuming the intensities I^+ and I^- to be constant within angles $\Delta\Omega^+$ and $\Delta\Omega^-$, respectively. Beyond these angles, we have $I^+=I^-=0$. The summation in Eqn (13) in two directions takes into account the geometry of the amplifying medium.

As for the transformation of the right-hand side of equation (8), because of a weak dependence of the solution on the noise intensity upon strong amplification, the volume noise sources can be replaced by equivalent surface sources located at the ends of the X-ray laser medium. In this case, angles $\Delta\Omega^+$ and $\Delta\Omega^-$ will be the angles of vision of the cross section from the point with coordinate z lying on the X-ray laser axis. Thus, the multidimensional equation (8) for the integrated intensity of laser radiation is approximately reduced to two one-dimensional equations. In the stationary case, we have

$$\left\{+\frac{\partial}{\partial z}-\frac{\alpha_0}{1+\left[I^+\Delta\Omega(z)+I^-\Delta\Omega(z-z_{\mathrm{L}})\right]/J_{\mathrm{sat}}}+\beta\right\}\times I^+(z)=0\,,\quad I^+(0)=\frac{Q_0}{\alpha_0}\,;$$

$$\left\{-\frac{\partial}{\partial z}-\frac{\alpha_0}{1+\left[I^+\Delta\Omega(z)+I^-\Delta\Omega(z-z_{\mathrm{L}})\right]/J_{\mathrm{sat}}}+\beta\right\}\times I^-(z)=0\,,\quad I^-(z_{\mathrm{L}})=\frac{Q_0}{\alpha_0}\,, \tag{14}$$

where z_L is the X-ray laser length. If the 'travelling wave' pumping scheme is considered, one can neglect the counter beam effect and solve only one of the equations (14). The solution of the transport equation in the 'angles of vision' approximation approximately determines the spatial distribution of the laser radiation energy in the X-ray laser medium, the effect of saturation on the gain coefficient, and also the average parameters of the ASE intensity in the main direction of propagation of radiation. In particular, by using balance relations, one can easily estimate the energy fraction of the laser radiation propagating along the X-ray laser axis and in the transverse direction. A detailed spectrum and the angular ASE distribution can be obtained from linear equation (8), in which the influence of saturation on the gain coefficient is taken into account in the 'angles of vision' approximation.

In the stationary approximation in the absence of ASE refraction, we have the obvious geometric relation $\Delta\Omega(z) = S/z^2$ for small angles of vision $\Delta\Omega \ll 1$, where S is the cross-section area and z is the distance to the end of the X-ray laser medium. In the presence of refraction, the effective angles of vision depend on the refractive length of ASE and the refractive index profile. For some refractive index profiles, the angles of vision can be determined analytically. The approach considered above also permits a phenomenological consideration of the diffraction restrictions imposed on the magnitude of the angular spectrum of laser radiation, if the magnitude of the angle of vision is restricted by the characteristic angle of diffraction of radiation from the aperture of the laser medium.

Comparison of the results of the numerical solution to the complete transport equation of ASE in the two-level system in the case of cylindrical geometry of the laser medium with the solution obtained in the 'angles of vision' approximation showed that the error of measurements of absolute values of the ASE angular spectrum based on the 'angles of vision' approximation does not exceed 30% over a broad range of gain lengths, diameters, and ratios of the refractive ASE length to the X-ray laser length. The 'angles of vision' approximation is also useful for studying lasing media with numerous laser transitions.

2.2 The parabolic equation for the field amplitude

The geometrical optics approximation can be used provided the qualitative criterion $kl_\perp^2 \gg z$ is satisfied (see, for example, Ref. [40]). This criterion means that the diffraction length on the lateral dimension of the optical inhomogeneity $l_\perp$ should be substantially greater than the X-ray laser length. A plasma contains comparatively small-scale optical inhomogeneities caused by various instabilities (see reviews [63, 64] and references cited therein and also more recent experimental papers [65–69]). In the case of the laser plasma, the inhomogeneities can result from nonuniform irradiation of a solid target, the filamentation of the pump beam in the plasma produced, stimulated scattering of the pumping radiation, turbulence, etc. They cause random variations in the dielectric constant and gain coefficient. For $l_\perp \sim 10$ μm and $\lambda = 0.2-100$ nm, we have $kl_\perp^2 \sim 0.6-300$ cm, which can be of the order of the characteristic length of the X-ray laser $\sim 1-100$ cm or even lower. For this reason, it is unlikely that methods of conventional geometric optics can take into account the effect of microscopic inhomogeneities on the partially coherent ASE. Note that the wave effects should also be considered in the description of the highly-coherent mode when the transverse coherence length is comparable with the beam width.

2.2.1 The wave equation. The dynamics of the radiation field in the presence of emitting ions and refraction of radiation in an isotropic polarizable electrically-neutral plasma is described by Maxwell's equations (see, for example, Ref. [70])

$$\begin{aligned} &\operatorname{div}\mathbf{B} = 0\,, \\ &\operatorname{div}\mathbf{D} = 0\,, \\ &\operatorname{rot}\mathbf{H} = \frac{4\pi}{c}\,\sigma\mathbf{E} + \frac{1}{c}\frac{\partial\mathbf{D}}{\partial t}\,, \\ &\operatorname{rot}\mathbf{E} = -\frac{1}{c}\frac{\partial\mathbf{B}}{\partial t}\,. \end{aligned} \tag{15}$$

Here, **B** and **D** are the magnetic and electric induction, respectively; **H** and **E** are the strengths of the electric and magnetic fields, respectively, where σ is the electric conductivity of a medium which takes into account the losses caused by all transitions except for the laser transition. The additional constitutive equations are taken in the form

$$\mathbf{B} = \mu\mathbf{H}\,, \qquad \mathbf{D} = \varepsilon\mathbf{E} + \mathbf{P}'\,, \tag{16}$$

where μ is the permeability of the medium, and ε is the permittivity of the medium characterizing its dielectric properties caused by all transitions except for the transition under study. Polarization related to the transition under study is separated and denoted as $\mathbf{P}'$.

Let us substitute the first equation from (16) into the last equation in (15), taking into account that $\mu = 1$ for a nonmagnetic plasma, and take the rot of the equation obtained. Then, taking into account the third equation in (15), we obtain

$$\operatorname{rot}\operatorname{rot}\mathbf{E} = -\frac{4\pi}{c^2}\frac{\partial}{\partial t}\,\sigma\mathbf{E} - \frac{1}{c^2}\frac{\partial^2\mathbf{D}}{\partial t^2}\,.$$

By substituting the second equation from (16) into this expression and assuming that σ and ε change in time much more slowly than **E**, we arrive at

$$\operatorname{rot}\operatorname{rot}\mathbf{E} = -\frac{4\pi\sigma}{c^2}\frac{\partial\mathbf{E}}{\partial t} - \frac{\varepsilon}{c^2}\frac{\partial^2\mathbf{E}}{\partial t^2} - \frac{1}{c^2}\frac{\partial^2\mathbf{P}'}{\partial t^2}\,. \tag{17}$$

The refractive index of the medium relating to all transitions except for the transition under study is $\eta = (\varepsilon\mu)^{1/2} = \varepsilon^{1/2}$. Let us introduce the absorption coefficient $\beta = 4\pi\sigma/c\eta$, so that in the absence of polarization the density of the flux of the plane wave propagating along the z-axis decreases as $\exp(-\beta z)$. Let us take into account the notation introduced and use the identity $\operatorname{rot}\operatorname{rot}\mathbf{E} = \operatorname{grad}\operatorname{div}\mathbf{E} - \nabla^2\mathbf{E}$. In an isotropic medium, $\operatorname{div}\mathbf{E} = 0$; therefore we obtain from Eqn (17)

$$\nabla^2\mathbf{E} - \frac{\eta^2}{c^2}\frac{\partial^2\mathbf{E}}{\partial t^2} - \beta\frac{\eta}{c}\frac{\partial\mathbf{E}}{\partial t} = \frac{1}{c^2}\frac{\partial^2\mathbf{P}'}{\partial t^2}\,. \tag{18}$$

In the approximation of the isotropic two-level medium, polarization $\mathbf{P}'$ and the population inversion $W = N_u - g_u N_l/g_l$ are described by the equations [71, 72]

$$\begin{aligned} \frac{\partial^2\mathbf{P}'}{\partial t^2} + \frac{2}{\tau_2}\frac{\partial\mathbf{P}'}{\partial t} + \omega_0^2\mathbf{P}' &= -\frac{2\omega_0}{\hbar}\frac{\eta^2+2}{3}\frac{|\mathbf{d}|^2}{3}\,W\mathbf{E} \\ &\cong -\frac{2\omega_0}{3\hbar}|\mathbf{d}|^2 W\mathbf{E}\,, \end{aligned} \tag{19}$$

$$\frac{\partial W}{\partial t}+\frac{W-W_0}{\tau_1}=\frac{2}{\hbar\omega_0}\,\mathbf{E}\frac{\partial \mathbf{P}'}{\partial t}\,, \tag{20}$$

where τ_1 and τ_2 are the longitudinal and transverse relaxation times, respectively; ω_0 is the frequency of the $l-u$ laser transition; $\mathbf{d}$ is the matrix element of the dipole moment operator for the $l-u$ transition, and W_0 is the population inversion in the absence of radiation. In Eqn (19), the condition $\eta^2 \cong 1$ is also used.

The system of equations (18)–(20) cannot be solved analytically in the general case. A numerical solution requires the specification of a spatial grid with a step smaller than λ, which is unacceptably small for the X-ray spectral range. An analogous problem appears for a step in time.

2.2.2 The quasi-optical approximation. The system of equations (18)–(20) can be simplified by passing to the quasi-optical approximation or the method of slowly varying amplitudes, when the laser radiation is treated as a 'quasi-plane and quasi-monochromatic wave'. The quasi-optical approximation to the wave equation, originally suggested in Ref. [73], has been widely used in the theory of optical lasers. Let us assume that the polarization of radiation does not change substantially on propagation, so that the scalar wave equation can be used instead of the vector equation (18). Let us further assume that the amplitude of such an 'almost plane wave' slowly changes along the propagation direction z and the laser beam size in the transverse plane (x, y) is much smaller than the characteristic sizes along the z-axis. Then, a solution of equation (18) can be sought in the form

$$\mathbf{E}(\mathbf{R},t)=\mathbf{i}_E\,\mathrm{Re}\,A(\mathbf{r},z,t)\exp(-\mathrm{i}kz+\mathrm{i}\omega t)\,. \tag{21}$$

Here, the complex function $A(\mathbf{r},z,t)$ is slowly varying (as compared to the exponential factor) complex amplitude of the laser radiation field describing the difference between the field and the plane wave; $\mathbf{r}=\mathbf{i}x+\mathbf{j}y$ is the transverse radius vector; ω is the characteristic frequency of a comparatively narrow emission line; $k=\eta_0\,\omega/c$ is the characteristic wave number in the inhomogeneous medium, and η_0 is the mean value of the refractive index. Thus, we assume that the wave number k varies in the medium considerably more weakly than the field amplitude A. Let us also suppose that the polarization $\mathbf{P}'$ related to the transition under study varies as the electric field $\mathbf{E}$, i.e.

$$\mathbf{P}'(\mathbf{R},t)=\mathbf{i}_P\,\mathrm{Re}\,P(\mathbf{r},z,t)\exp(-\mathrm{i}kz+\mathrm{i}\omega t)\,, \tag{22}$$

where P is a complex function of coordinates and time slowly varying compared to the exponential factor. By substituting (21) and (22) into (18) and (19), respectively, we obtain

$$\left[\nabla_\perp^2+\frac{\partial^2}{\partial z^2}-2\mathrm{i}k\frac{\partial}{\partial z}-k^2-\frac{\eta^2}{c^2}\left(\frac{\partial^2}{\partial t^2}+2\mathrm{i}\omega\frac{\partial}{\partial t}-\omega^2\right)\right.$$
$$\left.-\beta\frac{\eta}{c}\left(\frac{\partial}{\partial t}+\mathrm{i}\omega\right)\right]A=\frac{1}{c^2}\left(\frac{\partial^2}{\partial t^2}+2\mathrm{i}\omega\frac{\partial}{\partial t}-\omega^2\right)P\,, \tag{23}$$

$$\left[\frac{\partial^2}{\partial t^2}+2\mathrm{i}\omega\frac{\partial}{\partial t}-\omega^2+\frac{2}{\tau_2}\left(\frac{\partial}{\partial t}+\mathrm{i}\omega\right)+\omega_0^2\right]P$$
$$-\frac{2\omega_0}{3\hbar}|\mathbf{d}|^2WA\,, \tag{24}$$

where $\nabla_\perp^2$ is the Laplacian over transverse coordinates. It is assumed that the emission frequency ω_0 is close to the transition frequency ω_0, so that $\omega_0^2-\omega^2\approx 2\omega(\omega_0-\omega)$ in Eqn (24). In accordance with the physical assumptions made above, we also suggest that the following inequalities are satisfied:

$$\left|\frac{\partial^2 A}{\partial z^2}\right|\ll 2k\left|\frac{\partial A}{\partial z}\right|;\quad \left|\frac{\partial^2 A}{\partial z^2}\right|\ll k^2|A|;\quad \left|\frac{\partial^2 A}{\partial t^2}\right|\ll 2\omega\left|\frac{\partial A}{\partial t}\right|;$$
$$\left|\frac{\partial^2 A}{\partial t^2}\right|\ll \omega^2|A|;\quad \left|\frac{\partial A}{\partial t}\right|\ll \omega|A|;$$

$$\left|\frac{\partial^2 P}{\partial t^2}\right|\ll 2\omega\left|\frac{\partial P}{\partial t}\right|;\quad \left|\frac{\partial^2 P}{\partial t^2}\right|\ll \omega^2|P|;\quad \left|\frac{\partial P}{\partial t}\right|\ll \omega|P|\,.$$

Taking into account these inequalities, we obtain from (23)

$$\left[\frac{\partial}{\partial z}+\frac{\eta^2}{c\eta_0}\frac{\partial}{\partial t}+\frac{\mathrm{i}}{2k}\nabla_\perp^2+\frac{\mathrm{i}k}{2}\left(\frac{\eta^2}{\eta_0^2}-1\right)+\frac{\beta}{2}\frac{\eta}{\eta_0}\right]A=\frac{k}{2\mathrm{i}\eta_0}P\,.$$

Because $\varepsilon \cong 1$, the latter equation can be simplified, taking into account the inhomogeneity of ε only in the term responsible for refraction. Then, we obtain from here and (24) and (20):

$$\left[\frac{\partial}{\partial z}+\frac{1}{c}\frac{\partial}{\partial t}+\frac{\mathrm{i}}{2k}\nabla_\perp^2+\frac{\mathrm{i}k}{2}(\varepsilon-1)+\frac{\beta}{2}\right]A=\frac{k}{2\mathrm{i}}\,P\,, \tag{25}$$

$$\mathrm{i}\frac{\partial P}{\partial t}+\mathrm{i}\frac{P}{\tau_2}+\Delta\omega P=-\frac{1}{3\hbar}|\mathbf{d}|^2WA\,, \tag{26}$$

$$\frac{\partial W}{\partial t}+\frac{W-W_0}{\tau_1}=\frac{\mathrm{i}}{2\hbar}(A^*P-AP^*)\,, \tag{27}$$

respectively, where $\Delta\omega=\omega_0-\omega$. Expression (27) was obtained from (20) using the fact that a change in the population inversion W on the wavelength scale for a time of the order of the period of radiation vibrations is negligibly small.

The parabolic equation (25) represents the quasi-optical approximation to the classical wave equation (18) in the isotropic inhomogeneous absorbing (amplifying) medium. Together with equations (26) and (27), it forms a closed system of equations describing the interaction of the laser radiation with a two-level quantum medium.

The system of equations (25)–(27) describes the amplification of radiation incident on the medium from the outside. In our case, we should consider a spontaneous source in the medium. It was shown in [74] that the quantum-mechanical description of ASE is determined by a system of equations for the field and polarization operators, which is formally identical to the semiclassical system of equations (25)–(27) with the additional fluctuation Langevin force R in the equation for polarization (26):

$$\mathrm{i}\frac{\partial P}{\partial t}+\mathrm{i}\frac{P}{\tau_2}+\Delta\omega P=-\frac{1}{3\hbar}|\mathbf{d}|^2WA+R\,, \tag{28}$$

which is delta-correlated in time and space:

$$\big\langle R(\mathbf{r}_1,z_1,t_1)\,R(\mathbf{r}_2,z_2,t_2)\big\rangle=8\pi^2|\mathbf{d}|^2\varGamma N_u\delta^{(2)}(\mathbf{r}_1-\mathbf{r}_2)$$
$$\times\,\delta(z_1-z_2)\delta(t_1-t_2)\,, \tag{29}$$

where $\varGamma$ is the full linewidth.

Let the population inversion be independent of the radiation intensity, i.e. a linear amplification mode is being considered. Then, we omit equation (27) and in (25) and (28) pass to the new variable $\tau = t - z/c$ to obtain $\partial/\partial z + (1/c)\partial/\partial t = \partial/\partial z$ and $\partial/\partial t = \partial/\partial\tau$. Let us change equations (25) and (28) using the Laplace transform over the variable τ:

$$f^{\mathrm{L}}(\mathbf{r}, z, s) = L\big[f(\mathbf{r}, z, \tau)\big] = \int_0^\infty \exp(-s\tau) f(\mathbf{r}, z, \tau)\, \mathrm{d}\tau\,.$$

Let us next multiply (25) and (28) by $\exp(-s\tau)$ and integrate over τ from zero to infinity. Then, using properties of the Laplace transform $L\big[\mathrm{d}f(\tau)/\mathrm{d}\tau\big] = sf^{\mathrm{L}}(s) - f(0)$, the system of equations (25) and (28) is reduced to one parabolic equation for the Laplace transform of the field amplitude [75]:

$$\left[\frac{\partial}{\partial z} + \frac{\mathrm{i}}{2k}\nabla_\perp^2 + \frac{\mathrm{i}k}{2}(\varepsilon - 1) + \frac{\beta}{2} - \frac{\mathrm{i}k}{6\hbar}\frac{|\mathbf{d}|^2 W}{\mathrm{i}(s + \tau_2^{-1}) + \Delta\omega}\right]$$

$$\times A^{\mathrm{L}}(\mathbf{r}, z, s) = \frac{\mathrm{i}k}{2}\frac{R^{\mathrm{L}}(\mathbf{r}, z, s) + \mathrm{i}P(\mathbf{r}, z, \tau = 0)}{\mathrm{i}(s + \tau_2^{-1}) + \Delta\omega}\,. \quad (30)$$

The initial polarization in (30) is also assumed to be delta-correlated in space:

$$\big\langle P(\mathbf{r}_1, z_1, t = 0) P^*(\mathbf{r}_2, z_2, t = 0)\big\rangle$$

$$= 8\pi^2 |\mathbf{d}|^2 N_u \delta^{(2)}(\mathbf{r}_1 - \mathbf{r}_2)\delta(z_1 - z_2)\,. \quad (31)$$

2.2.3 The quasi-steady-state case. In the case of amplification saturation, i.e. when W depends on A, the problem becomes more complicated. The solution of practically important problems requires additional simplifications. Below, we consider two limiting cases.

In the first case, when the coherence time τ_c of the amplified radiation substantially exceeds τ_1 and τ_2, the medium has time to 'follow' pulsations of the field amplitude. This can be observed in a noticeable narrowing of the spectral line taking place at the stage of linear amplification. It was found [75] that the duration of the transient process related to the finite time τ_2 is equal to $\alpha_0 z\tau_2$ (where α_0 is the weak-signal gain, see below), which is substantially shorter than the characteristic generation time in the quasi-steady-state mode. By neglecting the time derivative in (26), i.e. transient phenomena, we obtain

$$P = -\frac{|\mathbf{d}|^2 WA}{3\hbar(\Delta\omega + \mathrm{i}/\tau_2)} = \chi A\,, \quad (32)$$

i.e. the complex polarization amplitude P is proportional to the complex field amplitude A with a proportional constant equal to the complex susceptibility χ. By separating it into real χ' and imaginary χ'' parts, we rewrite Eqn (25) in the form

$$\left[\frac{\partial}{\partial z} + \frac{1}{c}\frac{\partial}{\partial t} + \frac{\mathrm{i}}{2k}\nabla_\perp^2 + \frac{\mathrm{i}k}{2}(\varepsilon - 1) + \frac{\beta}{2}\right] A = \frac{k}{2\mathrm{i}}(\chi' + \mathrm{i}\chi'')A\,. \quad (33)$$

The term containing χ' in the right-hand part of (33) represents the contribution of the resonance transition to the refractive index. As was noted above, the effect of anomalous dispersion can be neglected in the case of X-ray lasers. The term of equation (33) containing

$$\chi'' = \frac{|\mathbf{d}|^2 W}{3\hbar\tau_2(\Delta\omega^2 + 1/\tau_2^2)} \quad (34)$$

describes the saturating absorption or amplification (depending on the sign of W) of laser radiation at the $u-l$ transition. By substituting (32) into (27), we obtain

$$\frac{\partial W}{\partial t} + \frac{W - W_0}{\tau_1} = -\frac{1}{\hbar}\chi''|A|^2\,. \quad (35)$$

After substitution (34) into (35), we find the stationary value of W:

$$W = W_0\left(1 + \frac{J}{J_{\mathrm{sat}}}\frac{1/\tau_2^2}{\Delta\omega^2 + 1/\tau_2^2}\right)^{-1}, \quad (36)$$

where

$$J = \frac{c\langle|\mathbf{E}|^2\rangle}{4\pi} = \frac{c|A|^2}{8\pi}\,, \quad J_{\mathrm{sat}} = \frac{3\hbar^2}{8\pi\tau_1\tau_2|\mathbf{d}|^2}$$

are the densities of the radiation and saturation fluxes, respectively. Therefore, in the quasi-steady-state case the system of equations (25)–(27) is reduced to a parabolic equation for the field

$$\left[\frac{\partial}{\partial z} + \frac{1}{c}\frac{\partial}{\partial t} + \frac{\mathrm{i}}{2k}\nabla_\perp^2 + \frac{\mathrm{i}k}{2}(\varepsilon - 1) + \frac{\beta}{2} - \frac{\alpha_0/2}{1 + J/J_{\mathrm{sat}} + \tau_2^2\Delta\omega^2}\right] A = 0\,,$$

where

$$\alpha_0 = k\tau_2|\mathbf{d}|^2\frac{W_0}{3\hbar}$$

is the gain coefficient of a weak signal. In so doing the effect of the amplifying medium is taken into account in the form of terms of the equation with linear or nonlinear spatially-nonuniform coefficients. Unfortunately, in the presence of a spontaneous source and the gain saturation, the system of equations (25), (27), and (28) cannot be rigorously reduced to the parabolic equation. A spontaneous delta-correlated source S is added to the right-hand side of the parabolic equation as a phenomenological term. Further, we will also assume that the carrier frequency ω in Eqns (21) and (22), corresponding to the laser line centre, coincides with the transition frequency, i.e. $\omega_0 = \omega$. Then, the parabolic equation takes the final form

$$\left\{\frac{\partial}{\partial z} + \frac{1}{c}\frac{\partial}{\partial t} + \frac{\mathrm{i}}{2k}\nabla_\perp^2 + \frac{\mathrm{i}k}{2}\big[\varepsilon(\mathbf{r}, z) - 1\big] + \frac{\beta(\mathbf{r}, z)}{2} - \frac{\alpha_0(\mathbf{r}, z)/2}{1 + J(\mathbf{r}, z)/J_{\mathrm{sat}}}\right\} \times A(\mathbf{r}, z) = S(\mathbf{r}, z)\,, \quad (37)$$

where

$$\alpha_0 = \frac{c^2}{4\omega^2} A_{ul} W_0(\mathbf{r}, z)\tau_2\,, \quad (38)$$

$$J_{\mathrm{sat}} = \frac{\hbar\omega^3}{2\pi c^2 A_{ul}\tau_1\tau_2}\,. \quad (39)$$

In expressions (38) and (39), we used a relation for the Einstein coefficient $A_{ul} = 4\omega^3|\mathbf{d}|^2/(3\hbar c^3)$ accepted in atomic physics. Relations (38) and (39) are qualitatively similar to relations (9) and (11) obtained by the transport equation method. The field amplitude A in (37) can be renormalized in such a way that $J = |A|^2$. Then, the source in the right-hand side of Eqn (37) satisfies the relation

$$\left\langle S(\mathbf{r}_1, z_1) S^*(\mathbf{r}_2, z_2) \right\rangle = \lambda^2 Q(\mathbf{r}_1) \delta^{(2)}(\mathbf{r}_1 - \mathbf{r}_2) \delta(z_1 - z_2)\,, \tag{40}$$

where Q is the average power of the spontaneous noise.

The term in equation (37), responsible for the nonlinear amplification, is close in form to the analogous term in the transport equation (8). Note, however, that the value of J in the denominator of the nonlinear term in (37) represents the instant value of the flux density rather than its mean value. The influence of the finite width of the spectral line on saturation in the transport equation (8) is taken into account by integrating over frequency in (10), whereas in (37) the finite linewidth is taken into account in the dependence of A on time. The characteristic time scale of variations in A (the reciprocal linewidth) is determined by the coherence time τ_c of ASE.

In the second case, when τ_c is shorter than τ_1 and τ_2, the medium 'has no time' to follow the field fluctuations. In this case, the stationary approximation in (26) and (27) is only valid for $\tau_c \ll \tau_1,\ \tau_2$, and J in (37) becomes a quantity averaged over a time much longer than τ_c (but much shorter than the characteristic time of variations of the mean values). The nonlinear gain coefficients in (37) and (8) have the same mean statistical sense. The dependence of the gain coefficient on the moment of the field in the stochastic equation (37) written for instantaneous field intensities makes the solution of this equation difficult. The closed equation for this moment can be obtained from (37) by statistical averaging (see below Section 2.3).

Note that in the case of saturation, in general the degeneracy of the laser levels should be taken into account, because the degenerate levels related to the same energy level interact differently with radiation. However, as was shown in Ref. [76], one can neglect the degeneracy and consider a single energy level if the rate of elastic collisions between ions and electrons is high. Fortunately, this is observed in many practical situations. Collisions produce mixing of populations of the degenerate states proportionally to their statistical weights even at high radiation intensities.

2.2.4 Methods for solving the parabolic equation. Equation (30) was solved in [75] by the method of Green functions satisfying equation (30) in which the right-hand side is replaced by the delta-function. The solution for the Laplace component of the field amplitude A^{L} is formally written as the multidimensional integral of the Green function G^{L}:

$$A^{\mathrm{L}}(\mathbf{r}, z, s) = \int \mathrm{d}\mathbf{r}_0 G(\mathbf{r}, \mathbf{r}_0, z, 0; s) A^{\mathrm{L}}(\mathbf{r}_0, 0, s)$$
$$+ \frac{\mathrm{i}k}{2} \int \mathrm{d}\mathbf{r}_0 \int_0^z \mathrm{d}z_0 G(\mathbf{r}, \mathbf{r}_0, z, z_0; s)$$
$$\times \frac{R^{\mathrm{L}}(\mathbf{r}_0, z_0, s) + \mathrm{i}P(\mathbf{r}_0, z_0, \tau = 0)}{\mathrm{i}(s + \tau_2^{-1}) + \Delta\omega}$$

with the subsequent inverse Laplace transform. From a practical point of view, this is quite unsuitable. In Ref. [75], the simplified solution of the problem was given for large Fresnel numbers $N_{\mathrm{F}} = ka^2/z \gg 1$ (a is the half-width of the gain region) in the geometrical optics approximation for the Green function and for parabolic transverse profiles of W and ε. In Ref. [77], the Wentzel–Kramers–Brillouin method used in [75] was generalized to two-dimensional media with profiles of W and ε close to parabolic.

In Ref. [78], the case of small Fresnel numbers N_{F} was considered using the mode expansion of the Laplace component of the field amplitude in the Gaussian–Laguerre functions:

$$A^{\mathrm{L}}(\mathbf{r}, z, s) = \sum_{m,n} c^{\mathrm{L}}_{mn}(z, s) U^n_m(\mathbf{r}, z)\,. \tag{41}$$

The Gaussian–Laguerre functions are solutions of the parabolic equation in free space

$$\left(\frac{\partial}{\partial z} + \frac{\mathrm{i}}{2k}\nabla^2_{\perp}\right) U^n_m(\mathbf{r}, z) = 0$$

and form a complete orthonormalized basis set. The substitution of (41) into (30) yields a system of coupled stochastic ordinary differential equations for the expansion coefficients c^{L}_{mn} from (41). The solution in the general case involves difficulties. This system was simplified in [78] for a particular case of special profiles of W and ε.

In papers [79–81], an equation of type (37)

$$\left\{\frac{\partial}{\partial z} + \frac{\mathrm{i}}{2k}\frac{\partial^2}{\partial x^2} + \frac{\mathrm{i}k}{2}\left[\varepsilon(x) - 1\right] - \frac{\alpha_0(x)}{2}\right\} A(x, z) = S(x, z) \tag{42}$$

was solved in the stationary two-dimensional case (with one transverse coordinate) in the absence of gain saturation ($J_{\mathrm{sat}} = \infty$) using the expansion of the field amplitude over the uncoupled modes

$$A(x, z) = \sum_n c_n(z) U_n(x)\,. \tag{43}$$

The substitution of (43) into (42) leads to the eigenvalue problem for eigenfunctions U_n with eigenvalues E_n:

$$\left\{\frac{\mathrm{i}}{2k}\frac{\mathrm{d}^2}{\mathrm{d}x^2} + \frac{\mathrm{i}k}{2}\left[\varepsilon(x) - 1\right] - \frac{\alpha_0(x)}{2}\right\} U_n(x) = -E_n U_n(x)\,. \tag{44}$$

Equation (44) is identical in form to the stationary Schrödinger equation with a complex potential; therefore, its eigenfunctions U_n are nonorthogonal in the ordinary sense, i.e. $\int U_n(x) U^*_m(x)\,\mathrm{d}x \neq \delta_{nm}$, but they satisfy the condition $\int U_n(x) U_m(x)\,\mathrm{d}x = \delta_{nm}$. Hence,

$$\frac{\partial c_n(z)}{\partial z} - E_n c_n(z) = \int S(x, z) U_n(x)\,\mathrm{d}x\,. \tag{45}$$

This approach is more useful as compared to that in Ref. [78], however, the incompleteness and nonorthogonality of the transverse basis set results in the nonphysical effect of so-called excess spontaneous noise. In Ref. [80], the method of reducing excess spontaneous noise due to the extension of the transverse basis set by introducing the functions of the continuous spectrum was considered. The mode analysis in the case of linear amplification allows one to simplify the initial problem and obtain practical results for some model profiles of α_0 and ε, when the transverse modes U_n are determined analytically. For the saturation regime, the mode approach has not been realized.

The direct solution of the parabolic equation (37), which can only be numerical in the general case in the presence of a spontaneous source, is more often applied in practice. In the case of strong amplification, the distributed source S can be replaced in Eqn (37) by a random source located in the input section of the gain medium. If the 'travelling wave' amplification mode is considered, it is sufficient to solve one equation (37) [82, 83]. But when, in the gain saturation mode, the counter-propagating ASE fluxes affect each other, equation (37) should be supplemented by the equation for the field of the counter beam, similar to Eqn (14) [84, 85].

The step of the transverse grid used for solving the parabolic equation is equal to $\Delta x \sim \lambda/\theta_s$, where θ_s is the angle of divergence of the source radiation. The value of θ_s should be sufficiently large because of the strong divergence of the spontaneous noise, while the value of λ in the X-ray range is small. For this reason, the number of points used in calculations is usually large and the step of integration over z, $\Delta z \sim k\Delta x^2$, is small. Because of this, modern computational facilities permit the consideration of two-dimensional media only. In addition, a single solution of the parabolic equation with a random source gives the result of a single statistical test (a realization of the random process). To obtain mean characteristics, which are of practical interest, the obtained solutions of the parabolic equation should be averaged over an ensemble of realizations [83] or in time [84, 85]. It is known that the convergence of this procedure is quite slow, and time-consuming computer calculations are usually required. Note that the additional consideration of the randomness of the medium parameters, which has not been taken into account in the literature on X-ray lasers in the framework of the parabolic equation approach, presents further difficulties.

2.3 The equation for the transverse correlation function of the field

In order to avoid the problem of averaging over an ensemble of realizations, one should obtain the equation for the required mean quantity from the stochastic parabolic equation (37). For this purpose, it is convenient to choose the transverse correlation function (TCF) of the radiation field $B = \langle A(\mathbf{r}_1, z) A^*(\mathbf{r}_2, z)\rangle$, where A is the slowly varying field amplitude from (21), and the angle brackets mean statistical averaging. The proceeding processes are assumed ergodic, and averaging over an ensemble is equivalent to time averaging over an interval much longer than the coherence time τ_c. The TCF determines the spatial correlation of the radiation field at the points $\mathbf{r}_1$ and $\mathbf{r}_2$ in the transverse plane $z = \mathrm{const}$. This function is a particular case of the mutual intensity function [43] and contains information on the average flux density, the angular distribution of the radiation intensity, and its transverse spatial coherence. The TCF and the intensity from Eqn (1) are related by the expression [40, 41]

$$B(\mathbf{r}, \mathbf{r}'; z) = \int I(\mathbf{n}, \mathbf{r}, z) \exp(\mathrm{i}k\mathbf{n}_\perp \mathbf{r}')\,\mathrm{d}\Omega_{\mathbf{n}}\,, \tag{46}$$

where $\mathbf{r}' = \mathbf{r}_1 - \mathbf{r}_2$, $\mathbf{r} = (\mathbf{r}_1 + \mathbf{r}_2)/2$, and $\mathbf{n}_\perp$ is the projection of the unit vector $\mathbf{n}$ defining the beam direction onto the transverse plane. Because we do not consider effects related to the finite linewidth, the correlation dependence of the TCF on time and the frequency dependence of the intensity are omitted in (46).

2.3.1 Derivation of the equation for the TCF. According to Refs [86–88], we will derive the equation for the TCF from the parabolic equation (37) in the stationary approximation, which is most typical, for example, for travelling-wave pumping. For this purpose, we multiply from the right equation (37) written for $A(\mathbf{r}_1, z)$ by $A^*(\mathbf{r}_2, z)$ and then combine the obtained equation with its complex conjugate equation by interchanging the subscripts 1 and 2 [89]. Then, by passing to new variables $\mathbf{r}' = \mathbf{r}_1 - \mathbf{r}_2$ and $\mathbf{r} = (\mathbf{r}_1 + \mathbf{r}_2)/2$, we obtain the equation for $\gamma(\mathbf{r}, \mathbf{r}'; z) \equiv A(\mathbf{r}_1, z) A^*(\mathbf{r}_2, z)$:

$$\left[\frac{\partial}{\partial z} + \frac{\mathrm{i}}{k}\frac{\partial^2}{\partial\mathbf{r}\partial\mathbf{r}'} + \frac{\mathrm{i}k\mu(\mathbf{r}, \mathbf{r}'; z)}{2}\right]\gamma(\mathbf{r}, \mathbf{r}'; z) = v(\mathbf{r}, \mathbf{r}'; z)\,, \tag{47}$$

where

$$\mu(\mathbf{r}, \mathbf{r}'; z) = \varepsilon(\mathbf{r}_1, z) - \varepsilon(\mathbf{r}_2, z) - \frac{\mathrm{i}}{k}\left[\beta(\mathbf{r}_1, z) + \beta(\mathbf{r}_2, z)\right] + \frac{\mathrm{i}}{k}\frac{\alpha_0(\mathbf{r}_1, z)}{1 + J(\mathbf{r}_1, z)/J_{\mathrm{sat}}(\mathbf{r}_1, z)} + \frac{\mathrm{i}}{k}\frac{\alpha_0(\mathbf{r}_2, z)}{1 + J(\mathbf{r}_2, z)/J_{\mathrm{sat}}(\mathbf{r}_2, z)}\,, \tag{48}$$

$$v(\mathbf{r}, \mathbf{r}'; z) = S(\mathbf{r}_1, z) A^*(\mathbf{r}_2, z) + S^*(\mathbf{r}_2, z) A(\mathbf{r}_1, z)\,. \tag{49}$$

Let us take into account the presence of optical microscopic inhomogeneities in a plasma, by representing ε, α_0, and β as the sum of regular and fluctuation components

$$\varepsilon = \bar\varepsilon + \tilde\varepsilon\,, \quad \alpha_0 = \bar\alpha_0 + \tilde\alpha_0\,, \quad \beta = \bar\beta + \tilde\beta\,;$$

then,

$$\mu = \bar\mu + \tilde\mu\,. \tag{50}$$

Fluctuations of parameters of the medium have zero mean values: $\langle\tilde\varepsilon\rangle = \langle\tilde\alpha_0\rangle = \langle\tilde\beta\rangle = \langle\tilde\mu\rangle = 0$.

According to the recipe [40, page 349], we will rewrite equation (47) in the identical form

$$\frac{\partial}{\partial z}\left\{\exp\left[\frac{\mathrm{i}k}{2}\int_0^z \mu(\mathbf{r}, \mathbf{r}'; z_1)\,\mathrm{d}z_1\right]\gamma(\mathbf{r}, \mathbf{r}'; z)\right\} = \exp\left[\frac{\mathrm{i}k}{2}\int_0^z \mu(\mathbf{r}, \mathbf{r}'; z_1)\,\mathrm{d}z_1\right]\left[-\frac{\mathrm{i}}{k}\frac{\partial\gamma(\mathbf{r}, \mathbf{r}'; z)}{\partial\mathbf{r}\partial\mathbf{r}'} + v(\mathbf{r}, \mathbf{r}'; z)\right].$$

The integration of this equation over z_2 from zero to z yields

$$\gamma(\mathbf{r}, \mathbf{r}'; z) - T(\mathbf{r}, \mathbf{r}'; 0, z)\gamma(\mathbf{r}, \mathbf{r}'; 0) = \int_0^z \mathrm{d}z_2\, T(\mathbf{r}, \mathbf{r}'; z_2, z)\left[-\frac{\mathrm{i}}{k}\frac{\partial^2\gamma(\mathbf{r}, \mathbf{r}'; z_2)}{\partial\mathbf{r}\partial\mathbf{r}'} + v(\mathbf{r}, \mathbf{r}'; z_2)\right], \tag{51}$$

where

$$T(\mathbf{r}, \mathbf{r}'; z_2, z) = \exp\left[\frac{\mathrm{i}k}{2}\int_{z_2}^z \mu(\mathbf{r}, \mathbf{r}'; z_1)\,\mathrm{d}z_1\right]. \tag{52}$$

Because the integrand factors in the right-hand side of equation (51) are statistically independent, it can be averaged:

$$B(\mathbf{r}, \mathbf{r}'; z) - \big\langle T(\mathbf{r}, \mathbf{r}'; 0, z)\big\rangle B(\mathbf{r}, \mathbf{r}'; 0) = \int_0^z \mathrm{d}z_2 \big\langle T(\mathbf{r}, \mathbf{r}'; z_2, z)\big\rangle \times \left[-\frac{\mathrm{i}}{k}\frac{\partial^2 B(\mathbf{r}, \mathbf{r}'; z_2)}{\partial\mathbf{r}\partial\mathbf{r}'} + \big\langle v(\mathbf{r}, \mathbf{r}'; z_2)\big\rangle\right]. \tag{53}$$

Thus, the function $T(\mathbf{r}, \mathbf{r}'; z_2, z)$ should be averaged, which finally reduces to averaging $\mu(\mathbf{r}, \mathbf{r}'; z)$. We will assume that fluctuations in $\tilde{\varepsilon}$, $\tilde{\alpha}_0$, and $\tilde{\beta}$ are described by Gaussian statistics. For the ASE coherence time $\tau_c < \tau_1$, τ_2, the values of $J(\mathbf{r}_1, z)$ and $J(\mathbf{r}_2, z)$ in the denominators of nonlinear terms in (48) can be considered in fact averaged over time or an ensemble (see Section 2.2.3). But for $\tau_c > \tau_1$, τ_2, when the populations of the laser levels have time to relax for the time τ_c, the values of $J(\mathbf{r}_1, z)$ and $J(\mathbf{r}_2, z)$ in (48) represent instantaneous values of the flux density. Then, averaging of the nonlinear terms in (48) responsible for amplification and depending on J presents difficulties. They can be averaged by the method of statistical linearization [89]. In our case, it consists in the replacement of the fluctuating flux densities $J(\mathbf{r}_1, z)$ and $J(\mathbf{r}_2, z)$ in (48) by their mean statistical values $B(\mathbf{r}_1, 0; z)$ and $B(\mathbf{r}_2, 0; z)$, respectively. Thus, for all relations between τ_c and τ_1, τ_2, the nonlinear terms in (48) have the same form and only the values of $\alpha_0(\mathbf{r}_1, z)$ and $\alpha_0(\mathbf{r}_2, z)$ fluctuate in them. Then, the statistics of $\tilde{\mu}$ and the integral of it in (52) is also Gaussian, and the averaging of (52) can be performed analytically [89]. Taking into account Eqn (50), we obtain from (52)

$$\left\langle T(\mathbf{r}, \mathbf{r}'; z_2, z)\right\rangle = \exp\left[-\frac{\mathrm{i}k}{2}\int_{z_2}^{z} \bar{\mu}(\mathbf{r}, \mathbf{r}'; z_1)\,\mathrm{d}z_1 - \frac{k^2}{8}\int_{z_2}^{z}\mathrm{d}z_1\int_{z_2}^{z}\left\langle \tilde{\mu}(\mathbf{r}, \mathbf{r}'; z_1)\tilde{\mu}(\mathbf{r}, \mathbf{r}'; z_1')\right\rangle \mathrm{d}z_1'\right].$$

If the longitudinal length of the ASE spatial coherence noticeably exceeds that of the mutual correlation of fluctuations of the medium parameters $\tilde{m}$ and $\tilde{n}$, the Markovian approximation can be used [40]. The Markovian approximation requires the validity of the necessary conditions

$$kl_\perp \gg 1\,, \qquad kl_\perp^2 \gg l_{||}\,, \tag{54}$$

where $l_\perp$ and $l_{||}$ are the transverse and longitudinal lengths of the mutual correlation of fluctuations of $\tilde{m}$ and $\tilde{n}$. The general criteria for the applicability of the Markovian approximation (54) are usually satisfied for X-ray lasers. Then, cross-correlation functions for $\tilde{m}$ and $\tilde{n}$ can be considered delta-correlated in the longitudinal direction:

$$\left\langle \tilde{m}(\mathbf{r}_1, z)\tilde{n}(\mathbf{r}_2, z')\right\rangle = A_{mn}(\mathbf{r}, \mathbf{r}'; z)\delta(z - z')\,, \tag{55}$$

where each symbol m and n denotes ε, α_0, or β. Note that the presence of correlations between fluctuations of various parameters of the gain medium is substantiated because they depend on the hydrodynamic parameters of the plasma such as its density and electron and ion temperatures. Taking into account (55), we have

$$\left\langle T(\mathbf{r}, \mathbf{r}'; z_2, z)\right\rangle = \exp\left[-\frac{\mathrm{i}k}{2}\int_{z_2}^{z} \bar{\mu}(\mathbf{r}, \mathbf{r}'; z_1)\,\mathrm{d}z_1 - \frac{\pi k^2}{4}\int_{z_2}^{z} H(\mathbf{r}, \mathbf{r}'; z_1)\,\mathrm{d}z_1\right].$$

Let us substitute the latter relation into (53), divide (53) by $\langle T(\mathbf{r}, \mathbf{r}'; 0, z)\rangle$, and differentiate with respect to z. Averaging (49) by the method of averaging of equations with delta-correlated coefficients [89] using condition (40) yields

$$\left\langle v(\mathbf{r}, \mathbf{r}'; z)\right\rangle = \lambda^2 Q(\mathbf{r})\delta^{(2)}(\mathbf{r}')\,.$$

Then, we finally obtain the equation for the TCF:

$$\left\{\frac{\partial}{\partial z} + \frac{\mathrm{i}}{k}\frac{\partial^2}{\partial\mathbf{r}\partial\mathbf{r}'} + \frac{\mathrm{i}k}{2}\left[\bar{\varepsilon}(\mathbf{r}_1; z) - \bar{\varepsilon}(\mathbf{r}_2; z)\right] + \frac{\bar{\beta}(\mathbf{r}_1; z) + \bar{\beta}(\mathbf{r}_2; z)}{2} + \frac{\pi k^2}{4}H(\mathbf{r}, \mathbf{r}'; z) - \frac{\bar{\alpha}(\mathbf{r}_1; z)/2}{1 + B(\mathbf{r}_1, 0; z)/J_{\mathrm{sat}}(\mathbf{r}_1; z)} - \frac{\bar{\alpha}_0(\mathbf{r}_2; z)/2}{1 + B(\mathbf{r}_2, 0; z)/J_{\mathrm{sat}}(\mathbf{r}_2; z)}\right\} B(\mathbf{r}, \mathbf{r}'; z) = \lambda^2 Q(\mathbf{r}; z)\delta(\mathbf{r}')\,, \tag{56}$$

where

$$\begin{aligned} H(\mathbf{r}, \mathbf{r}'; z) = {} & \frac{A_{\varepsilon\varepsilon}(\mathbf{r}_1, 0; z) + A_{\varepsilon\varepsilon}(\mathbf{r}_2, 0; z) - 2A_{\varepsilon\varepsilon}(\mathbf{r}, \mathbf{r}'; z)}{2\pi} \\ & - \frac{A_{\alpha\alpha}(\mathbf{r}_1, 0; z) + A_{\alpha\alpha}(\mathbf{r}_2, 0; z) + 2A_{\alpha\alpha}(\mathbf{r}, \mathbf{r}'; z)}{2\pi k^2\left[1 + B(\mathbf{r}, 0; z)/J_{\mathrm{sat}}(\mathbf{r}_\perp, z)\right]^2} \\ & - \frac{A_{\beta\beta}(\mathbf{r}_1, 0; z) + A_{\beta\beta}(\mathbf{r}_2, 0; z) + 2A_{\beta\beta}(\mathbf{r}, \mathbf{r}'; z)}{2\pi k^2} \\ & + \mathrm{i}\,\frac{A_{\varepsilon\alpha}(\mathbf{r}_1, 0; z) - A_{\varepsilon\alpha}(\mathbf{r}_2, 0; z) + A_{\varepsilon\alpha}(\mathbf{r}, \mathbf{r}'; z) - A_{\varepsilon\alpha}(\mathbf{r}, -\mathbf{r}'; z)}{2\pi k\left[1 + B(\mathbf{r}, 0; z)/J_{\mathrm{sat}}(\mathbf{r}_\perp, z)\right]} \\ & + \frac{A_{\alpha\beta}(\mathbf{r}_1, 0; z) + A_{\alpha\beta}(\mathbf{r}_2, 0; z) + A_{\alpha\beta}(\mathbf{r}, \mathbf{r}'; z) + A_{\alpha\beta}(\mathbf{r}, -\mathbf{r}'; z)}{2\pi k^2\left[1 + B(\mathbf{r}, 0; z)/J_{\mathrm{sat}}(\mathbf{r}_\perp, z)\right]} \\ & - \mathrm{i}\,\frac{A_{\varepsilon\beta}(\mathbf{r}_1, 0; z) - A_{\varepsilon\beta}(\mathbf{r}_2, 0; z) + A_{\varepsilon\beta}(\mathbf{r}, \mathbf{r}'; z) - A_{\varepsilon\beta}(\mathbf{r}, -\mathbf{r}'; z)}{2\pi k}\,. \end{aligned} \tag{57}$$

Relation (57) is satisfied when the mean density of the ASE flux weakly varies on the scale of the transverse correlation length for parameters of the medium.

In the case of quasi-uniform fluctuations of the medium when its mean parameters weakly vary on the scale of $l_\perp$, the transverse part of the cross-correlation function (55) has the form [40]

$$A_{mn}(\mathbf{r}, \mathbf{r}'; z) = 2\pi\int \Phi_{mn}(\mathbf{r}, \rho_\perp, \rho_{||} = 0, z)\exp(\mathrm{i}\rho_\perp\mathbf{r}')\,\mathrm{d}\rho_\perp\,,$$

where

$$\Phi_{mn}(\mathbf{r}, \rho_\perp, \rho_{||}, z) = (2\pi)^{-3}\int\langle\tilde{m}(\mathbf{r}_1, z)\tilde{n}(\mathbf{r}_2, z')\rangle \times \exp\left[-\mathrm{i}\rho_\perp\mathbf{r}' - \mathrm{i}\rho_{||}(z - z')\right]\mathrm{d}\mathbf{r}'\,\mathrm{d}(z - z')$$

is the mutual spatial spectrum of fluctuations of $\tilde{m}$ and $\tilde{n}$. For the Gaussian cross-correlation function

$$\langle\tilde{m}(\mathbf{r}_1, z)\tilde{n}(\mathbf{r}_2, z')\rangle = \sigma^2(\mathbf{r}, z)\exp\left[\frac{-|\mathbf{r}'|^2}{2l_\perp^2} - \frac{(z - z')^2}{2l_{||}^2}\right],$$

where σ^2 is the variance, we obtain

$$A_{mn}(\mathbf{r}, \mathbf{r}'; z) = (2\pi)^{1/2}\sigma^2(\mathbf{r}, z)l_{||}(\mathbf{r}, z)\exp\left[\frac{-|\mathbf{r}'|^2}{2l_\perp^2(\mathbf{r}, z)}\right]. \tag{58}$$

Thus, in the case of linear amplification, equation (56) for the TCF and the parabolic equation (37) have the same accuracy, while in the case of gain saturation the statistic linearization impairs the accuracy of the equation for the TCF at $\tau_c > \tau_1, \tau_2$. The error in the determination of the mean energy parameters of ASE caused by the statistical linearization in deriving the equation for the TCF was discussed in Refs [83, 90] in the absence of fluctuations of the medium parameters. In [83], comparison was made between the results of a single solution of equation (56) and the repeated solution of the 'exact' equation (37) by the method of statistical tests (the Monte-Carlo method) with averaging of the required parameters over an ensemble of realizations of the spontaneous noise. It was shown that the statistical linearization does not distort the profile of the mean angular distribution of ASE but overestimates the absolute values of the mean ASE intensity. This overestimation reaches a maximum of $\sim 30\%$ when the ASE intensity is close to the saturation intensity. In the cases of a weaker and stronger saturation, the error is reduced.

2.3.2 Analysis of the equation for the TCF. In contrast to the parabolic equation (37) with a random source, equation (56) for the TCF has analytic solutions. To obtain them, firstly, we represent the profile of $\bar{\varepsilon}$ inside the gain medium (for $|\mathbf{r}| \leqslant a$) in the form of a power function

$$\bar{\varepsilon}(\mathbf{r}) = \bar{\varepsilon}_m(\mathbf{r}) = 1 - \Delta\varepsilon\left(1 - \frac{|\mathbf{r}|^m}{a^m}\right), \tag{59}$$

where $m > 0$ (for $|\mathbf{r}| > a$, it is assumed that $\alpha_0 = 0$ and $\bar{\varepsilon} = 1$). Consider a particular case of the distribution (59), namely, the defocusing parabolic profile $\bar{\varepsilon} = \bar{\varepsilon}_2$. This profile is widely used in qualitative studies of ASE dynamics in X-ray lasers. Secondly, in the case of significant amplification, when $\exp(\alpha_0 z) \gg 1$, the distributed source in the right-hand side of equation (56) can be replaced by the delta-correlated source located at the X-ray laser end:

$$B(\mathbf{r}, \mathbf{r}'; 0) = I_s(\mathbf{r})\lambda^2\delta^{(2)}(\mathbf{r}'), \tag{60}$$

where I_s is the intensity (brightness) of the source radiation. Then, in the absence of fluctuations of the parameters of the medium and neglecting amplification, the solution of equation (56) for the TCF of ASE emerging from the opposite end of the X-ray laser has the form [86–88]

$$B_0(\mathbf{r}, \mathbf{r}'; z) = \frac{q_s}{\zeta^2} F\left(\frac{kar'}{\zeta}\right) \exp\left[-\mathrm{i}k\mathbf{r}\mathbf{r}' \frac{\cosh(z/z_r)}{\zeta}\right], \tag{61}$$

where $q_s = \int I_s(\mathbf{r})\,\mathrm{d}\mathbf{r} \cong I_s S$ is the strength of the source radiation, S is the source area, $\zeta = z_r \sinh(z/z_r)$, and

$$z_r = \frac{a}{(\Delta\varepsilon)^{1/2}} \tag{62}$$

is the refraction length determining the characteristic distance passed by the beam before its emerging from the active region. In the case of axial symmetry of the medium, we have

$$F(y) = \frac{\int_0^\infty I_s(ax)J_1(xy)x^2\,\mathrm{d}x}{\int_0^\infty I_s(ax)x\,\mathrm{d}x}, \tag{63}$$

where J_1 is the Bessel function. Expression (63) is analogous to the van Cittert–Zernike theorem [43, 89].

For $z < z_r$, when $\sinh(z/z_r) \ll 1$, the effect of refraction is minimal, and expression (61) takes the form

$$B_0(\mathbf{r}, \mathbf{r}'; z) = \frac{q_s}{z^2} F\left(\frac{kar'}{z}\right) \exp\left(-\frac{\mathrm{i}k\mathbf{r}\mathbf{r}'}{z}\right). \tag{64}$$

Relations (61) and (64) are characteristic of an infinite free space. Now we take into account the light amplification under the condition that the mean gain coefficient $\bar{\alpha}_0$ and the mean absorption coefficient $\bar{\beta}$ are uniform in the cross section of the X-ray laser, i.e. they have step-like profiles. The solution of equation (56) for the TCF of ASE emerging from the end of the X-ray laser, by neglecting the wave effects related to the limited cross section of the gain medium, has the form [91]

$$B_r(\mathbf{r}, \mathbf{r}'; z) = f(z)B_0(\mathbf{r}, \mathbf{r}'; z), \tag{65}$$

where f is the gain factor. By substituting (65) into (56), we obtain the equation

$$\left(\frac{\partial}{\partial z} - \frac{\bar{\alpha}_0}{1 + q_s f/J_{\mathrm{sat}}\zeta^2} + \bar{\beta}\right) f(z) = 0, \tag{66}$$

for the gain factor, which coincides in form with the transport equation (14) in the 'angles of vision' approximation. Comparison of (66) with (14) shows that $I = I_s f$ and the angle of vision of the source is $\Delta\Omega = S/\zeta^2$, and in the case of weak refraction, $\Delta\Omega = S/z^2$ [cf. the text after Eqn (13)]. Like the basic equation (56), equation (66) obtained from it is written in the approximation of the unidirectional photon flux for the travelling-wave pumping mode. Otherwise, equations (56) and (66) should be supplemented by equations for the TCF and the gain factor for the field of the counter beam, similar to Eqn (14).

Now we take into account fluctuations of parameters of the medium by assuming that their field is statistically uniform, i.e. $H(\mathbf{r}, \mathbf{r}'; z) \equiv H(\mathbf{r}')$. Then, in the approximation of a transversely unbounded medium, the solution of equation (56) is sought in the form [92]

$$B(\mathbf{r}_\perp, \mathbf{r}'_\perp; z) = B_r(\mathbf{r}_\perp, \mathbf{r}'_\perp; z)\exp\left[-V(\mathbf{r}'_\perp; z)\right], \tag{67}$$

where B_r is defined in Eqn (65).

By substituting (61) into (56), we obtain the equation

$$\left[\frac{\partial}{\partial z} + \frac{\mathbf{r}'\cosh(z/z_r)}{\zeta}\frac{\partial}{\partial \mathbf{r}'}\right] V(\mathbf{r}'; z) = \frac{\pi k^2}{4} H(\mathbf{r}');$$

the equations for the characteristic curves of this equation have the form

$$\frac{\mathrm{d}z}{\mathrm{d}s} = 1, \quad \frac{\mathrm{d}\mathbf{r}'_\perp}{\mathrm{d}s} = \mathbf{r}'_\perp \frac{\cosh(z/z_r)}{\zeta}, \quad \frac{\mathrm{d}V}{\mathrm{d}s} = \frac{\pi k^2}{4} H(\mathbf{r}'_\perp)$$

with conditions $z = 0$, $\mathbf{r}' = \mathbf{r}'_0$, and $V(\mathbf{r}'_0; 0) = 0$ for $s = 0$. From the first two equations for characteristic curves, we obtain $z = s$ and $\mathbf{r}'_\perp = \mathbf{r}'_0 \sinh(s/z_r)$. Taking this into account, we find from the third equation

$$V(\mathbf{r}'; z) = -\frac{\pi k^2}{4}\int_0^1 \mathrm{d}y H(y\mathbf{r}')\left[y^2 + \sinh^{-2}\left(\frac{z}{z_r}\right)\right]^{-1/2}. \tag{68}$$

Analysis of the real part of (57) shows that the contribution of fluctuations of $\tilde{\varepsilon}$, $\tilde{\alpha}_0$, and $\tilde{\beta}$ to (56) results in narrowing of the TCF over $\mathbf{r}'_\perp$, i.e. in the broadening of the angular spectrum and deterioration of coherent properties of ASE. This occurs because the corresponding terms of $H(\mathbf{r}, \mathbf{r}'; z)$ increase with increasing $\mathbf{r}'$. The presence of correlation between $\tilde{\alpha}_0$ and $\tilde{\beta}$, on the contrary, improves coherent properties because the term in (57) with $A_{\alpha\beta}$ decreases with increasing $\mathbf{r}'$. The imaginary terms in (57) responsible for the correlations of $\tilde{\varepsilon}$ with $\tilde{\alpha}_0$ and $\tilde{\beta}$ are in a certain sense analogous to the term in (56) describing the regular refraction from the $\bar{\varepsilon}$ profile. They cause the shift of the angular spectral components of ASE.

By considering (56) and (57) for $\mathbf{r}'_\perp = 0$, we obtain the local gain and nonresonance absorption coefficients

$$\alpha(\mathbf{r};z) = \frac{\bar{\alpha}_0(\mathbf{r},z)}{1+B(\mathbf{r},0;z)/J_{\mathrm{sat}}} + \frac{A_{\alpha\alpha}(\mathbf{r},0;z)}{2\left[1+B(\mathbf{r},0;z)/J_{\mathrm{sat}}\right]^2} + \frac{1}{2}A_{\beta\beta}(\mathbf{r},0;z)\,,$$

$$\beta(\mathbf{r};z) = \bar{\beta}(\mathbf{r};z) + \frac{A_{\alpha\beta}(\mathbf{r},0;z)}{2\left[1+B(\mathbf{r},0;z)/J_{\mathrm{sat}}\right]}\,.$$

Thus, upon scattering of ASE from fluctuations of $\tilde{\alpha}_0$ and $\tilde{\beta}$, additional (compared to the average level) amplification takes place, while the correlation between $\tilde{\alpha}_0$ and $\tilde{\beta}$ leads to additional absorption.

In the numerical integration of the equation for the TCF in the case of great Fresnel numbers, when the transverse coherence length is noticeably smaller than the beam width, the method of the equation for the TCF is substantially more 'economical' than the method of statistical tests of the parabolic equation [83]. This is explained not only by the absence of averaging over an ensemble but also by the smaller number of points on the transverse grid for calculations and a significantly larger integration step in z. As a rule, a medium with one transverse coordinate is considered, however, the results are also available for the axially symmetric medium [87]. For the wave approach, they are the only ones in the literature on X-ray lasers.

3. Basic features of the radiation dynamics of X-ray lasers

One of the important parameters of ASE is the strength of radiation emerging from the X-ray laser in the plane $z = \mathrm{const}$ at the angle $\theta = |\mathbf{n}_\perp|$ to the optical axis. In accordance with the approach chosen for studying ASE dynamics, it is written in the form

$$q(\mathbf{n}_\perp,z) = \int I(\mathbf{n},\mathbf{r},z)\,\mathrm{d}\mathbf{r} = \left\langle \left|\lambda^{-1}\int A(\mathbf{r},z)\exp(\mathrm{i}\mathbf{k}_\perp\mathbf{r})\,\mathrm{d}\mathbf{r}\right|^2\right\rangle = \lambda^{-2}\int\!\!\int B(\mathbf{r},\mathbf{r}';z)\exp(\mathrm{i}\mathbf{k}_\perp\mathbf{r}')\,\mathrm{d}\mathbf{r}\,\mathrm{d}\mathbf{r}'\,, \tag{69}$$

where $\mathbf{k}_\perp = k\mathbf{n}_\perp$ is the projection of the wave vector $\mathbf{k}$ onto the transverse plane. The strength of radiation is measured in W/sr. This determines the angular divergence of the radiation, i.e. the far-field distribution of its flux density, and is one of quantities being experimentally established. Expression (69) is valid for the geometrical optics and wave approximations in conjunction with relation (46) in the case of a statistically quasi-homogeneous field, when the flux density weakly varies on the scale of the transverse length of the spatial coherence L_c [41].

The ASE power is defined as

$$P(z) = \int q(\mathbf{n}_\perp,z)\Omega_{\mathbf{n}} = \int \left\langle |A(\mathbf{r},z)|^2\right\rangle \mathrm{d}\mathbf{r} = \int B(\mathbf{r},0;z)\,\mathrm{d}\mathbf{r}$$

and gives the ASE energy after integration over time.

The coherence length L_c in the vicinity of the point $(\mathbf{r},z)$ is determined from the drop of the coherence coefficient [43, 89]

$$\mu(\mathbf{r},\mathbf{r}';z) = \frac{|B(\mathbf{r},\mathbf{r}';z)|}{\left[B(\mathbf{r}_1,0;z)B(\mathbf{r}_2,0;z)\right]^{1/2}}\,, \tag{70}$$

from 1 (for $\mathbf{r}'=0$) to a certain level when $|\mathbf{r}'|$ varies. If the flux density weakly changes on the scale of the coherence length, i.e. when the quasi-homogeneity condition is met, then the estimate

$$L_c(\mathbf{r},z) \approx \frac{1}{k\Delta\theta_{\mathrm{loc}}} \tag{71}$$

follows from (46), where $\Delta\theta_{\mathrm{loc}}$ is the half-width of the angular distribution of I at the point $(\mathbf{r},z)$. Note that expression (71) represents only an appraisal. It can be reliably used only in the case when the angular distribution of I has one characteristic angular scale $\Delta\theta_{\mathrm{loc}}$. If such a scale is not the only one (for example, the distribution of I consists of a narrow bright corn and weak but extended wings), appraisal (71) will be overestimated. Note also that the quantity $\Delta\theta_{\mathrm{loc}}$ in (71) can be treated as the local divergence of ASE (although it is not measured in experiments). In the scientific literature, the relation $L_c(\mathbf{r},z) \approx 1/(k\Delta\theta)$ is often used, where $\Delta\theta$ is the total divergence of the ASE beam. It should be remembered that the angular divergence is determined by the TCF itself [see Eqn (69)], while the coherence length depends on the TCF modulus [see Eqn (70)]. For this reason, the coherence length is directly connected with the total divergence $\Delta\theta$ of the beam only when $\Delta\theta_{\mathrm{loc}}$ and the angle of maximum I are independent of $\mathbf{r}$ in the most important part of the beam. Note that these conditions are often not satisfied for ASE, so that the relation $L_c(\mathbf{r},z) \approx 1/(k\Delta\theta)$ is invalid in the general case.

3.1 A regular medium without refraction

The divergence and coherence of ASE are most simply determined in X-ray lasers in which the electron density gradient is negligible, resulting in weak refraction of ASE. For operating X-ray lasers [11–19], as a rule, the condition of large Fresnel numbers $N_F = ka^2/z \gg 1$ is satisfied, where $2a$ and z are the transverse size and length of the active region, i.e. diffraction effects from the X-ray laser aperture are small. We neglect here small-scale fluctuations of parameters of the medium, so that $\alpha_0 = \bar{\alpha}_0$ and $\beta = \bar{\beta}$ in this section.

3.1.1 Divergence and power. The divergence $\Delta\theta$ of ASE in X-ray lasers, as in a mirrorless IR laser [33], is substantially characterized by the aspect ratio $\theta_g = 2a/z$. For $a \sim 100$ μm and z of several centimetres, we obtain the value of $\theta_g \sim 1-10$ mrad, which exceeds the diffraction limit by several orders of magnitude. For appreciable values of $\alpha_0 z$ in the absence of saturation, ASE emerging through the end of the gain medium dominates, whereas ASE emerging through the side surface is only weakly amplified. The total divergence of ASE is characterized by the value of θ_g. The angular distribution of the end ASE, in the case of the uniform amplification, is described by a function with a maximum at $\theta = 0$ and monotonically decaying to zero with increasing θ up to $\theta = \theta_g$:

$$q_{\mathrm{end}}(\theta,z) = q_0(z)\left[\arccos\chi - \chi(1-\chi^2)^{1/2}\right]\,, \tag{72}$$

where $\chi = \theta/\theta_g$. In order to take into account the influence of noise in the medium volume, which is substantial for small $\alpha_0 z$, relation (72) should be integrated over z.

It follows from Eqn (8) that the increase in the strength of radiation along the axis, $q_0(z) \equiv q(0; z)$, with increasing z is exponential:

$$q_0(z) = \frac{Q_0}{\alpha_0}\left[\exp(\alpha_0 z) - 1\right], \tag{73}$$

where β can be neglected (or included in α_0). Expression (73) is related to the frequency component of radiation within the spectral line. If the X-ray line is too narrow to be experimentally resolved, the frequency dependences of α_0 and Q_0 should be taken into account [see Eqns (9) and (10)]. The result of integration of equation (73) over the frequency, which is valid for any shape of narrow line, has the form [93]

$$\int q_0(z)\,\mathrm{d}\omega = \frac{Q_0}{\alpha_0}\,\frac{\left[\exp(\alpha_0 z) - 1\right]^{3/2}}{\left[\alpha_0 z \exp(\alpha_0 z)\right]^{1/2}},$$

where the quantities α_0 and Q_0 in the right-hand side are already related to the centre of the spectral line. The observation of such a dependence in experiments represents the most conclusive demonstration of the laser action in a plasma [15].

As the X-ray laser length or α_0 increase and $\alpha_0 z$ reaches a value of 15–20, gain saturation is observed. ASE begins to affect the populations of the laser levels, by decreasing the real gain coefficient. By considering the travelling-wave pumping mode, we assume in the system of equations (14) that $I^+ = I$, $I^- = 0$, and $\Delta\Omega(z) = S/z^2$. Then the system is reduced to one equation for the intensity at the line centre [cf. Eqn (66)]

$$\left[\frac{\partial}{\partial z} - \frac{\alpha_0}{1 + I(z)S/(J_{\mathrm{sat}} z^2)} + \beta\right] I(z) = 0\,. \tag{74}$$

For weak nonresonance losses ($\beta z \ll 1$) and strong gain saturation, the solution of (74) yields the expression

$$q_0(z) = I(z)S \approx \frac{\alpha_0 z^3}{3}\, J_{\mathrm{sat}}\,,$$

which is independent of the noise power and determined by the inversion margin in the medium and the value of the saturation intensity. The fast exponential increase of $q_0(z)$ (73) changes to a slower cubic increase upon gain saturation. Then the powers of the end and side ASE are described by the expressions

$$P_{\mathrm{end}}(z) = q_0(z)\Delta\Omega(z) \approx \frac{\alpha_0 z}{3}\, P_{\mathrm{sat}}\,,$$
$$P_{\mathrm{side}}(z) \approx \alpha_0\left[\frac{2z}{3} - z_{\mathrm{sat}}\right] P_{\mathrm{sat}}\,, \tag{75}$$

where $P_{\mathrm{sat}} = SJ_{\mathrm{sat}}$ and z_{sat} are the saturation power and length, respectively. The power of the end ASE increases linearly over z. From Eqn (75), important conclusion follows that approximately one third of the total ASE power $P(z) \approx \alpha_0 z P_{\mathrm{sat}}$ emerges through the X-ray laser end (see also Refs [94, 95]). Approximately two thirds of the total power leaves the gain medium through its side surface. The angular distribution of the end ASE is still characterized by relations (71). Because the fraction of ASE leaving the X-ray laser through its side surface increases upon gain saturation, the total divergence of ASE exceeds the value of θ_g.

If the travelling-wave pumping mode is not used, then in the case of gain saturation, the interaction between the counter-propagating ASE fluxes should be taken into account. The estimate of the asymptotic solution of system (14) then yields

$$P^{+}_{\mathrm{end}}(z) = P^{-}_{\mathrm{end}}(z) \approx \frac{3\alpha_0 z}{8}\, P_{\mathrm{sat}}\,.$$

In the case of considerable nonresonance losses, when $\beta z > 1$, we have [91]

$$P_{\mathrm{end}}(z) \approx \frac{\alpha_0}{\beta}\, P_{\mathrm{sat}}\,.$$
$$P_{\mathrm{side}}(z) \approx \frac{\alpha_0}{\beta}\left[2\ln(\beta z) - 2 - \beta z_{\mathrm{sat}}\right] P_{\mathrm{sat}}\,. \tag{76}$$

The power of the end ASE tends to a constant value. However, even upon a complete halt to the increase in P_{end}, the total power $P(z)$ can still increase owing to ASE escape through the side surface and the logarithmic increase in P_{side}. The X-ray laser length can be increased to $z \sim ka^2$ for $\beta z \gg 1$ as well until diffraction begins to play a role, because the quantity q_0 continues to grow at constant P_{end} due to decreasing divergence. As z further increases in the diffraction regime, q_0 ceases to increase, while P_{side} will continue to increase slightly because of the diffraction escape of ASE through the side surface.

3.1.2 Coherence. One can see from Eqn (65) that the uniform amplification in the geometrical optics approximation affects the amplitude of the end ASE field rather than its phase. The coherence coefficient of the end ASE, by neglecting the volume noise in the case of a uniform source, is determined from (70) using (63). In the approximation of a uniform source, it follows from (63) that

$$\mu(\mathbf{r}, \mathbf{r}'; z) = 2\left|\frac{J_1(kar'/z)}{(kar'/z)}\right|,$$

where J_1 is the Bessel function. This gives a characteristic coherence length of ASE at the laser output in the form of

$$L_{\mathrm{c}}(z) \approx \frac{z}{ka}\,, \tag{77}$$

i.e. ASE represents the superposition of $\sim N_{\mathrm{F}}^2$ transverse modes. Coherent properties of ASE are the same as in free space [43, 89]. Relation (77) remains valid in the presence of gain saturation and consideration of the volume noise and the influence of the counter beam, as numerical calculations of stochastic parabolic equations (37) have shown [85].

For $\lambda = 0.2$–100 nm, $z \sim 5$ cm, and $a \sim 100$ μm, the value of $L_{\mathrm{c}}(z)$ lies in the range ~ 0.02–8 μm. Because it is difficult to experimentally determine such a small coherence length, the coherence is measured away from the X-ray laser, where the far-field condition is usually satisfied. In the on-axis far-field region ($\theta = 0$), we have according to (64)

$$L_{\mathrm{c}}(Z) \approx \frac{Z}{ka}\,, \tag{78}$$

where Z is the distance from the X-ray output to the plane of measurements. Thus, moving away from the X-ray laser allows one to increase the coherence length by a factor of Z/z, although at the expense of a decrease in the ASE flux density by a factor of $(Z/z)^2$. The power of the coherent ASE, defined as the integral of the flux density over the coherence plane, remains constant as the distance from the X-ray laser increases.

The beam quality is quite sensitive to the profile of α_0. When this profile in the X-ray laser is close to the stepwise profile, the coherence degree of the side far-field ASE is higher than that of the end ASE [96]. As the distance from the beam centre ($\theta = 0$) increases, $L_c(Z)$ increases, reaches a maximum at $\theta = \theta_g$, and then decreases. The ratio of $L_c(Z)$ at $\theta = \theta_g$ and $\theta = 0$ is equal to $\sim \alpha_0 z$ in the case of linear amplification and to 2–3 in the case of strong saturation. Thus, the coherent power of ASE also remains approximately constant over the cross section of the ASE beam for $\theta \leqslant \theta_g$.

In the case of linear amplification, the bell-shaped non-uniformity of the amplification results in an additional spatial selection of ASE and its 'pulling' into the vicinity of the maximum of α_0, which leads to a decrease in the divergence and an increase in the degree of coherence [89]. For example, for the parabolic profile of α_0 at the X-ray laser output [80, 81], one finds

$$L_c(z) \approx \left[\frac{\alpha_0(0)z}{3}\right]^{1/2} \frac{z}{ka},$$

i.e. a normal linear law (77) changes to the dependence $\sim z^{3/2}$. Due to a decrease in the size of the output source, the far-field value of $L_c(Z)$ increases compared to (78), and no on-axis hole is observed in the distribution of $L_c(Z)$ over the beam cross section [96]. The gain saturation makes the gain profile steeper, which results in the deterioration of coherent properties, approaching case (77), (78).

3.2 A regular symmetric medium with refraction

The electron density required for obtaining population inversion at the 3p–3s transitions in Ne-like ion X-ray lasers and at the 4d–4p transitions in Ni-like ion X-ray lasers is quite high: $\sim 10^{20}-10^{22}$ cm^{-3} [15]. In the first experiments at LLNL, a thin foil target was used [5, 6, 10–12] (a schematic of the experiment is shown in Fig. 1). The foil is exploded upon two- or one-sided irradiation with light from a pump laser with a wavelength of 0.53 μm, a pulse length of $\sim$ 0.5 ns, and an intensity of $\sim 10^{13}-10^{14}$ W/cm^2 on the foil. The width of the irradiated line along the y-axis is $\sim$ 100–300 μm. Due to 'burning through' the foil and two-sided expansion of the plasma produced, the profiles of the parameters are approximately symmetrical with respect to the target plane. The gradient of $N_e(x)$ formed in the expanding plasma is usually sufficient for regular refraction of the radiation to be appreciable for an X-ray laser length z of several centimetres.

In Ne-like ion X-ray lasers with targets in the exploding-foil form, the distribution $\bar{\varepsilon} = \bar{\varepsilon}_2$ from (59) approximately describes the real profile $\bar{\varepsilon}$ in the direction x perpendicular to the foil. Figure 3 shows the experimental distribution of the electron density $N_e(x)$ in an Ne-like selenium X-ray laser within 100 ps after the end of the pump pulse [6] and the parabolic approximation of it.

3.2.1 Divergence and power. As was noted above, a plasma column freely expanding into a vacuum with the refractive index increasing to the periphery is the defocusing medium. Consider a flat medium with $\bar{\varepsilon} = \bar{\varepsilon}(x)$, where $\bar{\varepsilon} \to 1$ for $x \to \infty$. We neglect small-scale fluctuations in parameters of the medium, assuming that $\alpha_0 = \bar{\alpha}_0$ and $\beta = \bar{\beta}$. Let us assume that after leaving the medium at $x \to \infty$, the beam propagates at an angle θ_1 to the optical axis. Then, we easily obtain from Eqn (2) [97]

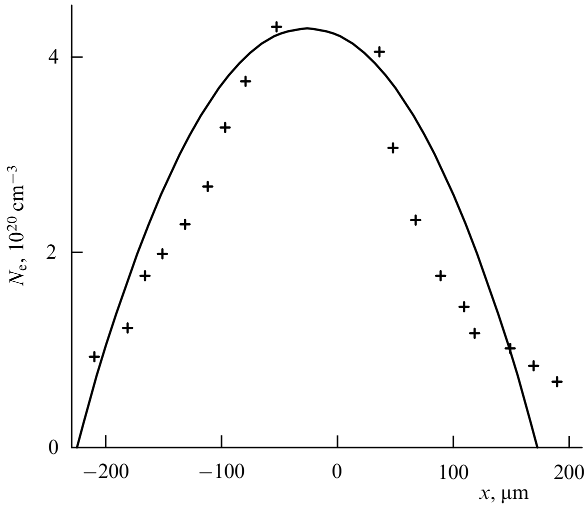

Figure 3. Experimental distribution of the electron density N_e in an Ne-like selenium X-ray laser perpendicular to a foil within 100 ps after the end of the pump pulse (+) [6] and a parabolic approximation of it (—).

$$\frac{dz}{dx} = \left[\frac{\bar{\varepsilon}(x)}{\cos^2\theta_1} - 1\right]^{-1/2}.$$

It follows from this equation that the beam was parallel to the axis at the point x_0, where $\bar{\varepsilon}(x_0) = \cos^2\theta_1$, which gives $\sin^2\theta_1 = 1 - \bar{\varepsilon}(x_0) = \Delta\varepsilon_0$, or for small angles, $\theta_1 = (\Delta\varepsilon)^{1/2}$. Thus, the beam emitted from the point with $\nabla\bar{\varepsilon} \neq 0$ parallel to the optical axis leaves the medium at an angle of $(\Delta\varepsilon_0)^{1/2}$, which is independent of the profile of $\bar{\varepsilon}$ and is only determined by the transverse variation in $\bar{\varepsilon}$.

Defocusing refraction leads to bending of the beam path and its premature escape to the peripheral regions of the space. Because the gain region occupies a plasma region that is comparatively narrow along the transverse coordinate, the refraction displacement of beams to the plasma column periphery causes undesirable reducing in the beam gain length and a decrease in the power and brightness of ASE.

The effect of refraction on the integral parameters of radiation can be qualitatively estimated from analysis of the propagation of the waves by means of the wave equation (18). By substituting $\mathbf{E}(\mathbf{r}, t) = \mathbf{i}_E E(\mathbf{r}) \exp(i\omega t)$ into (18), we obtain the Helmholtz equation for monochromatic radiation in a non-amplifying and nonabsorbing medium

$$\nabla^2 E - k^2 \bar{\varepsilon} E = 0,$$

which admits an analytic solution in the case of a flat Epstein layer with $\bar{\varepsilon}(x) = 1 - \Delta\varepsilon/\cosh^2(x/d)$. The fundamental mode of this solution has the form [98]

$$E \sim \cosh^s\left(\frac{x}{d}\right) \exp\left[ikz\left(1 - \frac{\Delta\varepsilon}{2}\right) - (\Delta\varepsilon)^{1/2}\frac{z}{2d}\right],$$

where $s = -1/2 - ikd(\Delta\varepsilon)^{1/2}$. It decreases exponentially with respect to z with the coefficient of intensity term $(\Delta\varepsilon)^{1/2}/d$. Based on this fact, an important conclusion was made [98] that refraction in the plasma column is similar to the nonresonance losses (from the point of view of the effect on the radiation intensity), which increase the gain threshold of the fundamental mode.

In the case of ASE, we consider the TCF (65), taking into account (61) and (66), obtained for the parabolic profile of $\bar{\varepsilon} = \bar{\varepsilon}_2$ from (59). According to (61), for $z < z_r$ ($\sinh \tilde{z} \ll 1$), the effect of refraction on ASE is small. Refraction is an analogue of the nonresonance losses, if $\sinh \tilde{z} \gg 1$. In this case, the flux density of the end ASE and the axial strength of radiation vary with the laser length as $\exp(\alpha_0 z - 2z/z_r)$. They increase exponentially along z for $\alpha_0 z_r > 2$, but because of the refraction escape of ASE from the gain region the observed gain coefficient decreases by the value of the coefficient of refraction losses

$$\beta_r = \frac{2(\Delta\varepsilon)^{1/2}}{a} = \frac{2}{z_r}\,. \tag{79}$$

For $\alpha_0 z_r < 2$, refractive losses dominate over the amplification, and no laser action is observed despite the positive gain coefficient α_0.

By substituting (65) into (69) and taking into account (61), we find that the divergence of the end ASE forming the on-axis peak in the directivity diagram, in the case of strong refraction ($\sinh \tilde{z} \gg 1$) does not change with increasing z and is equal to $\Delta\theta = \theta_r$, where $\theta_r = (\Delta\varepsilon)^{1/2}$ is the angle of refraction. For $z > 2z_r$, the value of θ_r exceeds the geometrical value θ_g of the divergence typical of a homogeneous medium. Therefore, refraction results not only in a decrease in the brightness and power but also in the deterioration of the divergence of the end ASE.

In Ref. [45], the formation of ASE was considered by the method of geometrical optics for linear amplification in a two-dimensional medium with parabolic distributions of $\bar{\varepsilon}$ and α_0. It was shown that the angular width of the on-axis peak corresponding to the end ASE is equal to $\theta_r/G_r^{1/2}$, where $G_r = \alpha_0(0)z_r$, i.e. by a factor of $G_r^{1/2}$ is smaller than for the uniform profile of α_0. This is explained by the fact that in the case of the bell-shaped profile of α_0, ASE is 'pulled in' to the region of enhanced amplification, resulting in a decrease in the divergence. Analysis of the amplification of a Gaussian beam shows [99] that under certain conditions imposed on the parameters of parabolic profiles of $\bar{\varepsilon}$ and α_0, in principle, beam channelling can be produced by means of amplification without refraction defocusing. However, experimental implementation of this idea presents difficulties.

The general picture of divergence deterioration caused by refraction is aggravated by the fact that ASE escaping through the side surface of the laser medium forms side peaks at $\theta \approx \pm\theta_r$ [45]. The angular distribution of the side ASE at $G_r > 1$ and $z > 3z_r$ has the form

$$q_{\text{side}}(\theta) \approx q_0 \frac{1}{G_r} \exp\left(G - \frac{G_r}{2}\right) \times \exp\left[-\frac{G_r}{8\exp(-2z/z_z)}\left(\frac{\theta}{\theta_r} - 1\right)^2\right].$$

It exponentially sharpens with increasing z. The ratio of powers of the side and end ASE tends to a constant with increasing z:

$$\frac{P_{\text{side}}}{P_{\text{end}}} = \frac{\sqrt{2/(\pi G_r)}\exp(-G_r/2)}{(G_r - 1)\operatorname{erf}(\sqrt{G_r/2})}\,,$$

which sharply decreases with increasing G_r. The ratio of the strength of radiation in the side peak to that in the cases of parabolic and uniform profiles of α_0 is equal to $\exp(z/z_r)/[2\pi\exp(G_r/2)]$ and $\exp(z/z_r)/(4G_r)$, respectively [100]. In the case of strong refraction, a narrow low-power side peak in the angular distribution of ASE dominates over the broad high-power on-axis peak.

Despite their identical influence on the axial strength of radiation, refraction differs from nonresonance absorption in a medium in that the radiation is 'displaced' through the side surface of the gain medium rather than lost inside it. In the case of gain saturation, this difference is especially interesting, because refraction can remove the restriction on the total radiation power of the X-ray laser existing in media without refraction [98] due to saturation of $P_{\text{end}}(z)$ and the weak logarithmic increase in $P_{\text{side}}(z)$ [see Eqn (76)]. In the case $\bar{\varepsilon} = \bar{\varepsilon}_2$ and uniform α_0, it follows from the solution of equation (66) at $z > z_r$ that [91]

$$P_{\text{end}}(z) \approx \frac{\alpha_0}{\beta + \beta_r} P_{\text{sat}}\,,$$
$$P_{\text{side}}(z) \approx \alpha_0\left(\frac{\beta_r z}{\beta + \beta_r} - z_{\text{sat}} - \frac{1}{\beta_r}\right) P_{\text{sat}}\,. \tag{80}$$

For $\beta z \ll 1$, refraction does not affect the total ASE power and only differently distributes it between P_{end} and P_{side} [cf. Eqn (75)]. For $\beta z > 1$, Eqn (80) gives a more rapid, linear increase in P_{side} instead of a slow logarithmic one. Thus, the total power increases linearly with increasing z, in accordance with the qualitative conclusion of Ref. [98], and the side ASE dominates over the end ASE.

In the far field, more powerful off-axis radiation peaks are formed, which are mainly determined by the side ASE and are located at angles of $\theta \approx \pm\theta_r$ (in an axially-symmetric medium, an angular distribution with an annular structure is formed). The half-width at half-maximum of the side peak is equal to [100]

$$\Delta\theta \approx 8\left(\frac{\pi}{4}\right)^{n-2}\theta_r \exp\left(-\frac{z}{z_r}\right).$$

It may be noticeably smaller than the values of the characteristic angles θ_g and θ_r. Thus, the useful radiation can be taken in a distributed way through the side surface. The numerical solution of the parabolic equations [84] showed that, taking into account the action of the counter beam, the qualitative structure of the angular distribution of the ASE intensity is retained.

Experiments with Ne-like selenium X-ray lasers ($\lambda = 20.6$ and 20.9 nm) at LLNL showed that the far-field ASE beam splits in the x direction perpendicular to the foil (see Fig. 1). As z increases, two peaks appear in the ASE intensity distribution at both sides from the X-ray laser axis, which are separated by a dip on the axis [10–12, 101, 102]. Figure 4 shows the time-integrated experimental distribution of the strength of radiation over x for the Ni-like Se X-ray laser at $\lambda = 20.6$ nm [102]. The divergence $\Delta\theta_x$ of ASE is of about 10 mrad. A certain asymmetry of the $q(x)$ profile is explained by the fact that selenium was deposited onto a Formvar ($C_{10}H_{16}O_5$) substrate. This results in some asymmetry in the plasma expansion and the location of the gain region. The beam splitting is unexpected, because numerical calculations and estimates at $\bar{\varepsilon} = \bar{\varepsilon}_2$ give the ASE distribution with one on-axis maximum.

Firstly, the beam splitting could be explained by the non-uniform distribution of the gain coefficient over x, which exhibits an on-axis dip [12, 45]. In this case, ASE is predominantly formed in the off-axis regions with enhanced

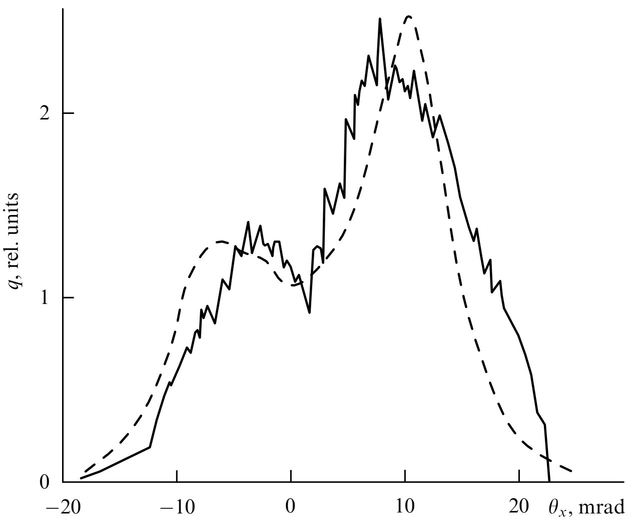

Figure 4. Experimental (—) [102] and theoretical (- - -) [104] time-integrated distributions of the strength of radiation q for an Ne-like selenium X-ray laser of length $z = 3$ cm perpendicular to a foil.

α_0, where the gradient of $\bar{\varepsilon}$ deflects beams from the axis. In the on-axis region, where refraction is weak, the ASE intensity is low. However, such an explanation of the effect casts doubt on the validity of the kinetic model, because kinetic calculations yield a bell-shaped profile for $\alpha_0(x)$ with a maximum on the axis. In addition, the experimental ASE distribution in the near field does not contain distinct off-axis maxima [102].

Secondly, the beam splitting in the case of the bell-shaped profile of α and $\bar{\varepsilon} = \bar{\varepsilon}_2$ can be explained by the refraction escape of ASE upon gain saturation [45, 84, 91]. In this case, the maximum of ASE emerging from the laser end is located at the zero angle. ASE coming out from the side surface of the laser can form bright off-axis peaks only upon gain saturation [see Eqn (80)]. Against this interpretation is the important fact that the ASE beam begins to split in experiments at values of z when saturation is not yet observed. For $z = 3$, the ASE beam splitting is absent in calculations [84], although it is distinctly manifested in experiments [10, 101].

Thirdly, it was found that the profile of the angular distribution of ASE strongly depends on the profile of $\bar{\varepsilon}$. In contrast to the profile of $\bar{\varepsilon} = \bar{\varepsilon}_2$, in the case of the profile of $\bar{\varepsilon}$ showing a noticeable nonuniformity in the on-axis region of the gain medium, for example, a linear profile, the distribution of end ASE exhibits a dip on the axis and off-axis peaks [86, 103]. Moreover, the axial dip in the distribution of the end ASE also appears for smooth profiles of $\bar{\varepsilon}$ of type (59) with $m < 2$ [104]. The closer m to 2, the greater the z at which the dip appears. The centre of the off-axis peak shifts to the value of the angle of refraction with increasing z. Because the side ASE still has side peaks centred at $\theta \approx \pm\theta_r$, for $m < 2$ the far-field ASE beam as a whole acquires an axial dip. For $m > 2$, the angular spectrum also contains an on-axis peak along with side peaks. The coefficient β_r of refractive losses is greater (for $m < 2$) or smaller (for $m > 2$) than the value from (79) obtained for the parabolic profile of $\bar{\varepsilon}$.

The presence of linear and concave parts in the profile of N_e, where the law of variation is much weaker than the parabolic one ($m < 2$), was confirmed in experiments (Fig. 3). Then the distribution of the end ASE splits both upon gain saturation and in its absence. The use of the experimental profile of $\bar{\varepsilon}$ in calculations [104] provides qualitative agreement with experimental angular ASE spectra [10, 101, 102] (Fig. 4). Note that the ASE beam splitting can also be caused by the nonstationary conditions of the laser plasma in the course of generation [10, 102].

The experimental angular distribution of the ASE intensity in the y direction parallel to the foil plane (Fig. 1) has a symmetric bell shape with a maximum on the axis [10, 101]. For $z = 3$ cm, the divergence $\Delta\theta_y$ is of about 20 mrad, which is also unexpected. X-ray lasing occurs during the action of the pump pulse for ~ 0.2 ns [10]. Because by the time of the onset of lasing and during lasing the plasma has no time to noticeably expand in the y direction [6], the width of the gain region in this direction cannot noticeably exceed the width of the line on a target irradiated by the pump laser. The profile of $\bar{\varepsilon}(y)$ should be quite steep (of type (59) for $m > 2$), and the role of refraction is less important than for $m = 2$. For an irradiated line of width 200 μm, the geometrical divergence is equal to $\theta_g \approx 7$ mrad, which is appreciably lower than the observed experimental value.

3.2.2 Coherence. By neglecting the volume noise for $\bar{\varepsilon} = \bar{\varepsilon}_2$, the coherence coefficient of the end ASE is found, in the case of uniform amplification and source, from (70), taking into account (61):

$$\mu(\mathbf{r}_\perp, \mathbf{r}'_\perp; z) = 2\left|\frac{J_1(kar'_\perp/\zeta)}{kar'_\perp/\zeta}\right|,$$

which yields the coherence length of ASE at the X-ray laser output

$$L_c(z) \approx \frac{\zeta}{ka} = \frac{z_r \sinh(z/z_r)}{ka}. \quad (81)$$

Comparison of (81) with (77) shows that the presence of defocusing refraction leads to a sharp increase in the coherence length of the end ASE. In the case of strong refraction, $L_c(z)$ increases exponentially. The value $L_c(z) \sim a$ is achieved for an X-ray laser length of $z \sim z_r \ln(ka^2/z_r)$, which can be easily obtained in the experiment. Thus, selecting the refraction mode accompanied by a decrease in the ASE flux density and an increase in the divergence, at the same time, represents an efficient mechanism for improving coherence. In the case of a parabolic profile of α_0 and linear amplification, the coherence length of ASE estimated from (71) for $\sinh(z/z_r) \gg 2z/z_r$ has the form [80]

$$L_c(z) \approx \left(\frac{G_r}{8}\right)^{1/2} \frac{z_r}{ka} \exp\left(\frac{z}{z_r}\right).$$

For the parabolic profile, $L_c(z)$ increases by a factor of $\sim (G_r)^{1/2}$ as compared to a uniform profile of α_0 in (81).

When $L_c(z)$ is considerably smaller than the characteristic width of the ASE beam, the power of coherent ASE at the laser output takes the form

$$P_c \approx S_\omega \frac{\lambda}{4}\left(\exp(\alpha_0 z) - 1\right),$$

i.e. in the case of low coherence, the coherent power is independent of the geometry of the medium and the presence of refraction. For sufficiently high z, when $L_c(z)$ reaches the beam size, we arrive at

$$P_c \approx S_\omega 2\left(\frac{\pi a \theta_r}{\alpha_0 z_r}\right)^2 \frac{\exp(\alpha_0 z) - 1}{\sinh(2z/z_r) - 2(z/z_r)},$$

i.e. in the case of high coherence, the coherent power sharply decreases with increasing refractive losses (note that here the geometric optics approximation becomes invalid).

According to Ref. [96], in the on-axis far-field region where the main contribution comes from the end ASE, we have for transversely uniform amplification:

$$L_c(Z) \approx Z\,\frac{\cosh(z/z_r)}{ka}\,, \tag{82}$$

i.e. the coherence in the presence of refraction is substantially higher than in its absence [cf. (78)]. For nonparabolic profiles of $\bar{\varepsilon}$ (59), the on-axis value of $L_c(Z)$ additionally increases (for $m < 2$) or decreases (for $m > 2$).

The far-field ASE coherence substantially varies over the beam cross section [96, 105]. In the direction $\theta = \theta_r$, where the radiation has maximum strength, the coherence coefficient takes the form [96]

$$\mu = \left|\sinh\frac{kaX'}{2Z\cosh(z/z_r)} + \frac{\cosh(z/z_r)}{\gamma z_r - \mathrm{i}kaX'/Z}\right| \times \left(1 + \frac{\cosh(z/z_r)}{\gamma z_r}\right)^{-1}, \tag{83}$$

where $\gamma = \alpha_0$ for linear amplification, and $\gamma = 1/z_r$ for strong saturation. For $\gamma z_r \ll \cosh(z/z_r)$, one finds $L_c(Z) \approx 2Z\gamma z_r/ka$, i.e. is independent of z and substantially smaller than its value in the on-axis region (82). The ASE coherence only weakly depends here on the profile of $\bar{\varepsilon}$. Thus, the beam region with enhanced radiation strength is characterized by a lower coherence, and vice versa, so that the coherent power is approximately independent of the profile of $\bar{\varepsilon}$ for $\theta \leqslant \theta_r$.

Figure 5 shows the time-integrated experimental distribution of the coherence coefficient $\mu(X, X'; Z)$ in an Ne-like selenium X-ray laser for $z = 4$ cm ($\lambda = 20.6$ and 20.9 nm) [106]. The measurements were performed at a distance $Z = 113.6$ cm from the X-ray laser in the direction perpendicular to the foil for $\theta = X/Z = 8$ mrad, i.e. in the vicinity of the point where the radiation strength was maximum (see Fig. 4). The diffraction pattern of ASE was analyzed after passing a diffraction grating with a variable step. The profile of μ over X' has the form (83), i.e. it consists of a narrow core and a long low-coherence wing. The coherence length is about 40 μm. In [106], the calculation was performed by the method of the parabolic equation [84] taking into account the counter beam, the nonuniform profile of α_0 under gain saturation and $\bar{\varepsilon} = \bar{\varepsilon}_2$ for $\Delta\varepsilon = 2 \times 10^{-4}$. The method of TCF under similar conditions (except for the inclusion of the counter beam) gave a distribution of μ [96] very close in the coherence region to that obtained in calculations [106]. Both calculated profiles of μ differ sharply from the experimental profiles and overestimate the coherence length by a factor of ~ 5 (see Fig. 5). This occurs because the value of $\Delta\varepsilon = 2 \times 10^{-4}$ used in the calculations, which qualitatively corresponds to the moment of the maximum gain, yields an angle for the maximum radiation strength equal to $\theta_r = 14$ mrad rather than 8 mrad. This results in an overestimation of the degree of coherence and an error in modelling the time-integrated distribution. The calculation performed in [96] for $\Delta\varepsilon = 6.4 \times 10^{-5}$ and $\theta_r = 8$ mrad was in good agreement with experimental data (Fig. 5). The experimental studies also did not show a noticeable change in the degree of coherence upon increasing z from 3 to 7.5 cm, in agreement with the theory [96].

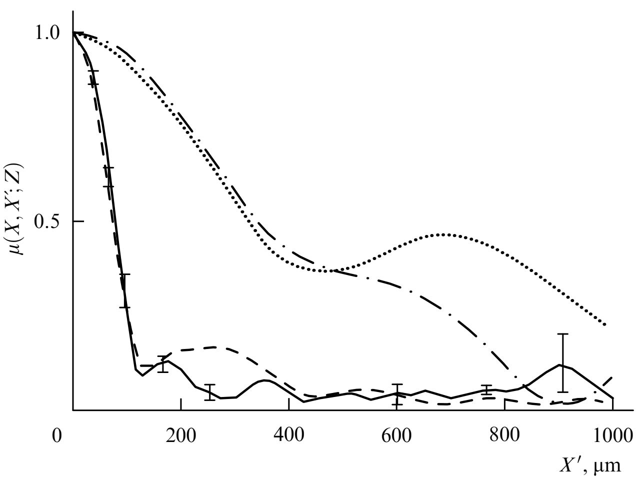

Figure 5. Distribution of the coherence coefficient μ at a distance of $Z = 113.6$ cm from an Ne-like selenium X-ray laser of length $z = 4$ cm for $\theta = X/Z = 8$ mrad perpendicular to a foil: experiment [106] (—); calculations [106] for $\Delta\varepsilon = 2 \times 10^{-4}$ (- · - · -); calculations [96] for $\Delta\varepsilon = 2 \times 10^{-4}$ (····) and $\Delta\varepsilon = 6.4 \times 10^{-5}$ (- - -).

Analysis of coherence and divergence in the experiment [106] in the direction parallel to the foil presents difficulties. For example, the size of a source at the X-ray laser output estimated from the width of the core in the distribution of μ is twice as large as the width 300 μm of the irradiated line. The narrowing of the irradiated line to 100 μm results in an improvement of coherence by a factor of 6, and the estimated size of the source corresponds to the width of the irradiated line.

3.3 A regular asymmetric medium with refraction

Later on, after experiments with thin foil targets, massive slab targets irradiated from one side were investigated [47, 107, 108]. In the case of massive slabs with chemical elements of small nuclear charges, there was a decrease in the required pumping intensity to $\sim 5 \times (10^{12} - 10^{13})$ W/cm^2 as compared to that for thin foils and a longer X-ray lasing of Ne-like ions at comparable gain coefficients. However, in the case of one-sided plasma expansion, the profile of N_e in the gain region is strongly asymmetric. Under these conditions, the ASE beam as a whole undergoes an angular shift and displacement from the gain region [47, 108]. Compared to the exploding-thin-foil X-ray laser scheme, the efficiency of the massive-slab X-ray laser is more strongly restricted by refraction with increasing laser length.

A thin-foil X-ray laser on the 3p – 3s transition in Ne-like yttrium is characterized by a high degree of monochromaticity, with the $J = 2 - 1$ line at 15.5 nm dominating [10]. In Ref. [48], a Nova laser was used for one-sided irradiation of a thicker target which was not burnt through during maximum amplification, thereby providing a strongly asymmetric distribution of N_e in the gain region, which was confirmed by calculations of the transversely two-dimensional hydrodynamics using LASNEX code [51] and of the population kinetics using XRASER code [57]. Pumping was performed with 0.53-μm, 0.5-ns, 1.4×10^{14}-W/cm^2 laser pulses. Figure 6 shows the time-integrated experimental and calculated far-field ASE distributions in the directions perpendicular (x) and parallel (y) to the target. The experiments were simulated using LASNEX and XRASER codes for three-dimensional nonstationary calculations of ASE along beam trajectories. For $z = 1.5$ cm, good agreement was observed between the calculated and experimental curves in the x direction (see Fig. 6a). However, for $z = 2.5$ cm, the calculated maximum of the distribution proved to be shifted by ~ 10 mrad relative to the experimental one. The divergence $\Delta\theta_x$ was equal to ~ 15 mrad. A more serious problem appears in modelling the ASE distribution in the y direction, where the divergence $\Delta\theta_y$ is ~ 25 mrad and the width of the experimental ASE distribution is twice as large as that of the calculated one (Fig. 6b). The experimental distribution of ASE over the y-axis does not change as the X-ray laser length varies from 1.5 to 2.5 cm and is independent of the width of the irradiated line.

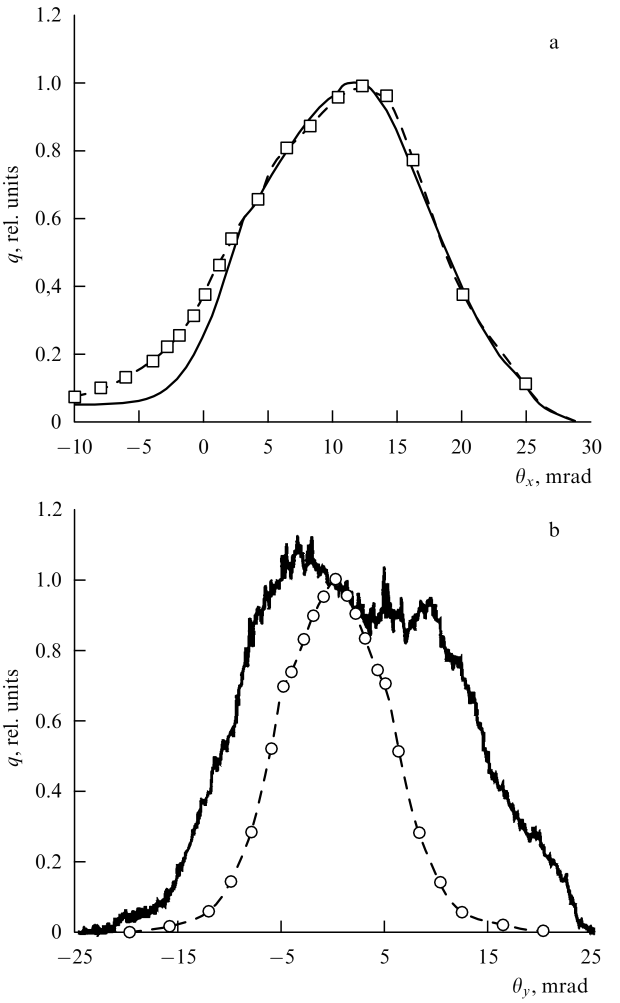

Figure 6. Time-integrated experimental (—) and calculated (□, ○) angular distributions of ASE for an Ne-like yttrium X-ray laser ($\lambda = 15.5$ nm) (a) perpendicular, and (b) parallel to a target [48].

In Ref. [50], an attempt was made to take into account the nonuniformity of plasma parameters over z caused by the longitudinal nonuniformity of the irradiated line on the target. Three-dimensional nonstationary calculations of the gain were performed in the geometrical optics approximation for a Ne-like germanium X-ray laser using LASNEX and XRASER codes. A separate calculation performed with a Cray supercomputer took at least 20 hours. The resulting angular distribution of ASE was not shifted from the centre along the x-axis, as has been observed in all experiments. All this demonstrates the complexity of the problems of three-dimensional modelling of experiments yet to be solved.

3.4 A randomly inhomogeneous medium

One can see from the preceding discussion that the interpretation of experimental data still involves a number of problems. Among these are the higher divergence and lower coherence observed in experiments as compared to calculations in the y direction parallel to the target in the case of Ne-like ion X-ray lasers with an exploding-foil [10, 102, 106] and massive-slab [48] targets. For an Ne-like argon capillary-discharge X-ray laser [25], an ASE distribution was obtained consisting of an on-axis core and low-intensity but long wings that may contain a considerable fraction of the energy. The appearance of the wings in the angular spectrum of ASE also needs interpretation. For this reason, some additional physical effects should be included in the theoretical models along with those considered in Sections 3.1 – 3.3.

One reason for the deterioration of coherence and divergence in experiments as compared to the theoretical expectations may be the presence of small-scale optical inhomogeneities in the amplifying medium. A plasma (including a laser plasma) possesses a number of instabilities (see reviews [63, 64] and references cited therein). In a laser plasma, they can be caused by the nonuniform structure of the target and its surface, nonuniform irradiation of the target, the presence of filaments in the pump beam in the plasma being formed, stimulated scattering of the pump radiation (SRS and SBS), turbulence, etc. These factors lead to a small-scale perturbation of the plasma density, velocity, and temperature, resulting in nonuniformity of the dielectric constant and gain. Such inhomogeneities in the form of filaments, jets, and vortices on the scale of $\sim 1-10$ μm were observed in experiments (see, for example, Refs [65 – 69]). The possibility of the presence of turbulent fluctuations in the plasma on the scale of 1 μm and lower was noted in Ref. [6]. A detailed experimental study of inhomogeneities on this scale presents serious difficulties.

Numerous successful X-ray laser experiments suggest that the instabilities developed during X-ray lasing are not sufficiently strong and do not drastically affect the ASE, as it would be the case for significant build-up and regularization of the perturbations. This fact, taking into account the great variety of possible instabilities, allows us to treat perturbations of plasma parameters theoretically as random. For this reason, ASE dynamics can be considered in an X-ray laser medium with a specified field of fluctuations of the dielectric constant with Gaussian statistics and correlation lengths equal to characteristic perturbation lengths obtained in experiments. This problem is solved with the help of the equation for the TCF (56).

Usually $\beta \ll \alpha_0$, so that the effect of fluctuations of $\tilde{\beta}$ on ASE can be neglected in many cases. For the same scale and amplitude of fluctuations in $\tilde{\varepsilon}$ and $\tilde{\alpha}_0$, the effect of the former on the angular and coherent properties of ASE is more substantial, because they directly affect the emission phase [88]. Therefore, we will neglect the influence of fluctuations of $\tilde{\alpha}_0$ and their statistical coupling with fluctuations of $\tilde{\varepsilon}$ on angular and coherent parameters of ASE. Then, we have from (57), taking into account (58):

$$H(\mathbf{r}_\perp, \mathbf{r}'_\perp; z) = \sqrt{\frac{2}{\pi}}\,\sigma^2(\mathbf{r}_\perp, z)\, l_{||}(\mathbf{r}_\perp, z) \times \left\{1 - \exp\left[-\frac{|\mathbf{r}'_\perp|^2}{2 l_\perp^2(\mathbf{r}_\perp, z)}\right]\right\}, \tag{84}$$

where σ^2, $l_\perp$ and $l_{||}$ are the variance, and the transverse and longitudinal correlation lengths of $\tilde{\varepsilon}$, respectively.

For the parabolic profile $\bar{\varepsilon} = \bar{\varepsilon}_2$ (59), uniform transversely unbounded amplification, and statistically uniform fluctuations of $\tilde{\varepsilon}$, the TCF of ASE has the form (67). By substituting (84) into (68), we obtain for weak refraction ($z < z_r$):

$$V(\mathbf{r}'; z) = \delta\left[1 - \frac{\sqrt{\pi}}{2}\,\frac{\operatorname{erf}(\sqrt{\rho})}{\sqrt{\rho}}\right], \tag{85}$$

and for strong refraction ($z > z_r$)

$$V(\mathbf{r}'; z) \approx \delta\,\frac{C + \ln\rho + E_1(\rho)}{2z/z_r}, \tag{86}$$

i.e. $V(\mathbf{r}'; z)$ changes with increasing z only for $r' \geqslant l_\perp \sinh(z/z_r)$. In (85) and (86), E_1 is the integral power function, $\rho = \mathbf{r}'^2/(2l_\perp^2)$, $\delta = (\pi/8)^{1/2}k^2\sigma^2 l_{||}z$, and $C \approx 0.58$ is Euler's constant.

From Eqn (69), taking into account (67) and (85), an important spatial scale—the scattering length of ASE, is determined as follows [109]:

$$z_{sc} = \left[6\left(\frac{2}{\pi}\right)^{1/2}\frac{(al_\perp)^2}{\sigma^2 l_{||}}\right]^{1/3}.$$

It gives the characteristic distance after passing which a noticeable fraction of ASE is scattered by fluctuations of $\tilde{\varepsilon}$ and comes out through the side surface of the gain medium. The ASE parameters depend on the relation between z_{sc} and the refraction length z_r.

It is possible that the case $z_{sc} < z_r$ is typical of the ASE development in Ne-like ion X-ray lasers [5, 6, 10–12, 48] in the y direction parallel to the target, where the profile of $\bar{\varepsilon}$ is quite steep and marked refraction is observed only at the periphery of the gain medium (see Sections 3.2.1 and 3.2.2). In this case, the ASE is predominantly affected by scattering from $\tilde{\varepsilon}$, while the role of diffraction can be neglected. As noted above, the laser action is experimentally manifested by an exponential increase in the axial strength of radiation with increasing z. Calculations in the plane-wave approximation showed [109] that in the case of a transversely restricted gain medium the analytic solution (67) takes place only at $z < z_{sc}$. Scattering of ASE by $\tilde{\varepsilon}$ and its displacement through the side surface of the X-ray laser is analogous to linear absorption of ASE with the coefficient of intensity $\varkappa_{sc}$. Therefore, fluctuations in $\tilde{\varepsilon}$ decrease the observed gain increment, as does regular refraction [see Eqn (79)].

The character of the dependence $\varkappa_{sc}(\sigma)$ is determined by the parameter $d \equiv kal_\perp/z_{sc}$. For strong fluctuations of $\tilde{\varepsilon}$, when $d^3 \geqslant 1$, we obtain [109]

$$\varkappa_{sc} \approx \frac{1}{z_{sc}}$$

[cf. Eqn (79)], i.e. $\varkappa_{sc} \sim \sigma^{2/3}$. In the case of an axially symmetric medium, this value, most likely, is doubled; however, this needs verification. For weak fluctuations of $\tilde{\varepsilon}$, when $d^3 \ll 1$, we obtain [110]

$$\varkappa_{sc} \approx \frac{3d^2}{z_{sc}}$$

and, therefore, $\varkappa_{sc}$ is independent of $l_\perp$ and a. Here, $\varkappa_{sc} \sim \sigma^2$ is similar to the coefficient of scattering of energy from a restricted coherent beam in an infinite randomly inhomogeneous gain medium [111]. Thus, the influence of $\tilde{\varepsilon}$ may be another reason for observing experimental gains that are typically lower than their values calculated using kinetics codes.

The scattering of ASE from $\tilde{\varepsilon}$ decreases its spatial coherence at the X-ray laser output, in accordance with experimental data obtained in the y direction [106]. In this case, the power of coherent ASE also decreases (for large Fresnel numbers as well), in contrast to the case of only regular refraction. There is the value of $l_\perp$ for which the coherence length L_c has a minimum, whereas for larger and smaller values of $l_\perp$ the influence of $\tilde{\varepsilon}$ on ASE is weaker [92]. As z increases, the value of L_c grows and tends to a constant value

$$L_c = \left[\frac{1-h}{2}\right]^{1/2}\frac{\lambda z_m}{\pi a},$$

where

$$z_m \approx \begin{cases} \left(\dfrac{2}{3}\right)^{1/3} z_{sc}, & \dfrac{6d^2}{1-h} \geqslant 1, \\[2ex] \dfrac{(2/9)(1-h)z_{sc}}{d^2}, & \dfrac{3d^3}{(1-h)^{3/2}} \ll 1. \end{cases}$$

For large values of d^2, we have $L_c < l_\perp$, while for small d^3, we obtain $L_c \gg l_\perp$. As for the far-field ASE coherence, in the case of the stepwise profile of α_0, the effect of $\tilde{\varepsilon}$ results in an insignificant increase in L_c, while for the bell-shaped profile of α_0, coherence, on the contrary, may become weaker.

The angular distribution of the ASE intensity is broadened upon scattering from $\tilde{\varepsilon}$. The decrease in the angular divergence with increasing z due to spatial filtration by the gain medium is followed by a tendency to the constant value $\Delta\theta \approx 2\theta_{sc}$, where $\theta_{sc} = a/z_{sc}$ is the characteristic angle of scattering [109]. The angle θ_{sc} exceeds the geometrical angle θ_g. As noted above, the excess of $\Delta\theta$ in the y direction over the geometrical angle and the independence of z have been observed in experiments with selenium [10–12, 101, 102] and yttrium [48] (Fig. 6), in accordance with the theory considered above. An example of possible inhomogeneities are filaments in a plasma of small size in the y direction and strongly elongated in the x direction, thus only weakly affecting the ASE distribution over x (see Fig. 4).

Note that in the case of an infinite medium, there is a restriction on the path length imposed by the Markovian approximation [112]. In the case of a gain medium of finite transverse size, this restriction is removed [92, 109].

Gain saturation results in an additional increase in $\Delta\theta$ and a decrease in L_c. Upon strong saturation, the angular distribution of ASE exhibits an off-axis peak which is mainly formed by ASE that has passed through the side surface of the X-ray laser, i.e. fluctuations of $\tilde{\varepsilon}$ cause splitting of the ASE beam [109]. In this case, the maximum radiation strength is observed in the direction $\theta \approx \theta_{sc}$.

The effect of $\tilde{\varepsilon}$ on the ASE coherence can be approximately neglected at X-ray laser lengths $z \leqslant z_m$. The estimate at the maximum density $N_e \sim 10^{21}$ cm^{-3}, $z \sim 5$ cm, and $l_\perp \sim 1-10$ μm shows that this effect will be noticeable when the level of fluctuations of $\tilde{\varepsilon}$ reaches several percent of its maximum value.

Consider now the case $z_{sc} > z_r$. This situation is probably typical of the development of ASE in the Ne-like selenium X-ray laser in the x direction where a smooth decrease in $\bar{\varepsilon}$ is observed due to predominant plasma expansion in this direction. Although in this case the ASE is mainly affected by regular refraction, nevertheless the role of scattering from $\tilde{\varepsilon}$ cannot be neglected. Scattering of ASE from $\tilde{\varepsilon}$ decreases the high degree of coherence of the end ASE at the laser output and in the far field and also decreases the coherent power. For $g \equiv kal_\perp/z_r < 1$ and $\delta > 1$, the behaviour of $|B|$ in (67) in the main interval $r' < l_\perp \sinh(z/z_r)$ is predominantly determined by the second factor and is independent of z, according to (86). As z increases and the influence of $\tilde{\varepsilon}$ grows, the exponential increase in $L_c(z)$ changes to the constant value

$$L_c \approx \begin{cases} \sqrt{\dfrac{\chi}{3}}\,\dfrac{\lambda z_{sc}}{\pi a}\,, & d^2 > \chi\,, \\ \sqrt{2}\,l_\perp \exp\left(\dfrac{\chi}{3d^2} - \dfrac{C}{2}\right), & d^2 < \dfrac{\chi}{2}\,, \end{cases}$$

where $\chi = (z_{sc}/z_r)\ln(1/h)$. In the first case, $L_c < l_\perp$, and in the second case, $L_c \gg l_\perp$; in both cases, L_c may be much smaller than the width of the ASE beam.

Calculations show that for $z_{sc} > z_r$, scattering of ASE by $\tilde{\varepsilon}$ is not analogous to linear absorption, as in the absence of refraction. The presence of fluctuations of $\tilde{\varepsilon}$ in the case of strong refraction results in the interesting effect of the so-called 'hidden' influence on ASE [92]. This effect is manifested in the destruction of the refraction-induced high degree of coherence at the X-ray laser output and in the far field, whereas the flux density changes only weakly, the broadening of the beam as a whole is comparatively weak, and the decrease in q_0 is relatively small. The effect of the hidden influence of $\tilde{\varepsilon}$ is demonstrated in Fig. 7 for parabolic profiles of $\bar{\varepsilon}$ and α_0 and linear amplification: when $L_c(Z)$ decreases by a factor of 3.5, the value of q_0 decreases by only 20%. The great difference between the values of $L_c(Z)$ for the end and side ASE, existing in the presence of refraction only, disappears. Upon gain saturation, only the prominent off-axis peak in the distribution of q broadens more noticeably. When the refraction coherence level is almost destroyed, a noticeable broadening of the beam and a decrease in $q_0(z)$ are observed with increasing z.

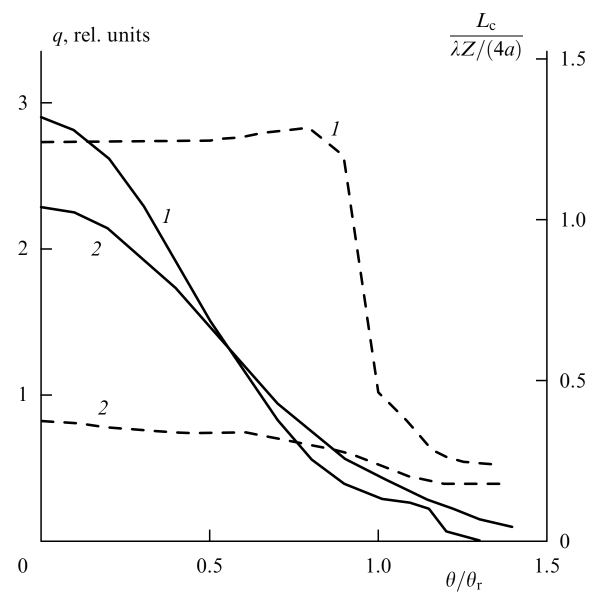

Figure 7. Calculated distributions of the strength of radiation q (—) and of the coherence length L_c (- - -) in the far field in the case of linear amplification on the parabolic profile of α_0, $\bar{\varepsilon} = \bar{\varepsilon}_2$, $\lambda = 21$ nm, $z = 4$ cm in the absence of $\tilde{\varepsilon}$ (*1*), and in the presence of $\tilde{\varepsilon}$ for $l_\perp = l_{||} = 1.4$ μm, $\sigma = 4 \times 10^{-5}$ (*2*) [92].

For $z_{sc} > z_r$, a rough estimate of the plasma irregularity at which full coherence can be achieved, shows that the level of fluctuations of the plasma electron density should not exceed several percent of its maximum regular value. This value is quite low and can be achieved in many cases.

Recently, significant fluctuations of $\tilde{\alpha}_0$ on a scale of ~ 10 μm and depth $\sigma_\alpha \sim 10$ cm^{-1} were detected for an average level of $\bar{\alpha}_0 \sim 25$ cm^{-1} in a Ne-like yttrium X-ray laser [69]. These results can be used for analysis of the influence of $\tilde{\alpha}_0$, by making the substitution $\sigma = \sigma_\alpha/k$. Then, the value of $\delta = (\pi/8)^{1/2}\sigma_\alpha^2 l_{||} z$ is of the order of unity. According to the necessary criterion $\delta \geqslant 1$ for the influence of fluctuations of $\tilde{\alpha}_0$ on ASE [88], the quality of the ASE beam may be noticeably affected at such a level of σ_α.

Thus, as is shown above, comparatively weak fluctuations of $\tilde{\varepsilon}$ reduce the quality of the ASE beam, which is inherently low in a multimode regime (except for coherence in the presence of strong regular refraction). However, one should bear in mind that the problem of small-scale inhomogeneities of parameters of the medium can become much more important in attempts to produce single-mode X-ray lasing. In Ref. [113], fluctuations of the plasma parameters caused by nonuniform irradiation of the target were considered within the framework of mode analysis [79–81]. The fluctuations were modelled by random displacements of parabolic profiles of $\bar{\varepsilon}(x)$ and $\bar{\alpha}_0(x)$ along x direction at different sections of z. It was shown that such a random transverse displacement of $\bar{\varepsilon}$ and $\bar{\alpha}_0$ profiles sharply reduce the ASE coherence in the regime close to the single-mode one.

4. Methods for improving the radiation parameters of X-ray lasers

A highly efficient, high-brightness, highly coherent, low-divergence X-ray laser can be developed by various methods. For example, one can search for conditions to obtain an X-ray laser medium with good optical properties. Having obtained a medium with an acceptable degree of optical homogeneity, one can use various approaches for increasing the power and brightness of the X-ray laser. However, in a number of cases, the great potential of the gain medium (the high gain coefficient) is very poorly realized because of optical losses during amplification, which can even result in no lasing. If the inhomogeneity of such a medium cannot be initially eliminated, one should search for the possibility to compensate for distortions of the phase front of the beam caused by optical inhomogeneities. In a number of cases, a combination of different methods for improving ASE parameters can be employed.

4.1 Improvement of the parameters of the gain medium

We consider here some procedures for improving the optical quality of an X-ray laser medium. The imposition of an axial magnetic field on a plasma, modification of the time profile of the pumping intensity, and the use of targets of special types result in a reduction in the large-scale electron density gradients in the gain region.

4.1.1 Magnetic confinement of a plasma. One of the first recombination pumped X-ray lasers [15] was the H-like carbon laser in which the laser plasma is produced by a long pulse and confined by a magnetic field [7, 114]. The geometry of the experiment differs from that shown in Fig. 1: the pump radiation is focused on a solid target to a small spot rather than to a line, and a plasma column is formed along the x-axis during plasma expansion in the direction opposite to the direction of pumping. In the (y, z) plane, the plasma is confined from expansion by a magnetic field. The magnetic field improves the uniformity of the electron density in the plasma column in the (y, z) plane, thereby minimizing refraction losses. The plasma is cooled not owing to the transverse expansion but due to radiation and thermal conductivity. The ASE beam in the recombination H-like carbon X-ray laser does not experience refraction deflection, and the experimental angular distribution of ASE has a maximum on the X-ray laser axis [114] (Fig. 8).

Note that the optimum electron density N_e required for producing the maximum population inversion in recombination H-like and Li-like ion X-ray lasers is noticeably lower than that in Ne-like and Ni-like ion X-ray lasers [15]. Correspondingly, the drop in the dielectric constant in the gain region is comparatively small, and in lasers with small lengths z refraction is not manifested even in freely expanding plasma, not confined by a magnetic field. However, in the event of relatively large z, the refraction length can become lower than z. In this case, the idea of magnetic confinement of a plasma used in Refs [7, 114] was applied to the Ne-like argon X-ray laser in a capillary discharge of length up to 24 cm [24, 25]. Calculations showed that the imposition of an axial magnetic field allows one to obtain a smoother angular distribution of the electron density during lasing [115]. The gradient of N_e decreases with increasing magnetic field strength, resulting in an improvement of the uniformity of the X-ray laser beam, which allows enhancement of the ASE intensity by an order of magnitude (Fig. 9). However, the intensity of the 46.9-nm laser line at first increases monotonically with the magnetic field strength and after reaching a maximum begins to decrease also monotonically. This is explained by the Zeeman splitting and broadening of the laser line, which becomes substantial in strong magnetic fields. One can see from Fig. 9 that the calculated results are in good agreement with experimental data [115].

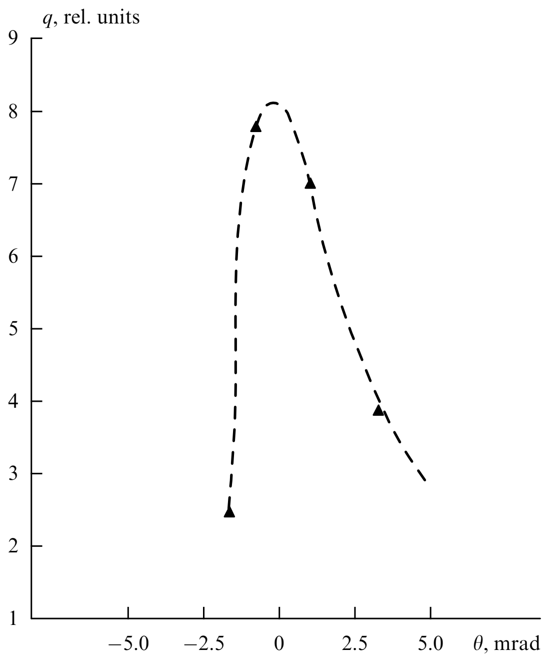

Figure 8. Experimental far-field distribution of the intensity of the 3 – 2 line of an H-like carbon X-ray laser at 18.2 nm with a magnetic induction of $B = 35$ kG [114].

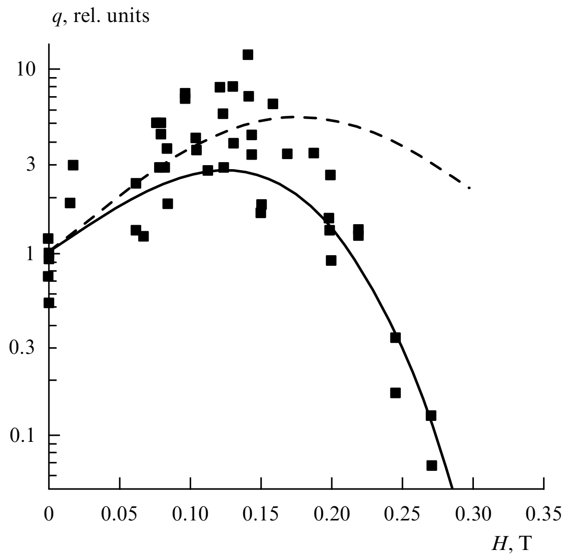

Figure 9. Integrated intensity of the 3p – 3s $J = 0 - 1$ line of the Ne-like argon X-ray laser at 46.9 nm in a capillary discharge of length $z = 10$ cm as a function of the strength of an external axial magnetic field [115]: experiment (■); calculations with (—) and without (- - -) regard for Zeeman splitting.

4.1.2 Temporal profiling of the pump. X-ray laser experiments using the Ne-like ion 3p – 3s quasi-steady-state inversion scheme and performed in the mid-1980s to early 1990s revealed an 'anomaly' which has been widely discussed [15 – 17]. It was found that two closely spaced lines, $[3/2, 3/2]_{J=2} - [3/2, 1/2]_{J=1}$ (or the $^1D_2 - {}^3P_1$ line in the LS-coupling notation) and $[1/2, 3/2]_{J=2} - [1/2, 1/2]_{J=1}$ ($^3P_2 - {}^1P_1$), dominated in the experimental ASE spectrum, whereas the kinetic calculations predicted the highest gain for the $[1/2, 1/2]_{J=0} - [1/2, 1/2]_{J=1}$ ($^1S_0 - {}^1P_1$) line. It was found later that this occurs, in particular, because of the high (and different for various lines) refraction losses. In the case of the $J = 0 - 1$ line, which is pumped exclusively by collisional monopole excitation from the ground state, the population inversion appears earlier in time and the distribution of the gain coefficient is localized closer to the target, i.e. at higher values of the electron density N_e and its gradient. Because pumping of the $J = 2 - 1$ line is further substantially determined by recombination of the F-like ions and subsequent cascade transitions from Ne-like highly excited ionic states [116], lasing at this line is observed later and for smaller values of N_e and its gradient. For this reason, the $J = 0 - 1$ line exhibits higher refraction losses compared to the $J = 2 - 1$ lines, so that the resulting gain on the $J = 0 - 1$ transition becomes smaller than that on the $J = 2 - 1$ transitions. These losses become so high for all lines on decreasing the nuclear charge of the target substance that lasing is no longer observed at all.

To compensate partially for refraction, a massive target is commonly irradiated by pump radiation with a low-energy prepulse [117, 118] or a pulse train [119]. The typical duration of the pump pulse is up to 1 ns when a prepulse is used, and

100 ps when a pulse train is used, with typical energies of 100 – 1000 J. The role of the prepulse (the first pulse) consists in preliminary heating and creation of the large-scale plasma region. The expanding plasma is cooled and becomes non-transparent for the pump radiation in the subcritical region with a low gradient of N_e. It is here, before achieving a critical surface, the main (next) pump pulse is strongly absorbed, resulting in rapid heating of the plasma up to the temperatures required for population inversion.

Figure 10 shows the calculated profiles of N_e and α_0 for the $J = 0 - 1$ transition of Ni-like titanium in the direction of plasma expansion, obtained with the help of the LASNEX code with and without a prepulse [118]. The energies of the main pulse and prepulse are 550 J and 3 J, respectively, the duration of the pulses is 0.6 ns, and the interval between the pulses is 7 ns. One can see that with the prepulse the role of refraction losses decreases in importance for two reasons: a decrease in the gradient of N_e and broadening of the gain region. When the conditions for the amplification of the $J = 0 - 1$ line change substantially, the corresponding conditions for the $J = 2 - 1$ line change more weakly [120].

The use of the prepulse permitted the observation of the laser lines, which otherwise were not observed due to refraction losses [117]. This resulted in substantial progress in the detection of lasing from ions with low nuclear charges [18, 19]. Later, the dependences of the ASE intensity on the fraction of the energy in the prepulse and the interval between pulses were experimentally investigated [121] and the possibility of combined use of a prepulse and multiple-pulse pumping was demonstrated [122].

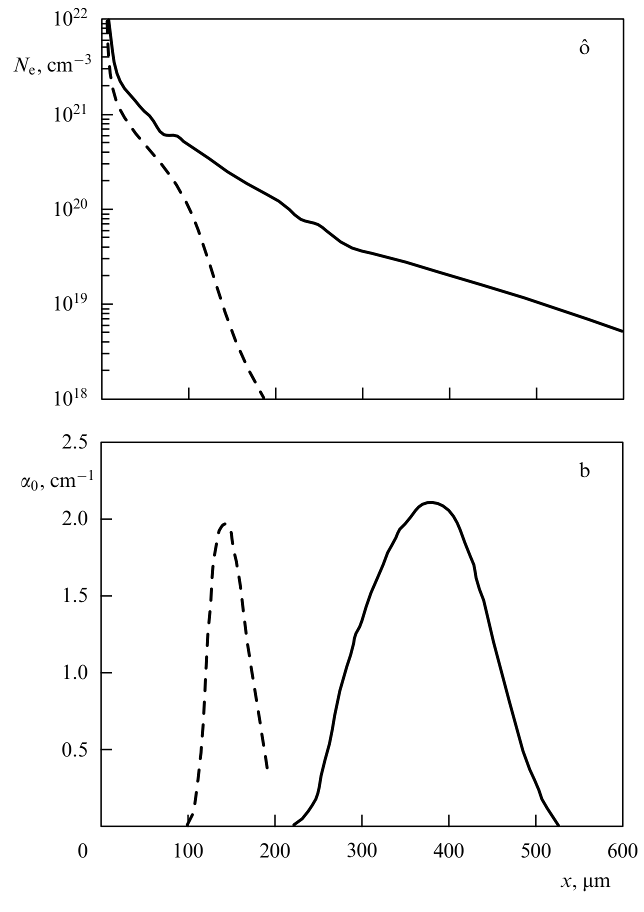

Figure 10. Calculated dependences of (a) the electron density and (b) the gain coefficient at the 3p – 3s $J = 0 - 1$ transition of an Ne-like titanium X-ray laser at 32.6 nm on the distance to the target surface in the direction of plasma expansion with (—) and without (- - -) a pump prepulse [118].

The technique of the prepulse allows one to reduce the refraction losses but does not completely eliminate the effect of refraction. Numerical calculations [118, 120] (see Fig. 10) and experiments [123] with prepulse and multipulse pumping showed that the gain region is characterized by a convex exponential profile of N_e, i.e.

$$\bar{\varepsilon}(x) = 1 - \Delta\varepsilon \exp\left(-\frac{x}{d}\right). \tag{87}$$

Detailed three-dimensional geometrical optics calculations of the gain were performed in Refs [120, 124]. The distributions of the far-field ASE intensity obtained in these papers qualitatively describe specific experiments on Ne-like germanium and zinc ions. The TCF calculations with profile (87) [125] showed that the amplification of radiation produced in a narrow transverse layer sharply decreases after passing a distance of $\sim z_r$, where $z_r = (8a/\nabla\varepsilon_0)^{1/2}$ and $\nabla\varepsilon_0$ is the gradient of $\bar{\varepsilon}$ at the point of maximum gain. As z further increases, this fraction of ASE is almost completely displaced from the gain region and the ASE power remains constant and proportional to $\exp(\alpha_0 z_r)$. Consideration of the noise source over the entire volume of the medium gives a linear increase in the ASE power for $z > z_r$: $P(z) \sim \exp(\alpha_0 z_r)(z - z_r)$. In the analogous case of a symmetric profile of $\bar{\varepsilon}$, refraction only reduces the real gain coefficient by the value of the coefficient of refraction losses (79), while the ASE power still increases exponentially. Thus, the asymmetric profile of $\bar{\varepsilon}$ reduces the pumping efficiency more significantly. The effect of the asymmetry of the $\bar{\varepsilon}$ profile on the behaviour of $P(z)$ is in some sense similar to the gain saturation in the case of a symmetric profile of $\bar{\varepsilon}$ [see Eqn (80)]. Note in this connection that saturation of the dependence $P(z)$ observed in experiments (see, for example, Ref. [126]) does not necessarily indicate gain saturation.

According to [125], the width of a source in the near field increases, as does its power, proportionally to z for $z \geqslant z_r$. The distribution of the radiation flux density is predominantly localized outside the gain region and has a quite flat top, in accordance with experiments [127]. The maximum value of $L_c(z)$ is achieved at the beam side far from the target and is estimated as $L_c \approx \lambda/(4\Delta\theta)$. It increases along z and tends to a constant value.

The use of a prepulse results in a decrease in the ASE divergence $\Delta\theta$ [120]. $\Delta\theta$ first decreases along z and then tends to a constant value $\Delta\theta \sim 1/z_r$. The far-field ASE distribution is also characterized by the angular displacement of the ASE beam from the target, which is observed upon single-pulse pumping (see Section 3.3). The angle of deflection θ_{max} of the ASE beam, for which $q = q_{max}$, at $z \leqslant z_r$ is equal to $\theta_{max} = (z/4)\nabla_0$, in accordance with experiment [128]. For $z > z_r$, the value of θ_{max} gradually tends to a constant value.

The degree of far-field ASE coherence significantly changes over the beam cross section [125]. The coherence length in the far field was estimated to be $L_c \approx \lambda Z/(4D)$, where D is the characteristic width of the distribution of I over x [96]. At the beam periphery from the side closest to the target, the contribution from weakly refracted and weakly amplified (but, however, noticeably exceeding the noise level) spontaneous radiation is significant for small θ, so that coherence here is independent of z and is mainly determined by the size of the gain region a: $L_c \approx \lambda Z/(4a)$. $L_c(Z)$ decreases with increasing angle, because this part of the angular spectrum is mainly determined by the region of the near field of size $D > 2a$, located outside the gain region. Because the source size in the near field increases linearly with z, at the beam centre $L_c \sim z^{-1}$. As z increases, the value of L_c at the beam centre becomes substantially smaller than at its periphery from the left. Therefore, the coherent power remains approximately constant with angle. The effect of the inhomogeneity of L_c in the far field was experimentally examined in Ne-like zinc ion [129], where a drop by a factor of 4 in the values of L_c at the beam wing closest to the target and at the beam centre was detected.

As was mentioned above, the population inversion in Ne-like ions in a conventional quasi-steady-state X-ray laser is produced by collisional and recombination pumping of the upper laser level followed by fast radiative depopulation of the lower level. In the case of more rapid plasma heating (for a time of the order of intraion relaxation processes), population inversion can be achieved through transient collisional processes proceeding with different rates [21]. According to calculations, such a transient, sharply nonstationary regime provides a gain coefficient that is one-two orders of magnitude higher and completely eliminates the problem of reabsorption of the resonance radiation. While in the quasi-steady-state case the use of a prepulse is not, in principle, always necessary to obtain lasing, in the transient regime it is inherently needed [20]. A long (~ 1 ns) pump pulse produces a plasma containing sufficient number of Ne-like ions, and the next short (~ 1 ps) pulse rapidly overheats the plasma and produces the conditions for lasing. The prepulse pump beam intensity is $\sim 10^{12}$ W/cm^2 and that of the picosecond pulse is $\sim 10^{15}$ W/cm^2. The energy per pulse is several joules. The gain coefficient on the 3p – 3s $J = 0-1$ transition of Ne-like titanium ion at 32.6 nm was measured to be $\alpha_0 = 19$ cm^{-1} and the gain – length product $\alpha_0 z \approx 10$ [20]. Because of the short time of the population inversion occurrence, the X-ray laser pulse is also short (~ 20 ps). Note that a combination of long and short pump pulses results in a quite high gradient of N_e, so that the actual path of the beam in the active region is smaller than a millimetre [130]. The gradient of N_e can be reduced by using an additional pump prepulse, which can be long, low-energy or short [131].

In the case of femtosecond pumping, the mechanism of interaction between radiation and matter is different. The irradiation of a gas or a preliminary prepared plasma by a very intense femtosecond pump pulse results in tunnelling ionization. The mechanism of producing the population inversion depends on the polarization of the pump radiation [22]. In the case of linear polarization, the ionized electrons are cold, and the laser levels are populated by recombination. In principle, the ground state may be the lower laser level, which allows one to substantially reduce the lasing wavelength compared to the quasi-steady-state collisional scheme. In the case of circular polarization of the pump radiation, hot electrons are produced and the levels are populated through collisional excitation by free electrons. The maximum gain-length product $\alpha_0 z \approx 11$ was achieved for the $4d^9 5d\,^1S_0 - 4d^9 5p\,^1P_1$ line in Pd-like xenon ion at 41.8 nm, pumped by a ~ 70 mJ, ~ 40 fs pulse [23]. The pump beam was focused longitudinally on a cell filled with gas. A serious problem encountered in this approach is the ionization-induced refraction caused by the self-action of the pump radiation. It is explained by the fact that upon longitudinal focusing of the pump beam with a bell-shaped intensity profile, an inhomogeneous transverse profile of the plasma electron density is produced which leads to defocusing refraction of the pump radiation and reduces its intensity. This limits the X-ray laser length and decreases $\alpha_0 z$.

4.1.3 Alternative targets. The uniformity of the transverse distribution of plasma parameters can be improved using solid targets of special construction, for example, with a modified surface. Calculations [131] showed that the use of a grooved target with a cylindrical longitudinal groove along the line of the pump radiation focusing allows one to obtain a smaller gradient of the plasma density. This explains the fact that the use of the same plane target in a series of experiments focusing the picosecond pump radiation onto the same spot improves the output parameters of the X-ray laser.

Another example is collisional Ne-like argon and Ni-like xenon X-ray lasers [132, 133] in which instead of the solid target in the scheme in Fig. 1, a gas puff is injected to a vacuum chamber through a narrow nozzle. In such a scheme, the uniformity of the distribution of N_e in the plasma produced is the same as that for the initial gas. In the case of a sufficiently uniform distribution of the gas density in the region being pumped, a small gradient of N_e in the plasma can be ensured and amplification in the X-ray laser with a length of ~ 3 cm can be achieved almost without refraction [133].

4.2 Improvement of the beam quality in a high-quality gain medium

If a method exists for obtaining a gain medium with high optical homogeneity, the intensity of ASE can in principle be increased, its divergence decreased, and coherence improved by increasing the X-ray laser length z [see Eqns (72), (73), (77)]. However, in order to obtain single-mode lasing which is realized at the Fresnel number $N_F \sim 1$, an X-ray laser length is required that cannot be provided by the available pumping conditions, degree of medium homogeneity, etc. For this reason, other methods for improving the radiation parameters of the homogeneous X-ray laser are used. Among them are the master ASE oscillator – amplifier scheme, the amplification mode with several ASE passages through the gain medium, and the travelling-wave pumping mode. These methods also provide a certain improvement in the ASE parameters in the presence of optical inhomogeneities in the X-ray laser medium.

4.2.1 The master oscillator – amplifier scheme. The quality of the X-ray laser beam can be improved by using the master ASE oscillator – amplifier scheme with spatial filtration [134]. Because the amplifier is far from the oscillator, the radiation incident on it possesses improved coherence and angular properties [see Eqn (78)]. Of course, the intensity of the oscillator ASE should substantially exceed the intensity of spontaneous amplifier noise in order to suppress the self-excitation of the latter. It is also necessary to provide the required time interval between the pump pulses for the oscillator and amplifier.

The master oscillator – amplifier scheme was used in an Ne-like yttrium X-ray laser on the 3p – 3s transition at 15.5 nm with the targets irradiated from one side [135]. The oscillator and amplifier lengths were 2.52 and 1.68 cm, respectively. Pumping was performed with a two-beam Nova laser facility operating at a wavelength of 0.53 μm, a pulse length of 0.5 ns, and an energy and intensity per pump beam of 2.52 kJ and

1.4×10^{14} W/cm^2, respectively. The time-integrated angular distribution of the oscillator ASE in the x direction perpendicular to the target has a maximum at an angle of about 13 mrad (see Section 3.3). The oscillator ASE reflected from a multilayer X-ray mirror was incident on the amplifier. The amplifier was located at an angle of 13 mrad and a distance of $\sim$ 30 cm from the oscillator. The time-integrated experimental distributions of the oscillator radiation passed through the amplifier and of the intrinsic ASE of the amplifier in the x direction in the far field showed that the excess of the amplified input signal over the intrinsic ASE of the amplifier is insignificant. After passage through the amplifier, the divergence of the radiation did not improve and the maximum of intensity somewhat shifted towards larger angles. It is obvious that one reason for the low efficiency of the scheme is the too high optical inhomogeneity of the amplifying medium. Nevertheless, note that an Ne-like yttrium X-ray laser is characterized by a maximum brightness of $\sim 10^{23}$ photon/(s mm^2 mrad^2) at the 0.01% band among other X-ray lasers.

The master oscillator – amplifier scheme can also be used to produce linearly polarized X-ray laser radiation [136] which is required in a number of applications [27]. The ASE itself is fully nonpolarized, as has been experimentally confirmed [136]. The oscillator ASE was made linearly polarized (with $\sim$ 98% degree of polarization) with the help of a grazing-incidence multilayer mirror and was incident on the amplifier input. After passage through the amplifier, the radiation completely retained its polarization.

4.2.2 The multipass amplification mode. In optical lasers, open resonators are widely used which require a gain coefficient sufficient to overcome losses in the resonator and a long time of population inversion occurrence to provide the multipass mode. Modern technology permits the manufacture of normal-incidence multilayer mirrors in the soft X-ray range with the reflectivities achieving up to several tens of percent under normal incidence [30]. However, because of the short time of the population inversion occurrence in an X-ray laser, the multipass amplification mode cannot be obtained. As a rule, X-ray lasers producing pulses of duration of several hundreds of picoseconds can operate in the double-pass amplification mode using a mirror located on one side of the laser and having the highest possible reflectivity. Such a mode was demonstrated in H-like carbon ion [7] and Ne-like selenium ion [137] X-ray lasers. In Ref. [138], triple-pass amplification was observed in an Ne-like selenium ion X-ray laser. The closer the mirror to the gain medium, the more efficient the system. However, for high ASE intensities the threat of mirror damage exists, resulting in a sharp decrease in the reflectivity (see, for example, Ref. [135]), whereas removing the mirror from the gain medium can eliminate the advantages of the amplification scheme.

At present, the use of a half-resonator in laboratory setups is quite common. In the case of an Ne-like zinc ion X-ray laser, the use and alignment of a curved mirror allows one to increase the ASE intensity by a factor of $\sim$ 80, thereby producing saturation with an output power of $\sim$ 1 mJ and an average power of 12 – 15 MW upon moderate pumping (450 ps, 450 J) [126], whereas in the single-pass mode, saturation is achieved for a pump energy $\geqslant$ 1 kJ. In addition, the spatial coherence of ASE is also improved [126].

For a tabletop Ne-like argon ion X-ray laser in a capillary discharge operating in double-pass amplification mode, an energy of 30 μJ was obtained and saturation was achieved at a lower discharge length [25]. Figure 11 shows the dependences of the ASE intensity on the 3p – 3s $J = 0 - 1$ transition of the Ne-like argon ion at 46.9 nm on the length of the capillary for single- and double-pass amplification modes.

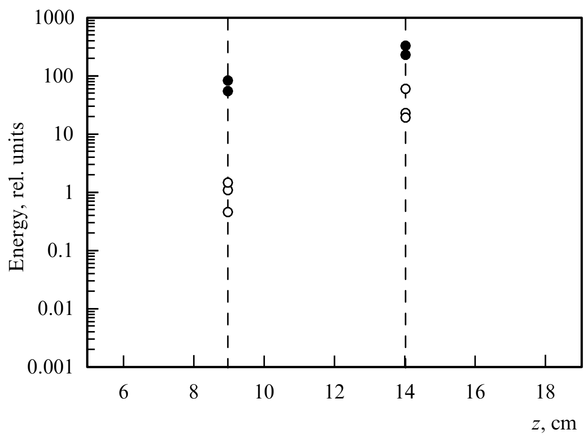

Figure 11. Experimental dependence of the ASE energy at the 3p – 3s $J = 0 - 1$ transition of an Ne-like argon X-ray laser at 46.9 nm in a capillary discharge on the capillary length for single-pass (○) and double-pass (●) amplification modes [25].

Upon irradiation of a massive target with a train of 16 laser pulses with energies of 1.5 – 2 J, the Li-like aluminium recombination X-ray laser produced pulses of duration longer than 1 ns [139]. This allows one not only to obtain the double-pass amplification mode but also to employ a resonator. The experiment showed a noticeable increase in the intensity of the 3d – 4f and 3p – 4d lines at 15.47 and 15.06 nm, respectively, when both stable and unstable resonators were used.

4.2.3 The travelling-wave pumping mode. For the time 100 ps, which is of the order of the time of the population inversion occurrence in the quasi-steady-state regime, ASE travels a distance of 3 cm which is close or even smaller than typical X-ray laser lengths. This means that the finite time of passage of the medium by photons can substantially limit the real gain length when simultaneously producing the gain medium over its entire volume. Travelling-wave pumping allows one to increase the effective gain length and thereby to use the potential of the gain medium more efficiently. In this case, the pump wave propagates through the medium not perpendicularly to the X-ray laser axis (see Fig. 1), i.e. to the direction of the ASE propagation, but as close to this direction as possible. Such a matching between the directions of propagation of the pump beam and ASE results in predominantly unidirectional X-ray lasing. The use of travelling-wave pumping reduces the divergence of ASE and increases its intensity.

Travelling-wave pumping has been demonstrated on the 3p – 3s transition in the Ne-like yttrium X-ray laser using exploding-foil targets [140]. Figure 12 shows the dependences of the ASE intensity on the X-ray laser length for the 3p – 3s $J = 0 - 1$ transition in an Ne-like germanium X-ray laser [119]. Here, a combination of travelling-wave and multipulse pumping was used. A massive target was irradiated on one side by a train of three 0.53-μm, 100-ps pump pulses separated

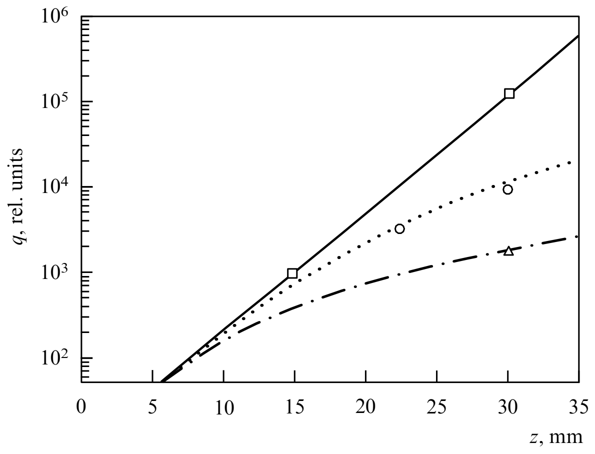

Figure 12. Dependences of the ASE intensity at the 3p – 3s $J = 0-1$ transition at 19.6 nm on the Ne-like germanium X-ray laser length [119]: calculations (—) and experiments with travelling-wave pumping (□); calculations (····) and experiments (○) without the travelling wave; calculations (-·-·-) and experiments (Δ) with a counter-propagating travelling wave.

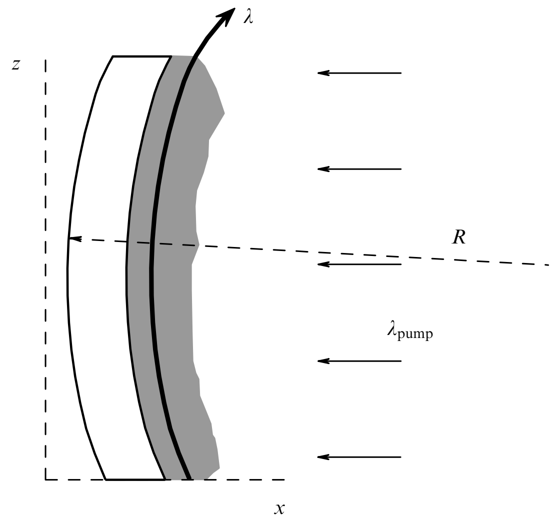

Figure 13. Schematic of an X-ray laser with a curved target.

by intervals of 400 ps. The intensity per pulse was 1.4×10^{14} W/cm^2. The main amplification was observed during the third pump pulse. For an angle of 45° between the direction of the pump propagation and the X-ray laser axis, the 10-fold increase in the intensity of the 'co-propagating' ASE beam was achieved compared to the case of perpendicular pumping. The intensity of the counter-propagating ASE beam was 100 times lower than that of the co-propagating beam.

In the case of promising tabletop X-ray lasers pumped by high-intensity picosecond and femtosecond pulses, the use of a travelling-wave pump seems to be necessary. For example, in a Pd-like xenon X-ray laser the maximum value of $\alpha_0 z \approx 11$ was obtained using longitudinal femtosecond pumping of a cell filled with xenon [23].

4.3 Compensation for refraction distortions

Refraction causes premature escape of the beams from the gain region, thereby decreasing the intensity of the ASE beam and reducing its quality. Below, we consider the cases when attempts are made to compensate for refraction distortions of ASE or to produce an inhomogeneity of a special type rather than to eliminate the large-scale inhomogeneity of the electron density in the plasma. In the first case, this is achieved using a curved target and an arrangement of two or more targets in series, and in the second case, by placing the targets in parallel.

4.3.1 A curved target. This method for compensation of refraction is based on the use of a massive target curved in the longitudinal direction with a constant radius of curvature [141] (see Fig. 13). Upon propagation, the beams are deflected due to refraction, but the plasma is also displaced to the defocusing side, so that the beam propagates through the plasma not leaving the gain region.

The effect of target curvature on ASE can be readily elucidated from analysis of equation (56) for the TCF. We assume that the radius of curvature R of the target is constant and satisfies the condition $(R/z)^2 \gg 1$. Then, distributions of $\bar{\alpha}_0$ and $\bar{\varepsilon}$ in the plasma can be approximately modelled with functions depending on $x + Cz^2/2$, where $C = 1/R$ is the curvature. By omitting in Eqn (56) fluctuations of the parameters of the medium, amplification, and a volume source and passing to the new variable $u = x + Cz^2/2$, we obtain in the two-dimensional case [125]:

$$\left\{\frac{\partial}{\partial z} + Cz\frac{\partial}{\partial u} + \frac{\mathrm{i}}{k}\frac{\partial^2}{\partial u\,\partial x'} + \frac{\mathrm{i}k}{2}\big[\varepsilon(u_1) - \varepsilon(u_2)\big]\right\}B(u, x'; z) = 0\,. \tag{88}$$

We seek the solution of equation (88) in the form $B(u, x'; z) = F(kx'/z)\exp(\mathrm{i}kux'/z)/z$, i.e. the TCF of radiation from a delta-correlated source located in the plane $z = 0$ [see Eqn (64)], propagating through a flat homogeneous medium. After substitution of the solution into (88), we obtain the relation $Cx' = \big[\bar{\varepsilon}(u_1) - \bar{\varepsilon}(u_2)\big]/2$, from which it follows that $C = \nabla\bar{\varepsilon}/2$ under the condition $\nabla\bar{\varepsilon} = \text{const}$. Thus, for a given value of C, the radiation from a delta-correlated source propagates in a curved medium without refraction. In a real plasma, the gradient $\nabla\bar{\varepsilon}$ is not constant; for this reason, the optimum value C_{opt} should be chosen based on the value of $\nabla\bar{\varepsilon}$ in the case of maximum amplification [141].

The approach [141] was implemented on the 3p – 3s transitions at 19.6 and 23.6 nm in an Ne-like germanium X-ray laser with a half-resonator [142]. Figure 14 shows the angular distributions of intensity for the $J = 0-1$ ASE line at 19.6 nm in the cases of flat and curved targets. One can see that a curved target with $R = 2.7$ m provides an increase in the maximum strength of radiation q_{max} by a factor of ~ 10 and reduces by a factor of ~ 2 its divergence $\Delta\theta$ in the x direction. Note that in these experiments a single-pulse pump was used (with a wavelength of 1.053 μm, a pulse length of 1 ns, and an intensity per pump beam of 1.7×10^{13} W/cm^2), so that the gradient $\nabla\bar{\varepsilon}$ was quite large. Later, the experiments were performed with curved targets irradiated by a prepulse and two or three subsequent pulses [144], which resulted in a reduction of $\nabla\bar{\varepsilon}$. In the case of two-pulse irradiation, the brightness of a given line increased by a factor of 25 compared to that for single-pulse irradiation. Three-pulse pumping leads to a further increase in the X-ray laser brightness and a decrease in the beam divergence due to further relaxation of $\nabla\bar{\varepsilon}$. The geometrical optics calculations of the angular distribution of the ASE intensity [144, 145] correspond to

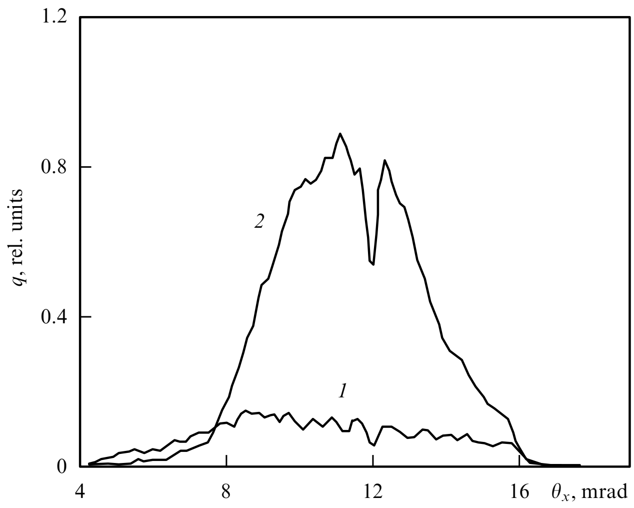

Figure 14. Experimental angular distributions of the ASE intensity for the 3p–3s $J = 0-1$ line of the Ne-like germanium ion laser at 19.6 nm for (*1*) a flat and (*2*) a curved target with a radius of curvature of 2.7 m [142].

the experimental data. Both experiments and calculations show that the use of curved targets results in more noticeable increase in $q_{\max}$ than a decrease in $\Delta\theta$ [125]. The maximum $q_{\max}$ and minimum of $\Delta\theta$ are observed for $C \approx C_{\text{opt}}$.

Figure 15 displays experimental dependences of the angle-integrated ASE intensity on the 3p–3s $J = 0-1$ transition of Ne-like germanium ion at 19.6 nm on the target curvature C for different ratios of the prepulse energy to the main pulse energy, which was 600 J [146]. When the fraction of energy in the prepulse was $\leqslant 1\%$, the use of a curved target resulted in an increase in the X-ray laser energy by two orders of magnitude. This positive effect decreased with increasing prepulse energy.

A curved target does not eliminate refraction completely because of the inhomogeneity of $\nabla\bar{\varepsilon}$ in the gain region. The residual effect of refraction in the case of a convex profile for $\bar{\varepsilon}$ (or a concave profile for N_{e}) of type (87) is of a focusing nature

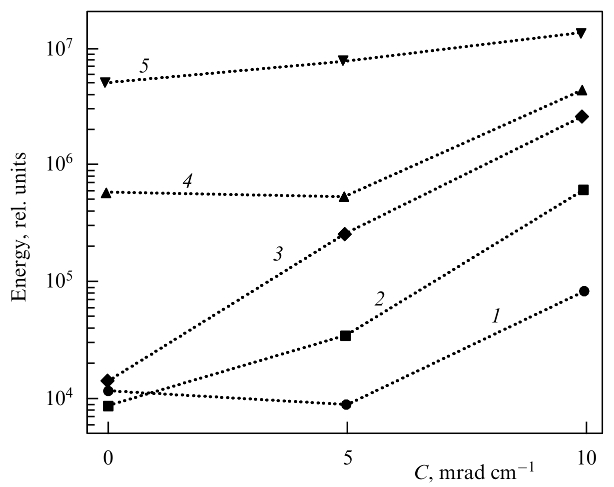

Figure 15. Experimental dependences of the ASE energy at the 3p–3s $J = 0-1$ transition of Ne-like germanium ion at 19.6 nm on the target curvature C for fractions of the energy in the prepulse (*1*) 0, (*2*) 0.087, (*3*) 0.165, (*4*) 1.65, and (*5*) 15% [146].

[47, 141, 142]. For this reason, in the case of a curved target, the residual focusing effect allows one to obtain a power that is even greater than in the absence of refraction [125].

A decrease in $L_{\text{c}}(Z)$ at the beam centre in the far field with increasing z, observed in the case of a plane target (see Section 4.1.2), changes to an increase in the case of a curved target [125]. Owing to the confinement of the ASE beam in the gain region, resulting in a decrease in the source size, the value of $L_{\text{c}}(Z)$ considerably exceeds the corresponding values in the case of a plane target. The use of a curved target not only substantially increases $L_{\text{c}}(Z)$ but also provides a quite flat distribution of it in the main part of the ASE beam (Fig. 16). Nevertheless, the values of $L_{\text{c}}(Z)$ are still smaller than in the absence of refraction because of the residual focusing effect. The values of $L_{\text{c}}(Z)$ can be increased provided the residual defocusing effect is obtained for the curved target by producing a concave profile of $\bar{\varepsilon}$ (or a convex profile of N_{e}) in the gain region. One can see from Fig. 16 that such an improvement in coherence is achieved at the expense of a substantial decrease in the ASE power and brightness and an increase in the beam divergence. However, this decrease in the power and brightness on passing from a concave to a convex density profile is not dangerous, because it will be substantially compensated by amplification saturation, while the effect of an increase in coherence remains because amplification saturation does not appreciably affect it.

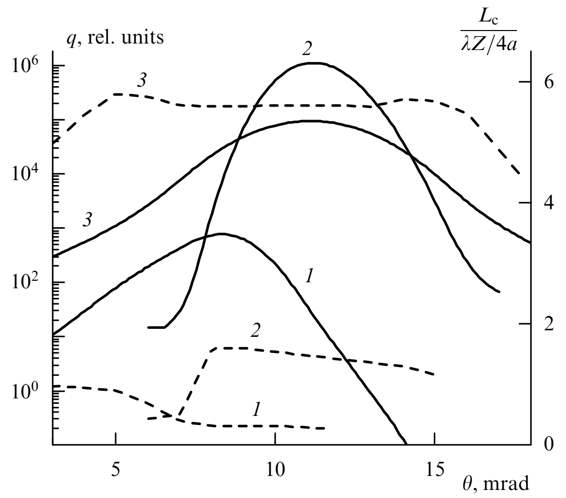

Figure 16. Calculated far-field distributions of the strength of radiation q (—) and the coherence length L_{c} (- - -) for $z = 5$ cm, $a = 50$ μm, and $\Delta\varepsilon = 2.6 \times 10^{-4}$ in the case of a convex profile of $\bar{\varepsilon}$ (87) for (*1*) $C = 0$ and (*2*) $C = C_{\text{opt}}$, and in the case of a concave profile of $\bar{\varepsilon}$ for (*3*) $C = C_{\text{opt}}$ [125]. The profile of $\bar{\alpha}_0$ is parabolic with the gain maximum at $x = 100$ μm and a gain region width of 100 μm.

4.3.2 Targets placed in series. Refraction losses can be also compensated for by using two massive targets placed in series and irradiated from the opposite sides [147]. Figure 17 demonstrates the principle of operation of such an X-ray laser. Plasma regions formed near each target expand in opposite directions. The ASE refracted in the first plasma bunch emerges from it and enters the second plasma bunch with an analogous profile of $\bar{\varepsilon}$ but with the opposite sign of $\nabla\bar{\varepsilon}$. The refraction distortion is compensated for during the ASE propagation through the second plasma volume. The use of a chain consisting of several pairs of such targets makes it

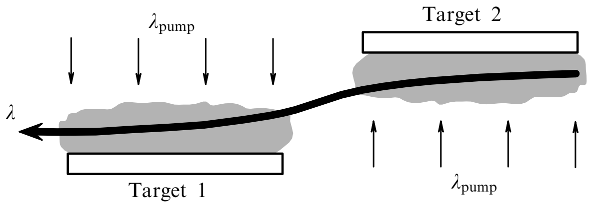

Figure 17. Schematic of the X-ray laser with targets placed in series.

possible to obtain stronger amplification. The efficiency of this system, which is obviously more complex than the configuration with one curved target, is substantially determined by the accuracy of its alignment.

Despite the complexity of such an approach, the operation of this scheme has been successfully demonstrated in experiments [148 – 150]. At present, such targets are commonly used in the Ne-like germanium ion X-ray laser in the Vulcan facility at the Rutherford Laboratory [151]. A pump with an energy of 1kJ using a prepulse makes it possible to achieve amplification saturation over a comparatively small length of 1.8 cm for both targets. The ASE divergence in the plane parallel to the targets is ~ 30 mrad and is 4 – 5 times larger than that in the plane perpendicular to the targets.

4.3.3 Targets placed in parallel. Plasma bunches produced upon irradiation of the inner surfaces of two targets placed parallel to each other expand toward each other and collide [152 – 154]. The profile of N_e has a hole in the gain region between the targets and possesses focusing properties.

In Ref. [46], radiation amplification was studied in an X-ray laser with a transverse parabolic increase of N_e to the periphery, i.e. with focusing properties. The gain coefficient was assumed to be proportional to N_e, but limited at high pressures. Thus, the laser medium was characterized by an enhanced gain at the periphery for $x \sim \pm x_m$.

It was found that upon amplification of the parallel beam of rays the distribution of the output emission periodically changed over z with the period $z_{per} = (\pi/2)z_r$ [46]. Generally, the angular distribution of emission consists of two peaks with coordinates $\theta_{peak} = \pm|\sin(2z/z_r)|\theta_m$, where $\theta_m = 2x_m/z_r$. For $z = (m + 1/2)z_{per}$, all the rays intersect at a node on the optical axis, and the angular distribution of emission has a maximum width of the localization area which somewhat exceeds $2\theta_m$. For $z = mz_{per}$, the rays are parallel to the optical axis, and the amplified emission forms one on-axis core in the far field with diffraction divergence, which is ideal for X-ray laser applications. Note that in this case refraction does not lead to additional losses in the gain coefficient over z of type (79): the gain is equal to a half-sum of the on-axis and maximum gain coefficients multiplied by the X-ray laser length. Therefore, the use of the focusing profile of N_e allows one to avoid refractive losses of the emission power.

The ASE regime gives the same rate of power increase over z as upon amplification of a parallel beam of rays. However, attempts to obtain a collimated beam during amplification have failed. For any z, the width of the angular distribution of ASE somewhat exceeds $2\theta_{max}$.

Finally, note that the methods for compensation of the ASE refraction described in this section permit improvement of the beam quality only in the transverse x direction parallel to the target, whereas in the perpendicular y direction the negative effect of refraction by the symmetric profile of N_e on the ASE power and divergence remains. One method for improving the situation consists in creating a hole in the distribution $N_e(y)$ [155]. The hole can be produced using a prepulse or multipulse pumping. In this case, the subsequent pulse (pulses) should be focused to a narrower line in a preliminary prepared plasma as compared to the previous pulse (pulses), which provides more rapid expansion of the plasma in the central region.

5. Conclusions

At present, stable laser action has been obtained in soft X-ray region in multiply-charged ion plasmas at large unique laser facilities. The minimum lasing wavelength achieved lies within the 'water window'. A number of tabletop soft X-ray lasers have been demonstrated which, although having modest energies and wavelengths, are more accessible. X-ray lasers are already used for the diagnostics of high-temperature plasma. However, from the point of view of the problem of coherence and divergence discussed in this review, existing X-ray lasers do not yet satisfy the standards commonly accepted in quantum electronics.

Nevertheless, the studies performed from the early 1980s have made it possible to understand principal macroscopic effects reducing the X-ray laser beam quality and to suggest a number of methods for reducing the negative action of these effects. In our opinion, the discrepancy between some experimental data and theoretical results can be eliminated by more detailed studies of plasma effects leading to a comparatively small-scale perturbation of the optically uniform X-ray laser medium. At present, studies on the possibilities of improving the beam quality are being developed along with a search for new X-ray laser schemes aimed at obtaining shorter X-ray laser wavelengths and pulses.

Acknowledgments
The authors are grateful to A N Anisimov, V A Volkov, V M Gerasimov, G G Kochemasov, Yu K Kochubei, V K Ladagin and V D Urlin for useful discussions of the problems considered in the review, and also to G A Kirillov, V D Pis'mennyi, Yu A Romanov, Yu A Trutnev and L P Feoktistov for their support and interest in this work.

This work was partially supported by the International Scientific Technological Centre (ISTC), project No. 076-95.

References

1. Prokhorov A M *Science* **149** 828 (1965) [Translated into Russian: *Usp. Fiz. Nauk* **85** 599 (1965)]
2. Robinson C A *Aviation Week and Space Technol.* **114** 25 (1981)
3. Canavan G H, Bloembergen N, Patel C K N "Debate on APS directed-energy weapons study" *Physics Today* **40** (11) 48 (1987) [Translated into Russian: *Usp. Fiz. Nauk* **155** 661 (1988)]
4. Broad W J *Teller's War* (New York: Simon & Schuster, 1992)
5. Matthews D L et al. *Phys. Rev. Lett.* **54** 110 (1985)
6. Rosen M D et al. *Phys. Rev. Lett.* **54** 106 (1985)
7. Suckewer S et al. *Phys. Rev. Lett.* **55** 1753 (1985)
8. Elton R C *Appl. Optics* **14** 97 (1975); Zherikhin A N, Koshelev K N, Letokhov V S *Kvantovaya Elektron.* **3** 152 (1976) [*Sov. J. Quantum Electron.* **6** 82 (1976)]; Vinogradov A V, Sobel'man I I, Yukov E A *Kvantovaya Elektron.* **4** 63 (1977) [*Sov. J. Quantum Electron.* **7** 32 (1977)]
9. Gudzenko L I, Shelepin L A *Zh. Eksp. Teor. Fiz.* **45** 1445 (1963) [*Sov. Phys. JETP* **18** 998 (1964)]; Pert G J *J. Phys. B* **9** 3301 (1976); **12** 2067 (1979)
10. Matthews D L et al. *J. Opt. Soc. Am. B* **4** 575 (1987)

11. Keane C J et al. *J. Phys. B* **22** 3343 (1989)
12. London R A et al. *J. Phys. B* **22** 3363 (1989)
13. Skinner C *Phys. Fluids B* **3** 2420 (1991)
14. Fill E E, in *Laser Interaction with Matter* (IOP Conf. Ser., Vol. 140, Ed. S J Rose) (Bristol: IOP Publ., 1995) p.111
15. Elton R C *X-Ray Lasers* (Boston: Academic Press, 1990)
16. *X-Ray Lasers 1990* (IOP Conf. Ser., Vol. 116, Ed. G J Tallents) (Bristol: IOP Publ., 1990)
17. *X-Ray Lasers 1992* (IOP Conf. Ser., Vol. 125, Ed. E E Fill) (Bristol: IOP Publ., 1992)
18. *X-Ray Lasers 1994* (AIP Conf. Proc., Vol. 332, Eds D C Eder, D L Matthews) (Williamsburg: AIP Publ., 1994)
19. *X-Ray Lasers 1996* (IOP Conf. Ser., Vol. 151, Eds S Svanberg, C-G Wahlström) (Bristol: IOP Publ., 1996)
20. Nickles P V et al. *Proc. SPIE* **2520** 373 (1995)
21. Afanas'ev Yu V, Shlyaptsev V N *Kvantovaya Elektron.* **16** 2499 (1989) [*Sov. J. Quantum Electron.* **19** 1606 (1989)]
22. Eder D C et al., in Ref. [19] p. 136
23. Lemoff B et al. *Phys. Rev. Lett.* **74** 1574 (1995)
24. Rocca J J et al. *Phys. Rev. Lett.* **73** 2192 (1994)
25. Rocca J J et al., in Ref. [19] p. 176
26. Matthews D L, in Ref. [19] p. 32
27. *Applications of X-Ray Lasers* (Eds R London, D Matthews, S Suckewer) (San Francisco: Nat. Tech. Inform. Serv. Doc. No. LLNL-CONF-9206170, 1992)
28. Koch J A et al. *Phys. Rev. Lett.* **68** 3291 (1992)
29. London R A *Phys. Fluids B* **5** 2707 (1993)
30. Vinogradov A V et al. *Zerkal'naya Rentgenovskaya Optika* (X-Ray Mirror Optics) (Leningrad: Mashinostroenie, 1989); Chakraborty P *Int. J. Modern Phys. B* **5** 2133 (1991)
31. Allen L, Peters G I *Phys. Lett. A* **31** 95 (1970)
32. Peters G I, Allen L *J. Phys. A* **4** 238 (1971); Allen L, Peters G I *J. Phys. A* **4** 377 (1971); *J. Phys. A* **4** 564 (1971)
33. Peters G I, Allen L *J. Phys. A* **5** 546 (1972)
34. Michalas D *Stellar Atmospheres* (San Francisco: W.H. Freeman and Co., 1978) [Translated into Russian (Moscow: Mir, 1982)]
35. Biberman L M, Vorob'ev V S, Yakubov I T *Kinetika Neravnovesnoĭ Nizkotemperaturnoĭ Plazmy* (Kinetics of Nonequilibrium Low-Temperature Plasma) (Moscow: Nauka, 1982) [Translated into English (New York: Consultants Bureau, 1987)]
36. Rautian S G, Smirnov G N, Shalagin A M *Nelineinye Rezonansy v Spektrakh Atomov i Molekul* (Nonlinear Resonances in Spectra of Atoms and Molecules) (Novosibirsk: Nauka, 1979)
37. Gasparyan P D et al. *Zh. Eksp. Teor. Fiz.* **105** 1593 (1994) [*JETP* **78** 858 (1994)]
38. Zemtsov Yu K, Sechin A Yu, Starostin A N *Zh. Eksp. Teor. Fiz.* **110** 1654 (1996) [*JETP* **83** 909 (1996)]
39. Maitland A, Dunn M H *Laser Physics* (Amsterdam: North-Holland Publ. Co., 1969) [Translated into Russian (Moscow: Nauka, 1978)]
40. Rytov S M, Kravtsov Yu A, Tatarskiĭ V I *Vvedenie v Statisticheskuyu Radiofiziku* Part 2 (Principles of Statistical Radiophysics) (Moscow: Nauka, 1978) [Translated into English (Berlin: Springer-Verlag, 1989)]
41. Apresyan L A, Kravtsov Yu A *Teoriya Perenosa Izlucheniya* (Theory of Radiation Transfer) (Moscow: Nauka, 1983)
42. Landau L D, Lifshitz E M *Elektrodinamika Sploshnykh Sred* (Electrodynamics of Continua Media) (Moscow: Nauka, 1981) [Translated into English (New York: Pergamon Press, 1984)]
43. Born M, Wolf E *Principles of Optics* 4th ed. (Oxford, New York: Pergamon Press, 1964) [Translated into Russian (Moscow: Nauka, 1970)]
44. Gudzenko L I, Yakovlenko S I *Plazmennye Lazery* (Plasma Lasers) (Moscow: Atomizdat, 1978)
45. London R A *Phys. Fluids* **31** 184 (1988)
46. Boswell B et al. *Phys. Fluids B* **2** 436 (1990)
47. Boehly T et al. *Opt. Commun.* **79** 57 (1990)
48. Ratowsky R P et al. *ICF Quart. Rep.* UCRL-LR 105821-94-2 (Livermore: LLNL) **4** (2) 63 (1994)
49. Plowes J A, Pert G J, Holden P B *Opt. Commun.* **116** 260 (1995)
50. Wan A S, Mayle R W, Kato Y, Osterheld A L, in *Laser Interaction and Related Plasma Phenomena* (AIP Conf. Proc., Vol. 369, Eds S Nakai, G N Miley) (New York: AIP Conf., 1996) part 2, p. 778
51. Zimmerman G B, Kruer W L *Comments Plasma Phys. Controlled Fusion* **11** 51 (1975)
52. Avrorin E N et al. *Pis'ma Zh. Eksp. Teor. Fiz.* **32** 457 (1980) [*JETP Lett.* **32** 437 (1980)]
53. Craxton R S, MacCrory R L *LLE Reports* 99 and 108 (Rochester: University of Rochester, 1980)
54. Sofronov I D et al., in *Konstruirovanie Algoritmov i Reshenie Zadach Matematicheskoĭ Fiziki* (Construction of Algorithms and Solution to Problems of Mathematical Physics) (Eds G P Voskresenskiĭ, V V Zabrodin) (Moscow: Inst. of Problems in Mechanics, USSR Acad. Sciences, 1989)
55. Klisnick A et al., in Ref. [17] p. 305
56. Klapisch M et al. *J. Opt. Soc. Am.* **67** 148 (1977)
57. Hagelstein P L *LLNL Report* UCRL-53100 (Livermore: LLNL, 1981)
58. Voinov B A et al. *Vopr. Atom. Nauki Tekhn., Ser. Matem. Model.* (2) 65 (1993)
59. Politov V Yu, Lykov V A, Shinkarev M K *Proc. SPIE* **1928** 157 (1993)
60. Makhrov V et al. *J. Phys. B* **27** 1899 (1994)
61. Holden P B et al. *J. Phys. B* **27** 341 (1994)
62. Derzhiev V I et al. Preprint IOFAN No. 235 (Moscow: Inst. Gen. Phys. Publ., 1987); Derzhiev V I, Zhidkov A G, Yakovlenko S I *Trudy IOFAN* **40** 52 (1992)
63. Limpoukh Ĭ, Rozanov V B *Kvantovaya Elektron.* **11** 1416 (1984) [*Sov. J. Quantum Electron.* **14** 955 (1984)]
64. Rosen M D *Phys. Fluids B* **2** 1461 (1990)
65. Willi O et al. *Phys. Fluids B* **2** 1318 (1990)
66. Kieffer J C et al. *Phys. Fluids B* **3** 463 (1991)
67. Nantel M et al. *Phys. Fluids B* **5** 4465 (1993)
68. La Fontaine B et al. *Phys. Rev. E* **47** 583 (1993)
69. Wan A S et al., in Ref. [19] p. 504
70. Hora H *Physics of Laser Driven Plasmas* (New York: John Wiley and Sons, 1981) [Translated into Russian (Moscow: Energoatomizdat, 1986)]
71. Pantell R H, Puthoff H E *Fundamentals of Quantum Electronics* (New York: Plenum Press, 1969) [Translated into Russian (Moscow: Mir, 1972)].
72. Allen L, Eberly J H *Optical Resonance and Two-Level Atoms* (New York: John Wiley and Sons, 1975) [Translated into Russian (Moscow: Atomizdat, 1978)]
73. Leontovich M *Izv. Akad. Nauk SSSR, Ser. Fiz.* **8** 16 (1944)
74. Hopf F A, Meystre P *Phys. Rev. A* **12** 2534 (1975); Raymer M G, Mostowski J *Phys. Rev. A* **24** 1980 (1981); Raymer M G et al. *Phys. Rev. A* **32** 332 (1985)
75. Hazak G, Bar-Shalom A *Phys. Rev. A* **38** 1300 (1988)
76. Sureau A, Holden P B *Phys. Rev. A* **52** 3110 (1995)
77. Ratowsky R P, London R A *Phys. Rev. A* **51** 2361 (1995)
78. Hazak G, Bar-Shalom A *Phys. Rev. A* **40** 7055 (1989)
79. London R A, Strauss M, Rosen M D *Phys. Rev. Lett.* **65** 563 (1990)
80. Amendt P, London R A, Strauss M *Phys. Rev. A* **44** 7478 (1991)
81. Amendt P, London R A, Strauss M *Phys. Rev. A* **47** 4348 (1993)
82. Borovskiĭ A V, Galkin A L, Korobkin V V *Kvantovaya Elektron.* **15** 1457 (1988) [*Sov. J. Quantum Electron.* **18** 915 (1988)]; Borovskiĭ A V, Galkin A L *Trudy IOFAN* **41** 103 (1993)
83. Ladagin V K, Starikov F A, Volkov V A, in Ref. [19] p. 336
84. Feit M D, Fleck J A, Jr. *J. Opt. Soc. Am. B* **7** 2048 (1990)
85. Feit M D, Fleck J A, Jr. *Opt. Lett.* **16** 76 (1991)
86. Starikov F A *Vopr. Atom. Nauki Tekhn., Ser. Teor. Prikl. Fiz.* (4) 14 (1989)
87. Starikov F A *Vopr. Atom. Nauki Tekhn., Ser. Teor. Prikl. Fiz.* (2) 33 (1990)
88. Starikov F A, Urlin V D *Kvantovaya Elektron.* **18** 436 (1991) [*Sov. J. Quantum Electron.* **21** 393 (1991)]
89. Akhmanov S A, D'yakov Yu E, Chirkin A S *Vvedenie v Statisticheskuyu Radiofiziku i Optiku* (Introduction to Statistical Radiophysics and Optics) (Moscow: Nauka, 1981)
90. Starikov F A *Vopr. Atom. Nauki Tekhn., Ser. Teor. Prikl. Fiz.* (3) 20 (1990)
91. Starikov F A *Kvantovaya Elektron.* **19** 527 (1992) [*Sov. J. Quantum Electron.* **22** 483 (1992)]
92. Starikov F A, in *Fizika Yaderno-Vozbuzhdaemoĭ Plazmy i Problemy Lazerov s Yadernoĭ Nakachkoĭ* Vol. 2 (Proceedings of the Second

International Conference on Physics of Nuclear-Excited Plasmas and Problems of Nuclear-Pumped Lasers) (Arzamas-16: VNIIEF, 1995) p. 260; *Kvantovaya Elektron.* **23** 205 (1996) [*Quantum Electron.* **26** 199 (1996)]
93. Linford G J et al. *Appl. Optics* **13** 379 (1974)
94. Kryuchenkov V B et al. *Kvantovaya Elektron.* **17** 189 (1990) [*Sov. J. Quantum Electron.* **20** 146 (1990)]
95. Mokhov Yu V *Vopr. Atom. Nauki Tekhn., Ser. Teor. Prikl. Fiz.* (1) 29 (1991)
96. Starikov F A *Kvantovaya Elektron.* **21** 343 (1994) [*Quantum Electron.* **24** 320 (1994)]
97. Chirkov V A *Kvantovaya Elektron.* **11** 2253 (1984) [*Sov. J. Quantum Electron.* **14** 1497 (1984)]
98. Bunkin F V, Bykov V P *Kvantovaya Elektron.* **13** 869 (1986) [*Sov. J. Quantum Electron.* **16** 569 (1986)]
99. Fill E E *Opt. Commun.* **67** 441 (1988)
100. Ladagin V K, Starikov F A, Urlin V D *Kvantovaya Elektron.* **20** 471 (1993) [*Quantum Electron.* **23** 406 (1993)]
101. MacGowan B J et al. *Proc. SPIE* **688** 36 (1986)
102. Whelan D A et al. *Proc. SPIE* **831** 275 (1987)
103. Zhidkov A G, Terskikh A O, Yakovlenko S I *Kratk. Soobshch. Fiz.* (9) 27 (1988); Gulov A V et al. *Kvantovaya Elektron.* **17** 753 (1990) [*Sov. J. Quantum Electron.* **20** 675 (1990)]
104. Volkov V A et al. *Kvantovaya Elektron.* **18** 1329 (1991) [*Sov. J. Quantum Electron.* **21** 1214 (1991)]
105. Zahavi O, Hazak G, Zinamon Z *J. Opt. Soc. Am. B* **10** 271 (1993)
106. Trebes J E et al. *Phys. Rev. Lett.* **68** 588 (1992)
107. Lee T N, McLean E A, Elton R C *Phys. Rev. Lett.* **59** 1185 (1987)
108. O'Neil D M et al. *Opt. Commun.* **75** 406 (1990)
109. Starikov F A *Kvantovaya Elektron.* **20** 477 (1993) [*Quantum Electron.* **23** 412 (1993)]
110. Starikov F A, in Ref. [19] p. 315
111. Sutton G W *AIAA Journal* **7** 1737 (1969)
112. Lutovinov V S, Chechetkin V R *Zh. Eksp. Teor. Fiz.* **93** 1602 (1987) [*Sov. Phys. JETP* **66** 916 (1987)]
113. Amendt P, Strauss M, London R *Phys. Rev. A* **53** R23 (1996)
114. Suckewer S et al. *Phys. Rev. Lett.* **57** 1004 (1986)
115. Tomasel F G, Shlyaptsev V N, Rocca J J *Phys. Rev. A* **54** 2474 (1996)
116. Nilsen J *Phys. Scr.* **T47** 83 (1993)
117. Boehly T et al. *Phys. Rev. A* **42** 6962 (1990)
118. Nilsen J et al. *Phys. Rev. A* **48** 4682 (1993)
119. Moreno J C, Nilsen J, Da Silva L B *Opt. Commun.* **110** 585 (1994)
120. Holden P B, Rus B *Opt. Commun.* **119** 424 (1995)
121. Li Y, Pretzler G, Fill E E *Phys. Rev. A* **51** R4341 (1995); *Opt. Commun.* **119** 557 (1995); Li Y, Pretzler G, Fill E E, Nilsen J *J. Opt. Soc. Am. B* **13** 742 (1996)
122. MacPhee A G et al., in Ref. [19] p. 50
123. Tallents G J et al., in Ref. [19] p. 372
124. Plowes J A, Pert G J, Holden P B *Opt. Commun.* **117** 189 (1995)
125. Starikov F A *Kvantovaya Elektron.* **24** 691 (1997) [*Quantum Electron.* **27** 673 (1997)]
126. Jaegle P et al., in Ref. [19] p. 1
127. Nilsen J et al. *Phys. Rev. A* **55** 827 (1997)
128. Lu P, Li Y, Fill E E *Phys. Rev. A* **54** 5193 (1996)
129. Albert F et al., in Ref. [19] p. 427
130. Shlyaptsev V N et al., in Ref. [19] p. 215
131. Bonnet L, Jacquemot S, in Ref. [19] p. 53; Schegel Th, Nickles P V, Sandner W, in Ref. [19] p. 91
132. Fiedorowicz H et al. *Phys. Rev. Lett.* **76** 415 (1996)
133. Fiedorowicz H et al., in Ref. [19] p. 76
134. Rosen M D, Trebes J E, Matthews D L *Comments Plasma Phys. Controlled Fusion* **10** 245 (1987)
135. Shimkaveg G M et al., in Ref. [17] p. 61
136. Rus B et al. *Phys. Rev. A* **51** 2316 (1995)
137. Ceglio N M et al. *Appl. Opt.* **27** 5022 (1988)
138. Ceglio N M et al. *Opt. Lett.* **13** 108 (1988)
139. Hara T et al., in Ref. [19] p. 200
140. Da Silva L B et al. *Proc. SPIE* **2012** 158 (1993)
141. Lunney J G *Appl. Phys. Lett.* **48** 891 (1986)
142. Kodama R et al. *Phys. Rev. Lett.* **73** 3215 (1994)
143. Daido H et al. *Opt. Lett.* **20** 61 (1995)
144. Yuan G et al. *Phys. Rev. A* **52** 4861 (1995)
145. Plowes J A, Pert G J, Holden P B *Opt. Commun.* **116** 260 (1995)
146. Nilsen J et al. *Opt. Commun.* **124** 287 (1996); **130** 415 (1996)
147. Hagelstein P L *Plasma Phys.* **25** 1345 (1983)
148. Lewis C L S et al. *Opt. Commun.* **91** 71 (1992)
149. Wang S et al. *J. Opt. Soc. Am. B* **9** 360 (1992)
150. Carillon A et al. *Phys. Rev. Lett.* **68** 2917 (1992)
151. Key M H et al., in Ref. [19] p. 9
152. Shvarts D et al. *Proc. SPIE* **831** 283 (1987)
153. Boehly T et al. *Proc. SPIE* **831** 305 (1987)
154. Boehly T et al. *Appl. Phys. B* **50** 165 (1990)
155. Pert G J et al., in Ref. [19] p. 260